Experimental Techniques

St. Andrews, Scotland
23 Aug - 5 Sept 1998

Introduction

Observables and their Measurement

Experimental Challenge at LHC

Magnets and Muon Detectors

Electromagnetic and Hadronic Calorimetry

Inner Tracking

Signal Processing, Trigger and Data Acquisition

T. S. Virdee
CERN / Imperial College

References

Books

Techniques for Nuclear and Particle Physics Experiments,
W. R. Leo, Springer, 1994.

Single Particle Detection and Measurement,
R. S. Gilmore, Taylor and Francis, 1992

Experimental Techniques in High Energy Physics, ed. T. Ferbel, Addison Wesley, 1987.

Physics of Particle Detectors,
D. Green, Cambridge University Press, to be be published

Review of Particle Physics, Euro. Phys. J **C3**(1988)1.
http://pdg.lbl.gov/

Many Journals and Proceedings of Conferences

D. Fournier and L. Serin, Experimental Techniques, 1995 European School of HEP, CERN 96-04.

N. Ellis and T. S. Virdee, Experimental Challenges in High-luminosty Collider Physics, Ann. Rev. Nucl. Part. Sci. **44**(1994)609

Technical Design Reports of Experiments

CERN Academic Training Programme

C. Joram, Particle Detectors (1998)
Lecture Series on LHC pp Detectors

Tracking	**L. Rossi**
Calorimetry	**B. Mansoulie**
Muon Systems	**A. Benvenuti**
Electronics	**G. Hall**
Trigger/DAQ	**P. Sphicas**

Particle Physics

Aim to answer the two following questions:

What are the elementary constituents of matter ?

What are the forces that control their behaviour at the most basic level ?

Experimentally

Aim to measure the energies, directions and identity of the products of hard interactions as precisely as possible

Bubble Chambers

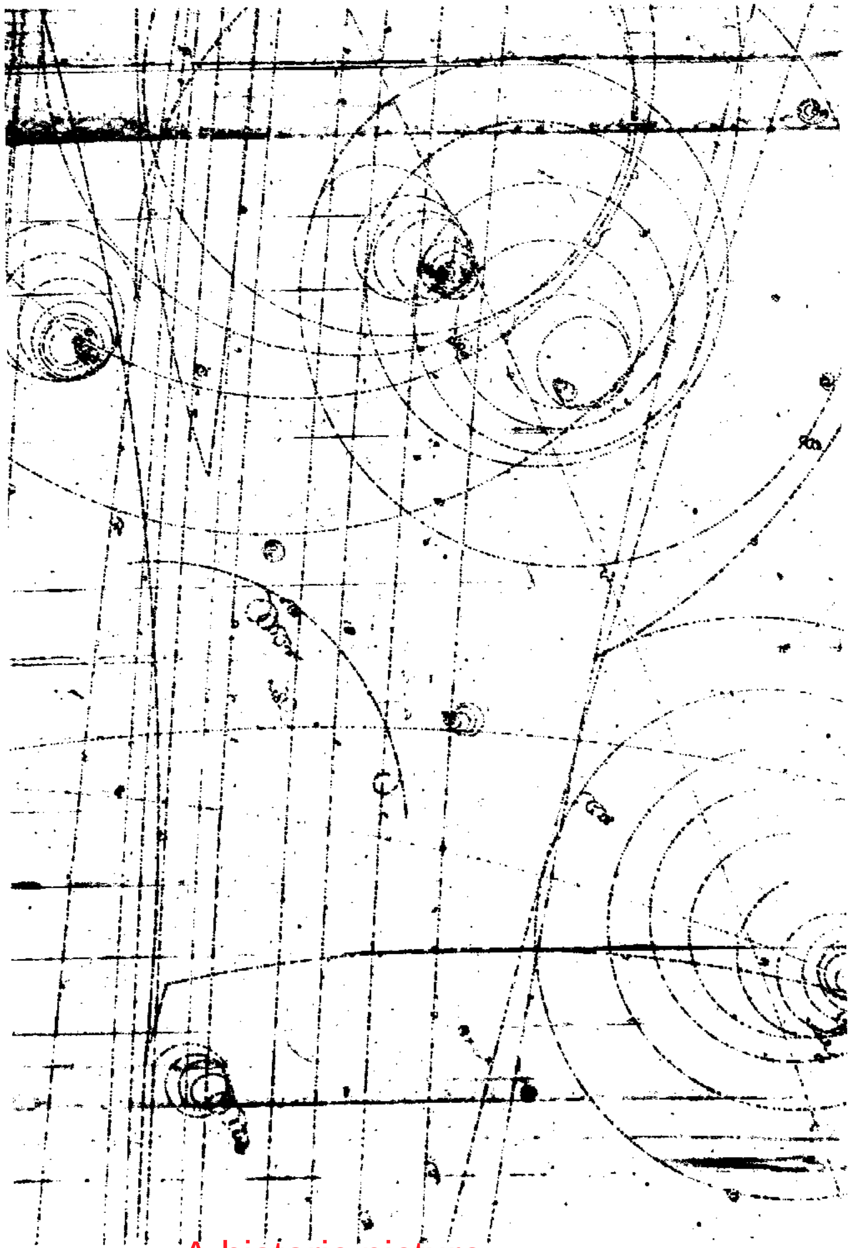

A historic picture

1964 : Production and decay of an Ω meson

$$K^- p \rightarrow K^0 \Omega^- K^+$$

$$\Omega^- \rightarrow \Xi^0 \pi^-$$

$$\Xi^0 \rightarrow \Lambda^0 \pi^0$$

$$\pi^0 \rightarrow \gamma \gamma$$

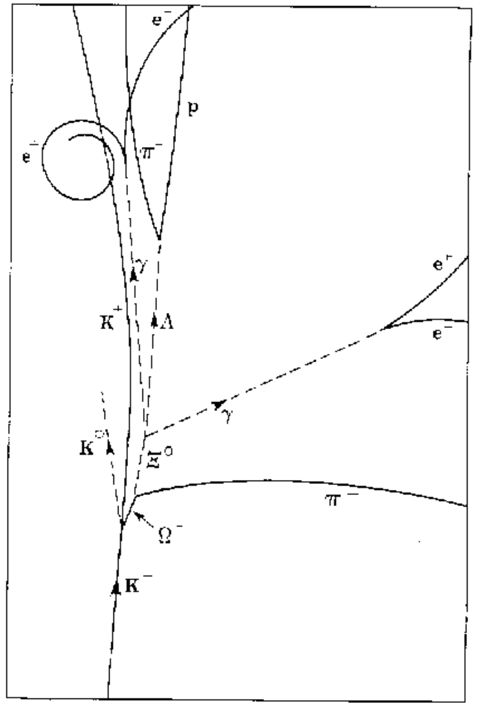

SM Higgs as a Benchmark

At the LHC the SM Higgs provides a good benchmark to test the performance of a detector

SM Higgs production at the LHC

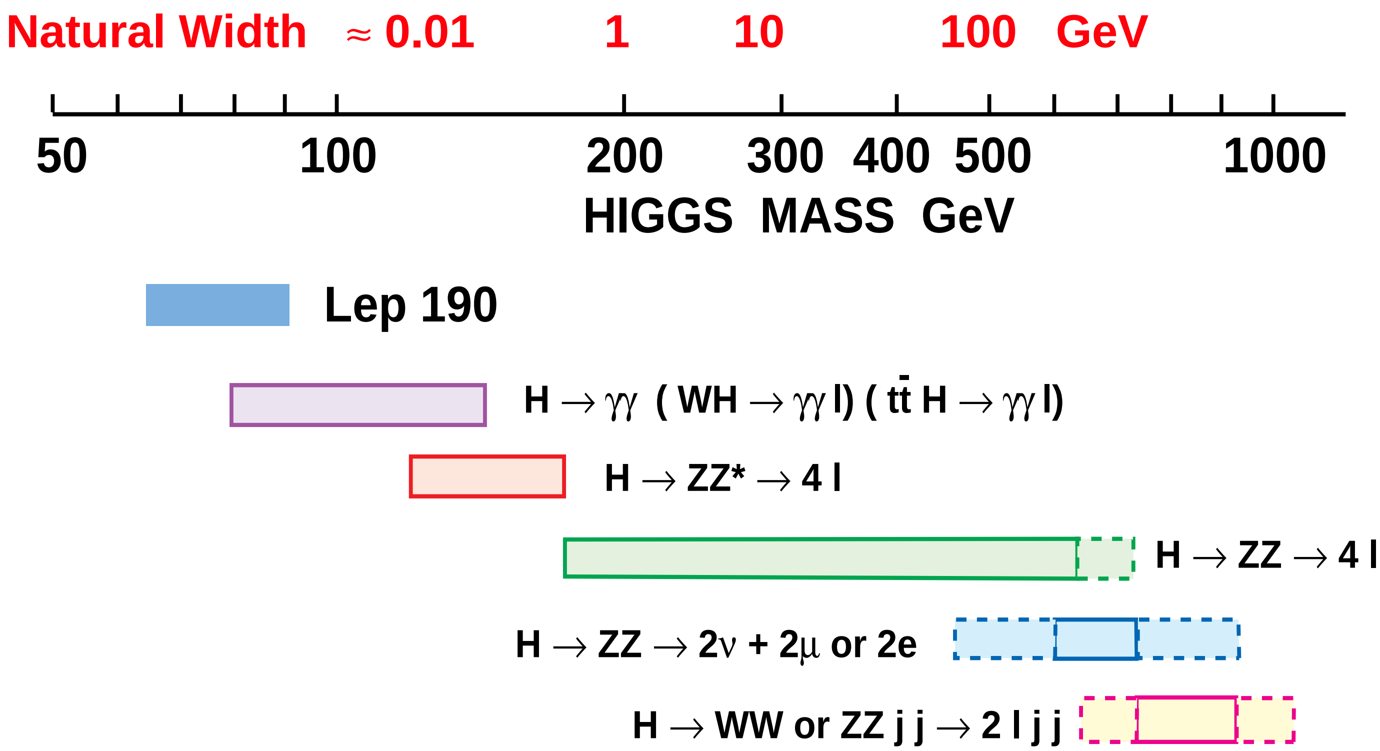

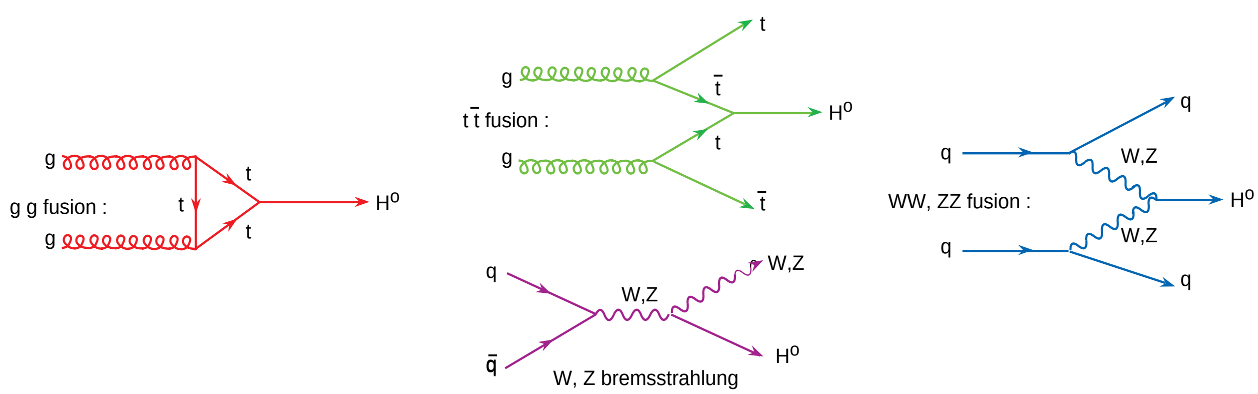

Reaction Rates

Colliders

Reaction rate, **R = σ L**

where σ is the cross-section (in units of cm^2) and L is the 'luminosity' (in units of $cm^{-2}s^{-1}$)

For two oppositely moving beams of relativistic particles

$$L = f.n\frac{N_1 N_2}{A}$$

where N_1,N_2 are no, of particles in each bunch,
n is the number of bunches in either beam around the ring,
A is the cross-sectional area of the beams assuming complete overlap, and f is the revolution frequency

e.g. at LHC, N_1,N_2 ≈ 10^{11} protons, n = 2835, transverse <radius> ≈ 20µm, f ≈ 10^4
giving L ≈ 10^{34} $cm^{-2}s^{-1}$.
Since σ ≈ 100 mb, R ≈ 10^9 interaction/s

Interaction of Radiation with Matter

Observables

Use the example of SM Higgs production at the LHC

Muons and electrons

SM, MSSM : H $\rightarrow$ Z Z* or ZZ $\rightarrow$ 4l or 2e 2μ

Z' $\rightarrow$ 2l and F-B asymmetry

Photons

SM, MSSM : H $\rightarrow$ 2γ

Jets

Jet tagging : high mass Higgs, strong WW scattering

Missing E_t

SM : H $\rightarrow$ ZZ $\rightarrow$ 2e 2ν, MSSM : gluinos, squarks

b-Jets

b-jet tagging: SUSY gluino and squark cascade decays, H$\rightarrow$bb, CP violation

Taus

MSSM : $H^+ \rightarrow \tau\nu$, A^0,h^0 and $H^0 \rightarrow \tau\tau$

$\pi^\pm$ and K^0

CP violation

Onion-like Structure of HEP Experiments

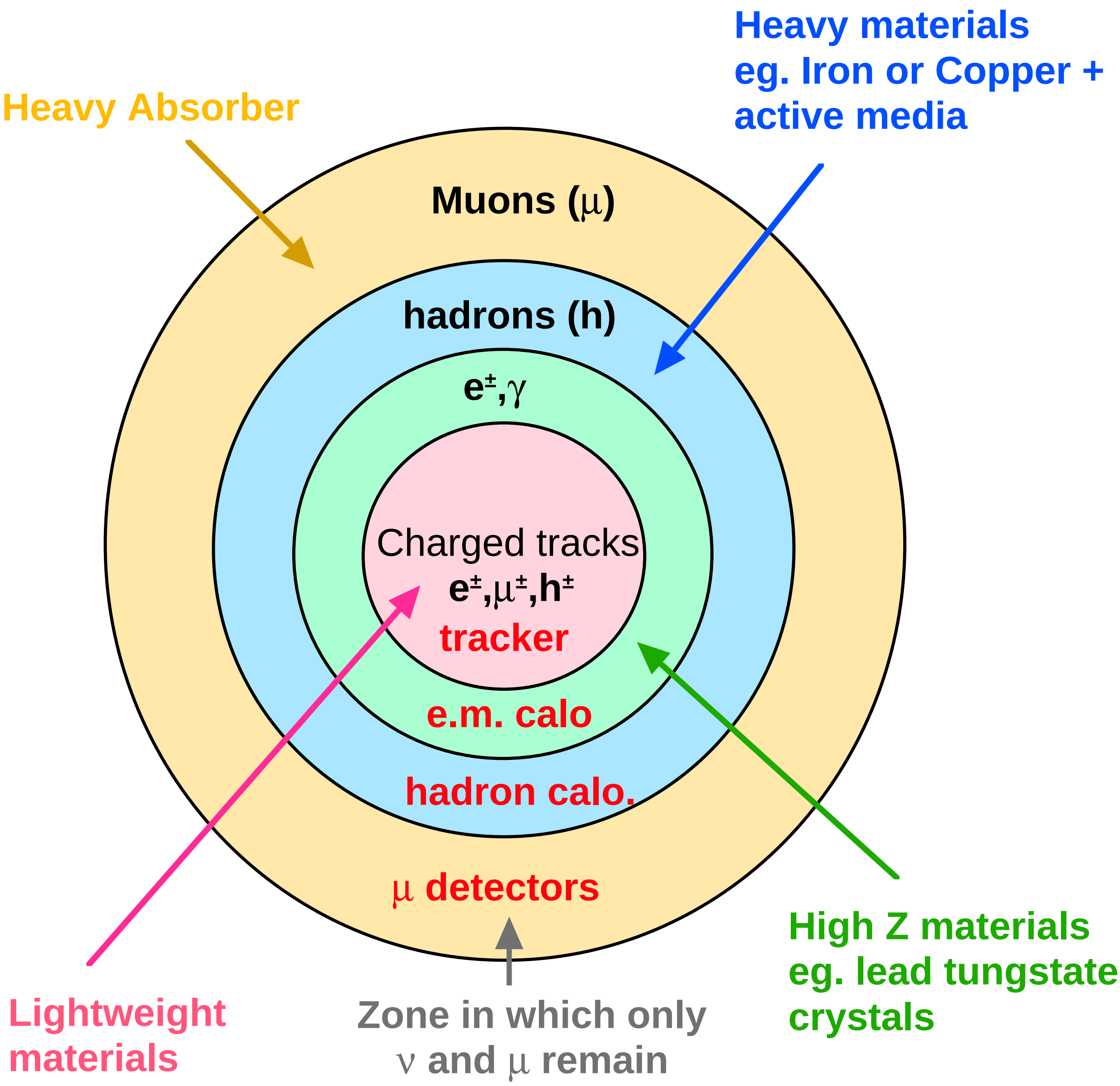

Each layer identifies and measures (or remeasures) the energy of particles unmeasured by the previous layer

Onion-like Structure of HEP Experiments

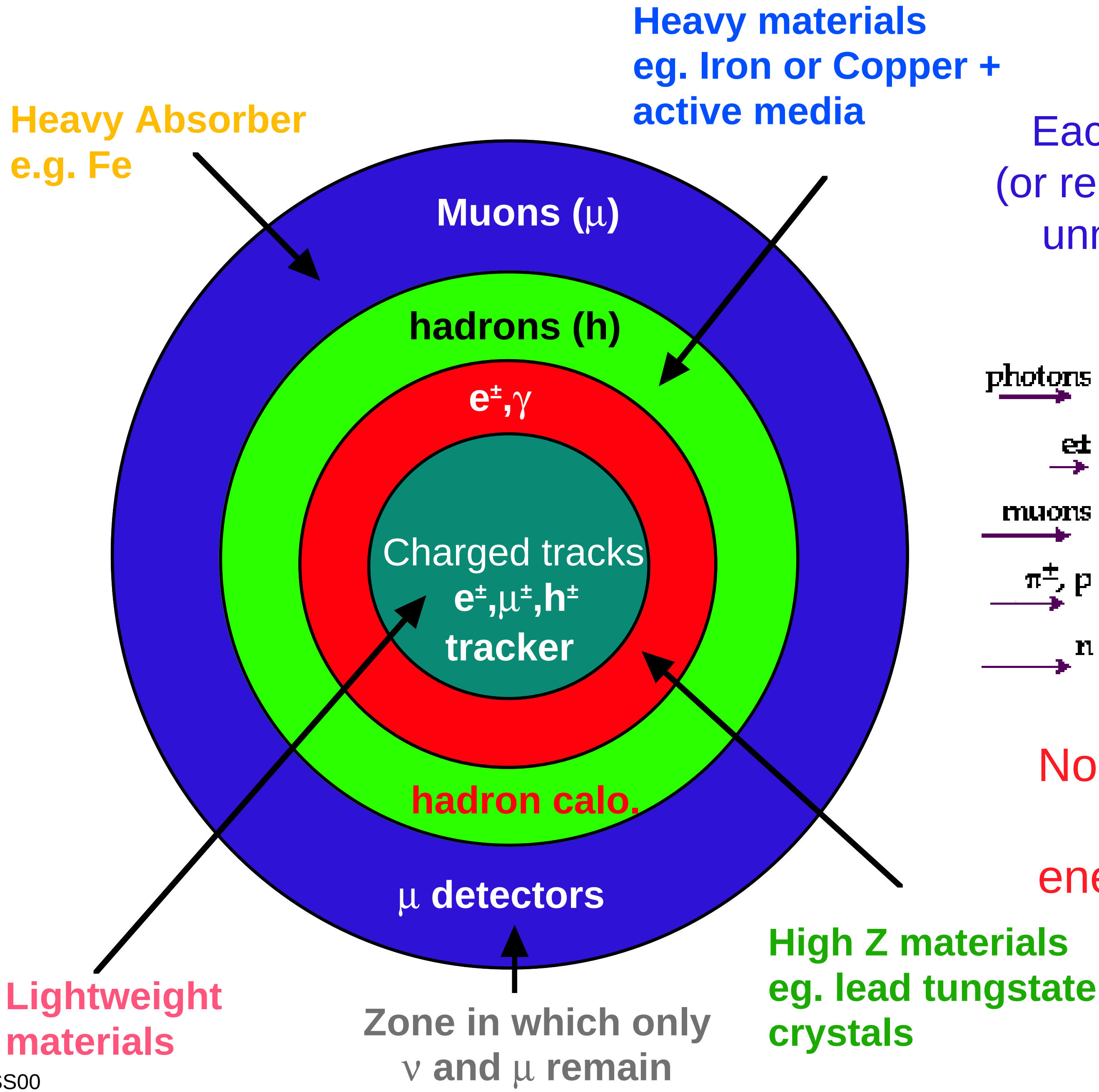

Each layer identifies and measures (or remeasures) the energy of particles unmeasured by the previous layer

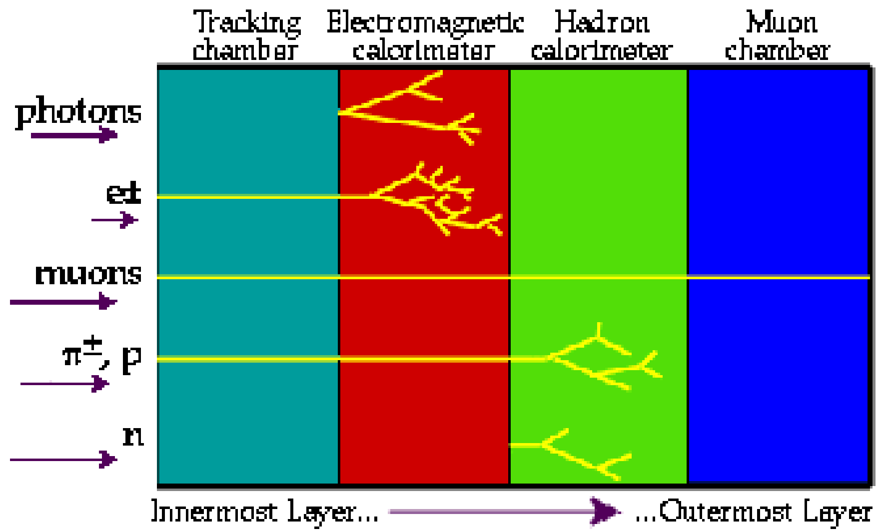

No single detector can determine identity and measure energies/momenta of all particles

Transverse View of CMS

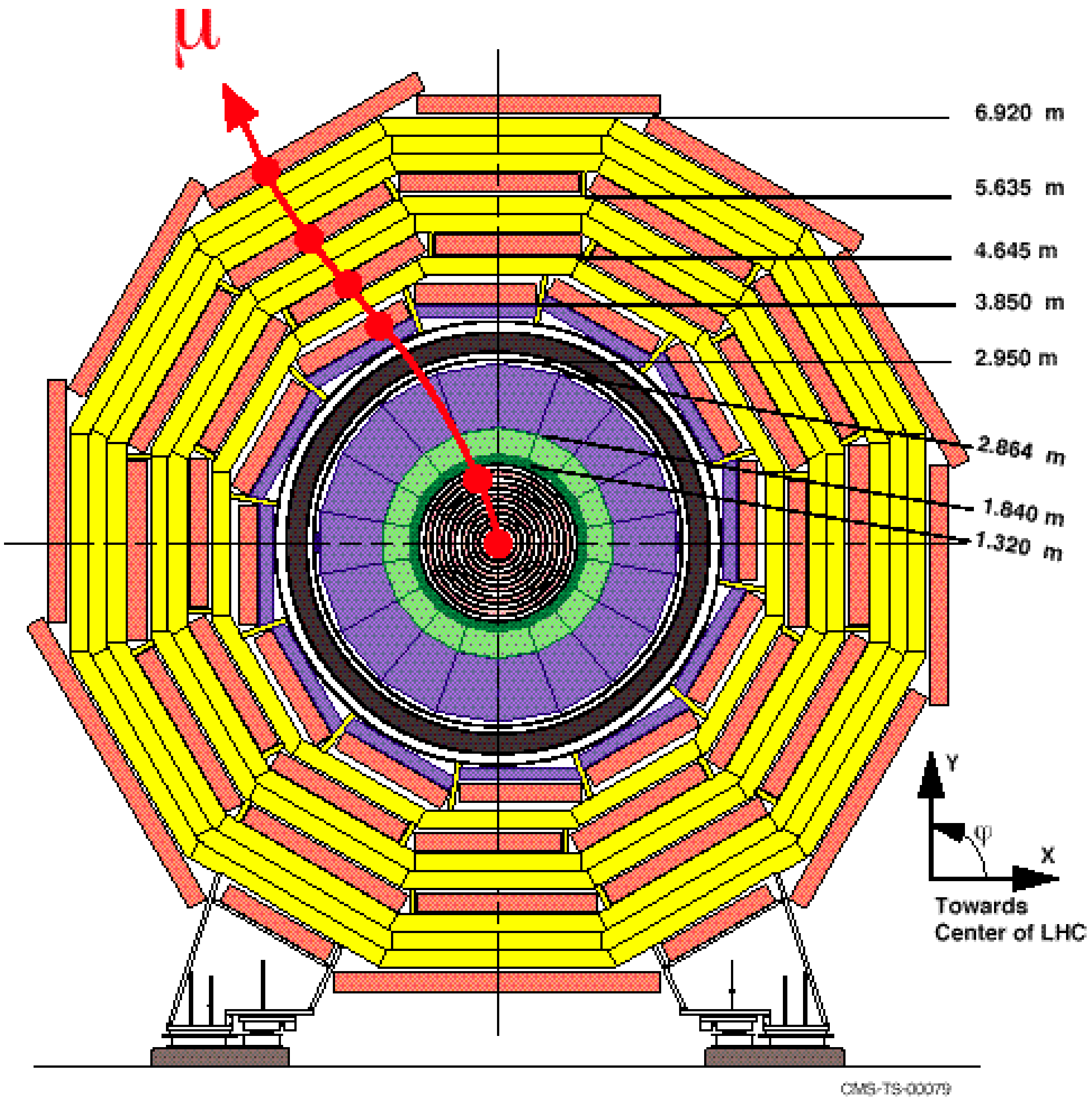

Transverse View

Experimental Measurements

Measurement of Momentum

- Charged particle in a magnetic field
- Multiple scattering

Measurement of Energy

- characteristics of e.m. cascades
- characteristics of hadronic cascades
- e.m energy resolution
  - homogeneous calorimeters
  - sampling calorimeters
- hadronic energy resolution
- energy measurement of jets

Identification of Particles

- electrons, photons
- pions / kaons / protons
- muons
- b-jets
- neutrinos (and jets)

Measurement of Momentum

- Charged Particle in a Magnetic Field
- Relative Momentum Resolution
- Multiple Scattering

Charged Particle in a Magnetic Field

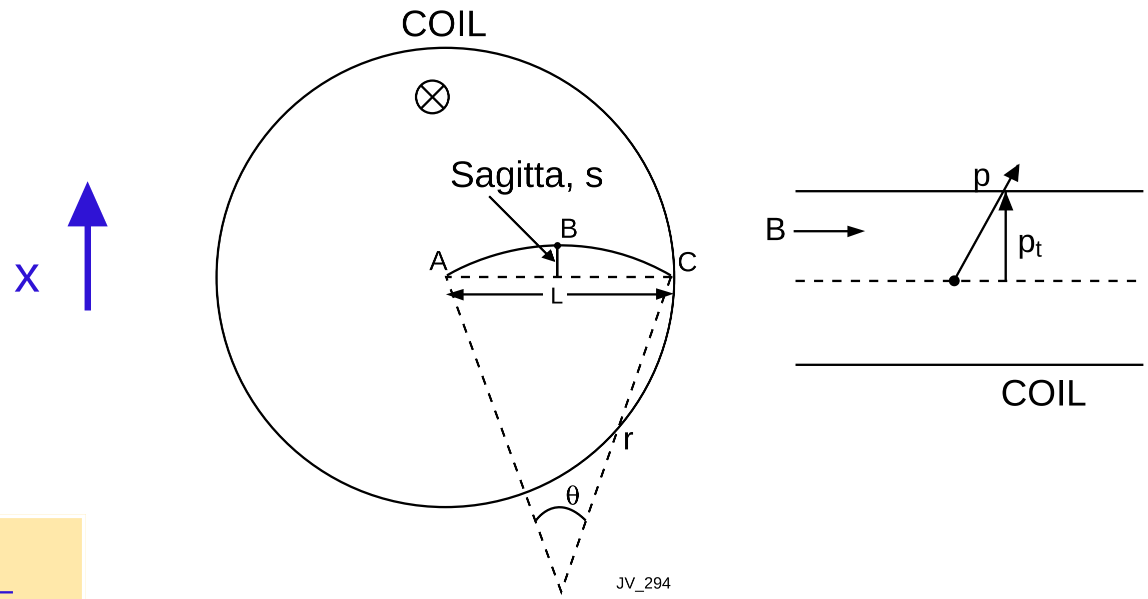

Radius of curvature

$$r = \frac{p_T}{0.3B}$$

If r>>L then

$$\sin\frac{\theta}{2} = \frac{L}{2r} \quad \Rightarrow \quad \frac{\theta}{2} \approx \frac{L}{2r} \quad \Rightarrow \quad \theta \approx \frac{0.3BL}{p_T}$$

Sagitta

$$s = r - r\cos(\theta/2)$$

$$\approx r\left[1 - \left(1 - \frac{1}{2}\frac{\theta^2}{4}\right)\right]$$

$$= \frac{r\theta^2}{8} \approx \frac{0.3BL^2}{8p_T}$$

e.g. s ≈ 3.75 cm
for p_T=1 GeV/c, L=1m and B=1T

Relative Momentum Resolution

$$\frac{dp_T}{p_T} = \frac{\sigma_s}{s} = \frac{\sqrt{(3/2)}\ \sigma_x}{s}$$

$$\frac{dp_T}{p_T} = \frac{\sqrt{3}}{2}\sigma_x \frac{8p_T}{0.3BL^2} \qquad (2)$$

Momentum resolution degrades linearly with increasing momentum, improves for higher field and the larger radial size of tracking cavity (quadratic in L)

Arrangement of measuring points

Uniform spacing

$$\frac{dp_T}{p_T} = \frac{\sigma_x p_T}{0.3BL^2}\sqrt{\frac{720}{N+4}}$$

e.g. $dp_T/p_T \approx 0.5\%$ for p_T=1 GeV/c, L=1m, B=1T, σ_x = 200 µm and N=10

BUT in a real tracker errors due to multiple scattering has to be included .

Multiple Scattering

- Electric field close to atomic nucleus may give large acceleration to a charged particle.
- For a heavy charged particle ($m \geq m_\mu$) results in a change of direction

Small impact parameter

single large angle scatter can occur (Rutherford Scattering)

$$\frac{d\sigma}{d\Omega} \propto \frac{1}{\sin^4 \theta/2}$$

Large impact parameter

- more probable

nuclear charge partly screened by atomic electrons, scattering angle is small

- thick material $\rightarrow$ large no. of random and small deflections - multiple Coulomb scattering

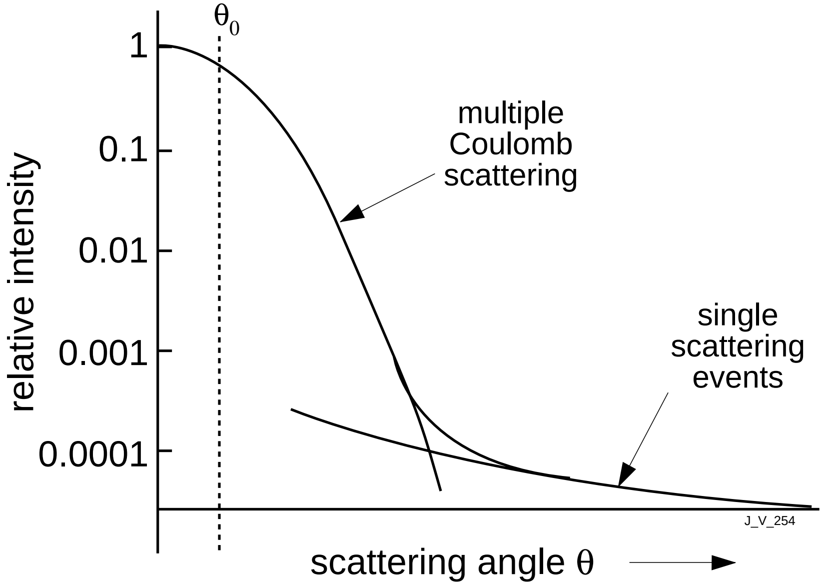

rms of scattering angle

$$\theta_0 \approx \frac{13.6\ MeV}{\beta pc} Z_{inc} \sqrt{\frac{L}{X_0}}$$

Multiple Scattering

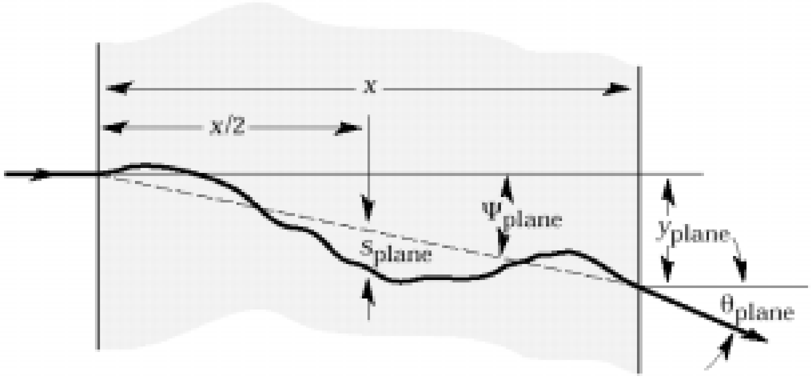

Figure 23.5: Quantities used to describe multiple Coulomb scattering. The particle is incident in the plane of the figure.

s_p - sagitta in plane

Apparent sagitta due to multiple scattering $s_p = \frac{L\theta_0}{4\sqrt{3}}$

If extrapolation error from one plane to next is larger than the point resolution then momentum resolution is degraded i.e. if

$$\theta_0 \; \Delta r \; > \; \sigma_x$$

Relative momentum resolution due to multiple scattering is

$$\therefore \; \frac{s_p}{s} = \left.\frac{dp}{p}\right|_{ms} \approx 0.05 \frac{1}{B\sqrt{LX_0}} \quad \text{since } s = \frac{0.3BL^2}{8p}$$

B in T, L and X_0 in m

i.e. Resolution is independent of p and α 1/B

e.g. argon gas, L = 1 m, B = 1 T

$$\left.\frac{dp}{p}\right|_{ms} \approx 0.5\%$$

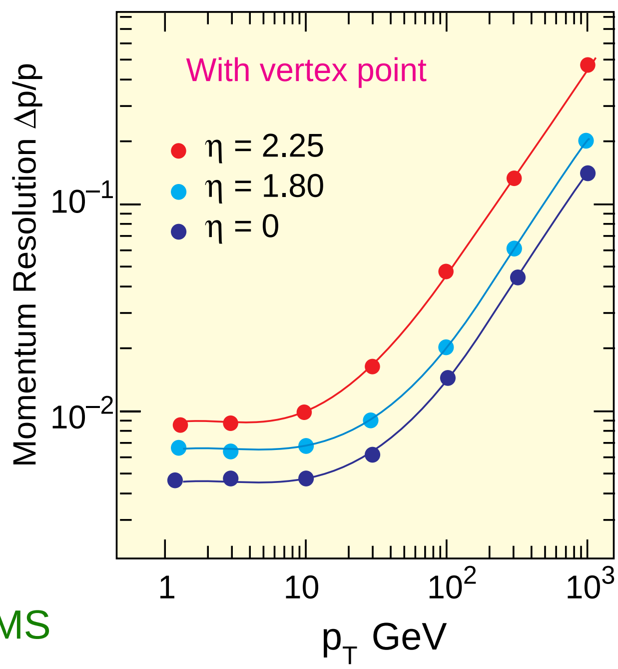

Estimated Momentum Resolution v/s p_T in CMS

Experimental Measurements

Measurement of Momentum

- Charged particle in a magnetic field
- Multiple scattering

Measurement of Energy

- characteristics of e.m. cascades
- characteristics of hadronic cascades
- e.m energy resolution
  - homogeneous calorimeters
  - sampling calorimeters
- hadronic energy resolution
- energy measurement of jets

Identification of Particles

- electrons, photons
- pions / kaons / protons
- muons
- b-jets
- neutrinos (and jets)

What is a Calorimeter

Neutral and charged particles incident on a block of material deposit their energy through destruction and creation processes

The deposited energy is rendered measurable by ionisation or excitation of the atoms of matter in the active medium.

The active medium can be the block itself (totally active or homogeneous calorimeter) or

a sandwich of dense absorber and light active planes (sampling calorimeters).

The measurable signal is usually linearly proportional to the incident energy.

An Electron Shower in a Bubble Chamber

Big European Bubble Chamber filled with Ne:H_2 = 70%:30%,
3T Field, L=3.5 m, X_0≈34 cm, 50 GeV incident electron

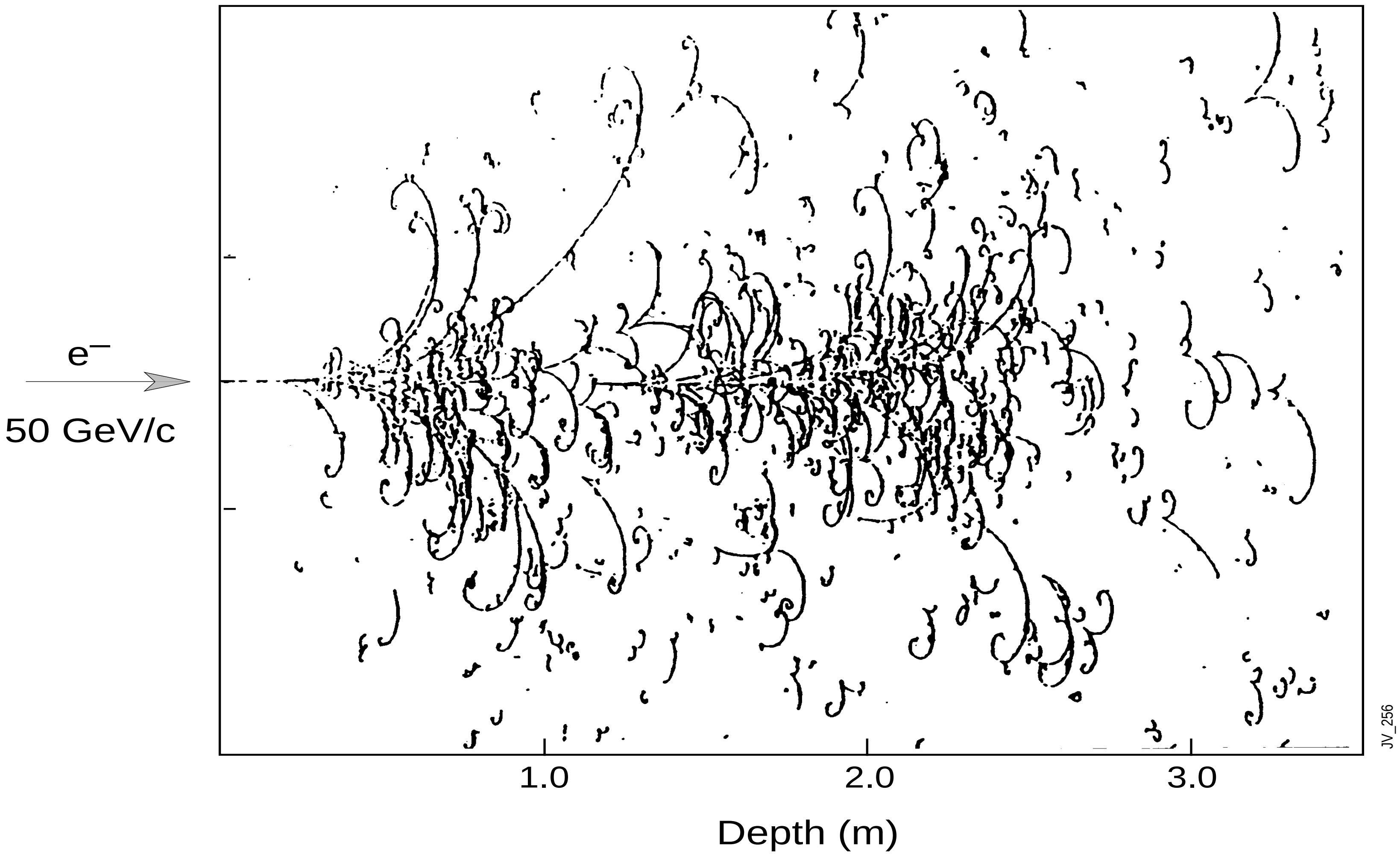

Hadron Showers in Copper

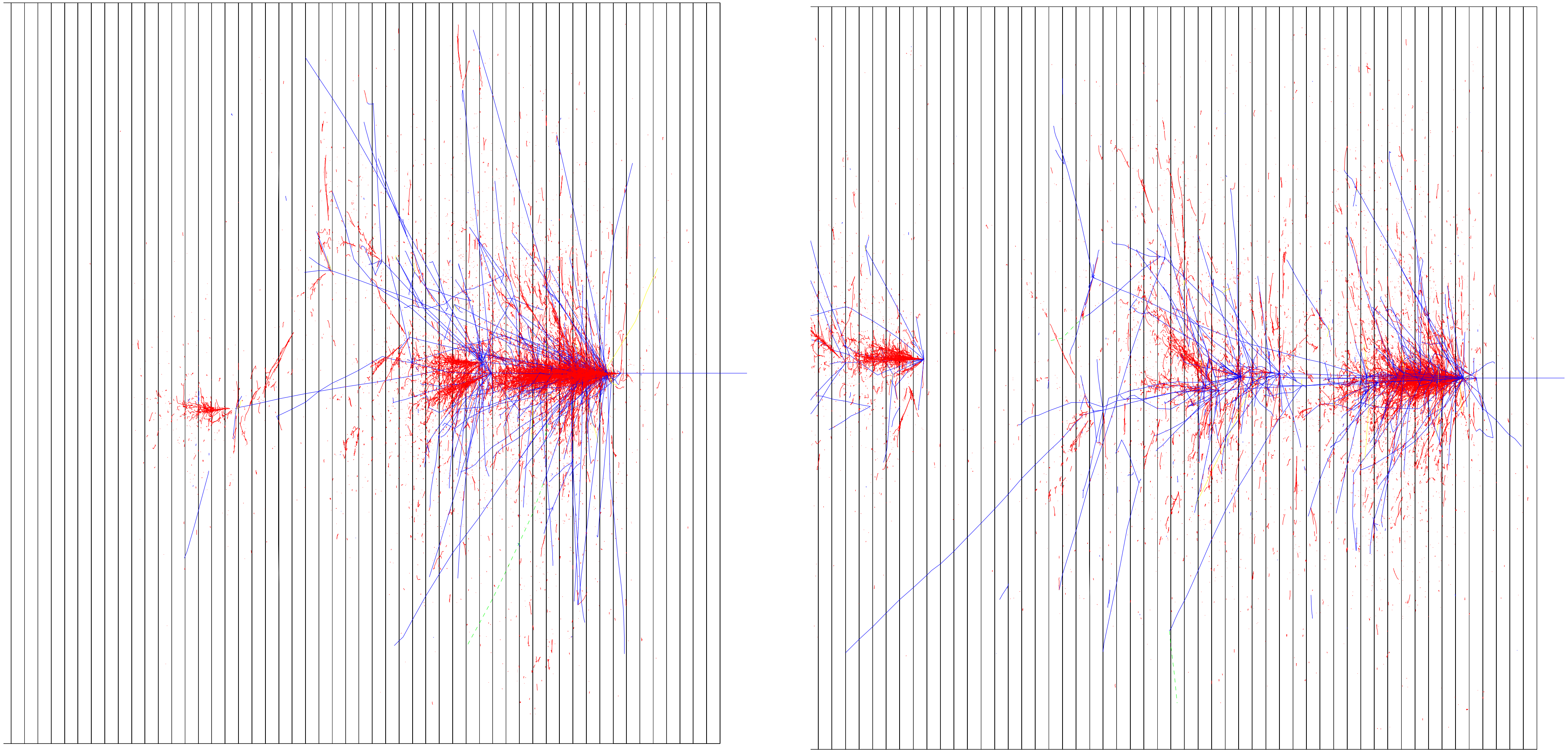

red - e.m. component
blue - charged hadrons

The Electromagnetic Cascade

- em Cascade - Longitudinal Development
- Radiation Length
- Critical Energy and Moliere Radius
- e.m. Cascade - Longitudinal Development
- e.m. Cascade - Longitudinal Development

em Cascade - Longitudinal Development

A high energy e or γ incident on a thick absorber initiates a cascade of $e^{\pm}$'s, γ's via bremstrahlung and pair production. With increasing depth the number of secondary particles increases while their mean energy decreases.

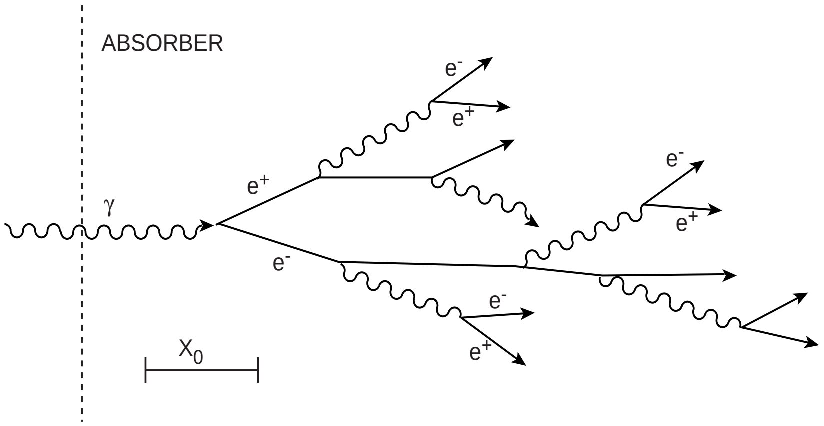

JV217.c

The multiplication continues until the energies fall below the critical energy ε. Further dissipation of energy is dominated by ionization or excitation rather than generation of more shower particles.

Consider a simplified model of shower development for e/γ of energy E. It is convenient to describe shower development using scaled variables

$$t = \frac{x}{X_0} \quad and \quad y = \frac{E}{\varepsilon}$$

.

In one radiation length,1 X_0, an electron loses about 2/3rd of its energy and a high energy photon has a probability of 7/9 of pair conversion

Naively take X_0 as a generation length.

Assume that after each generation the number of particles increases by a factor of 2.

After t generations,

$$energy \ \ of \ \ particles \quad e(t) = \frac{E}{2^t}$$

$$number \ \ of \ \ particles \quad n(t) = 2^t$$

Radiation Length

In dealing with electrons and photons at high energies striking blocks of materials (e.g. calorimeters) it is convenient to measure the depth and radial extent of the resulting cascades in terms of :
Radiation Length (X_0) and Moliére Radius (R_M)

Consider the bremstrahlung process

A free electron cannot radiate a photon. In classical electro-magnetism a charged particle emits radiation when it is subjected to acceleration or deceleration. The acceleration/deceleration is greater if the particle is lighter.

$$-\frac{dE}{dx}\Big|_{rad} = \left[4n\,\frac{Z^2\alpha^3(\hbar c)^2}{m_e^2c^4}\,\ln\frac{183}{Z^{1/3}}\right] E$$

$$-\frac{dE}{dx} \propto E \;\Rightarrow\; \frac{dE}{E} = -\,A\;dx \;\Rightarrow\; E = E_0\;e^{-Ax}$$

where A is a constant.

Thus, on average, the distance over which the electron loses all but 1/e of its energy, called the radiation length X_0 (=1/A), is

$$X_0 = \left[4n\,\frac{Z^2\alpha^3(\hbar c)^2}{m_e^2c^4}\,\ln\frac{183}{Z^{1/3}}\right]^{-1}$$

e.g. for Pb, Z = 82, n = 3.3 10^{28} /m^3
X_0 ~ 5.3 mm which is close to 5.6 mm in PDG

$$\frac{dE}{dx} = -\,\frac{E}{X_0} \quad \text{and} \quad X_0 \approx \frac{180A}{Z^2}\;g.cm^{-2}$$

Critical Energy and Moliere Radius

Critical Energy, ε

Defined to be the energy at which the energy loss due to ionisation* (at its minimum i.e. β≈0.96) and radiation are equal (over many trials)

$$i.e.\quad \frac{(dE/dx)_{rad}}{(dE/dx)_{ion}} = 1$$

$$\Rightarrow \quad \varepsilon = \frac{560}{Z} \quad (E \ \ in \ \ MeV)$$

PDG gives ε =610/(Z+1.24)

Fractional Energy Loss by Electrons

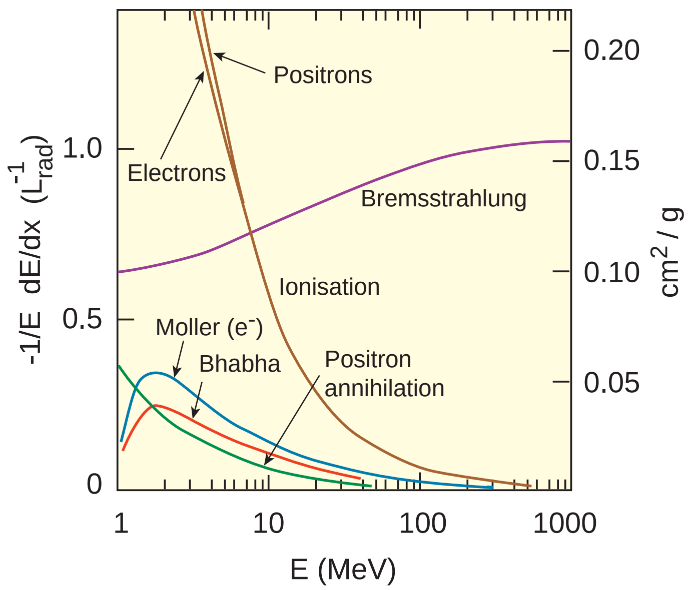

Moliere Radius, R_M

This gives the average lateral deflection of critical energy electrons after traversing 1 X_0 and can be parameterised as :

$$R_M = \frac{X_0 E_s}{\varepsilon} = \frac{21_{MeV} X_0}{\varepsilon} \approx \frac{7A}{Z} \quad g.cm^{-2}$$

	Z	ρ	I/Z	(1/ρ) dT/dx	X_0	ε	λint
		$g.cm^{-3}$	eV	$MeV/g{\cdot}cm^{-2}$	cm	MeV	cm
C	6	2.2	12.3	1.85	~19	103	38.1
Al	13	2.7	12.3	1.63	8.9	47	39.4
Fe	26	7.87	10.7	1.49	1.76	24	16.8
Pb	82	11.35	10.0	1.14	0.56	6.9	15.1
U	92	18.7	9.56	1.10	0.32	6.2	10.5

---

* $$-\frac{dE}{dx}\Big|_{ion} = N_A \frac{Z}{A} \frac{4\pi\alpha^2(\hbar c)^2}{m_e c^2} \frac{Z_i^2}{\beta^2} \left[\ln \frac{2m_e c^2 \gamma^2 \beta^2}{I} - \beta^2 - \frac{\delta}{2} \right]$$

e.m. Cascade - Longitudinal Development

At shower max. where e ~ ε

$$no.\ of\ \ particles\quad n(t_{max}) \approx \frac{E}{\varepsilon} = y$$

$$and\qquad t_{max} \approx \ln\frac{E}{\varepsilon} = \ln\ y$$

After shower maximum
Critical energy electrons do not travel far (~ 1 X_0) and the remaining energy of the cascade is carried forward by photons giving the typical exponential falloff of energy deposition caused by attenuation of γ's .

Longitudinal development of 10 GeV showers in Al, Fe and Pb.
It can be noted that the shower max. is deeper for higher Z materials because multiplication continues down to lower energies. The slower decay beyond the max. is due to the lower energies at which electrons can still radiate. Both of the above are due to lower ε for higher Z materials.

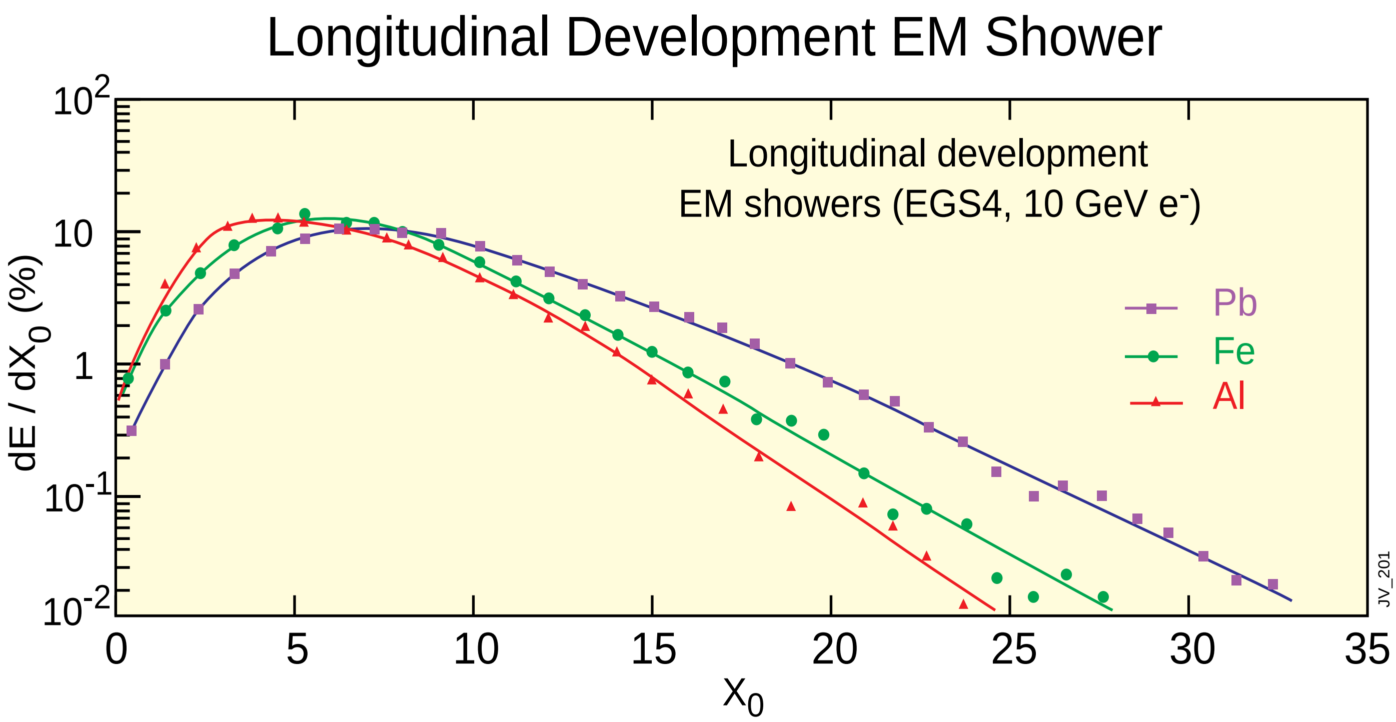

Need a depth of > 25 X_0 to contain high energy em showers

e.m. Cascade - Longitudinal Development

Mean longitudinal profile of energy deposition is given by

$$\frac{dE}{dt} = Eb\frac{(bt)^{a-1}e^{-bt}}{\Gamma(a)}$$

The maximum occurs at t_{max} = (a-1) / b

Fits to t_{max} give t_{max} = ln y - 0.5 for e-induced cascades

and t_{max} = ln y + 0.5 for γ-induced cascades

Coefficient a can be found using t_{max} and assuming b ~ 0.5.

The photon showers are longer since the energy deposition only starts after the first pair conversion has taken place. The mean free path length for pair conversion of a high energy photon is

$$X_\gamma = \frac{9}{7} X_0 \quad i.e.\ \text{Prob. of conversion is } e^{-\frac{7}{9}X_0}$$

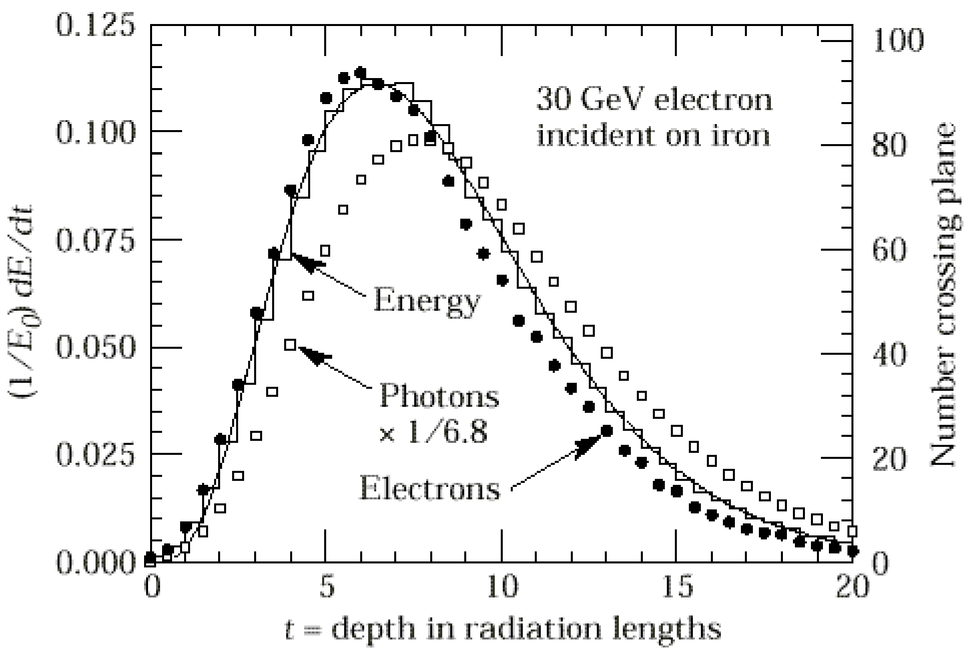

NB. The gamma distribution is flat near the origin while the EGS4 cascade (or a real cascade) increases more rapidly. As a result the above formulas fails badly for about the first two X_0.

e.m. Cascade - Lateral Development

The lateral spread of an e.m. shower is determined by multiple scattering of $e^{\pm}$ away from the shower axis and by minimally attenuated photons

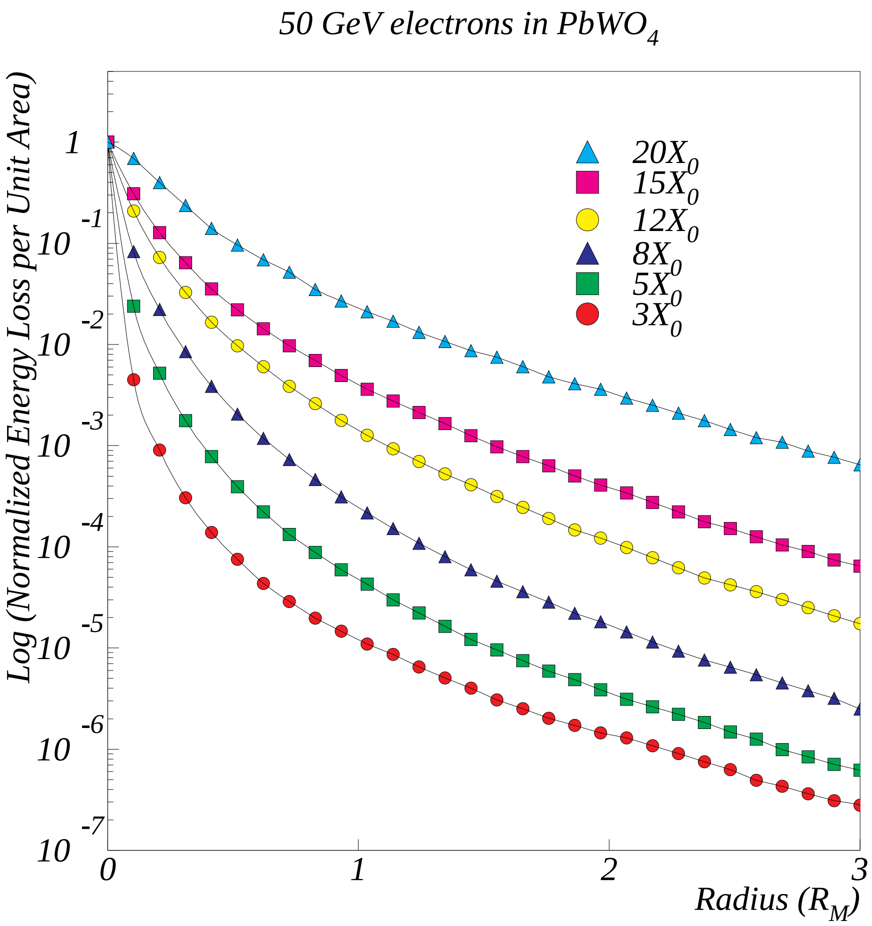

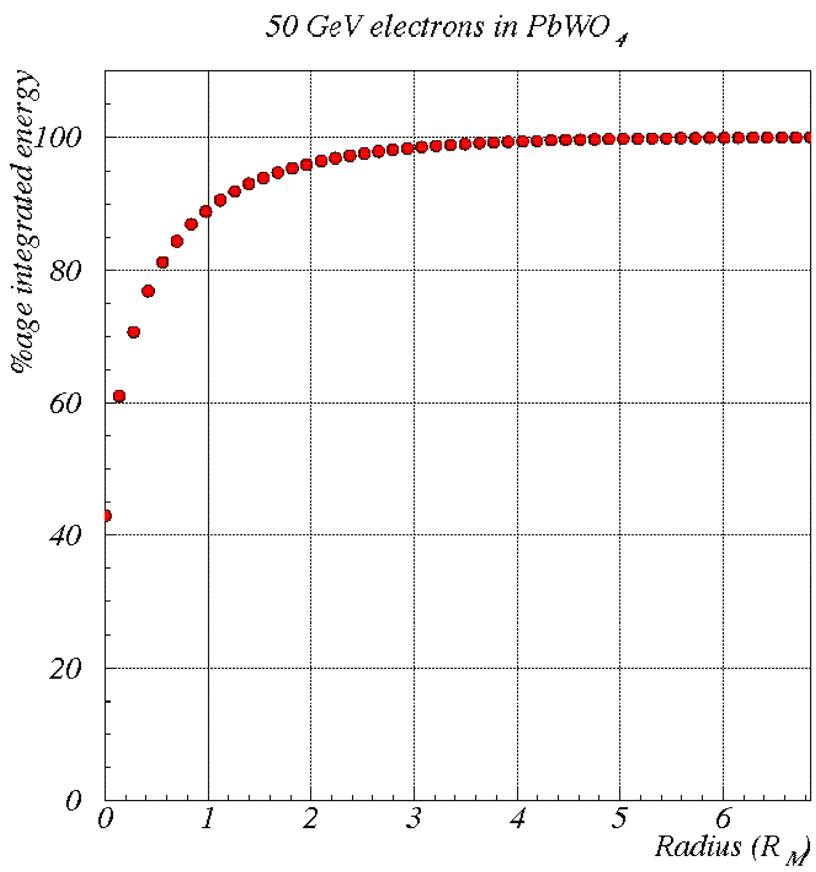

An infinite cylinder with a radius of $2R_M$ contains ≈ 95% of the shower energy.

The Hadronic Cascade

- Hadronic Cascade

  Longitudinal Development

Hadronic Cascade Longitudinal Development

- A situation analagous to that for em showers exists. The interaction responsible for shower development is the strong one instead of Coulomb.
- A high energy hadron striking an absorber interacts with a nucleus leading to multi-particle production consisting of mesons (e.g. $\pi^{\pm}$, π^0, K etc.). The hadrons in turn interact with further nuclei leading to a growth in the number of secondary particles.
- Nuclei may breakup leading to spallation neutrons.
- Multiplication continues until the pion production threshold (E_{th}) is reached.

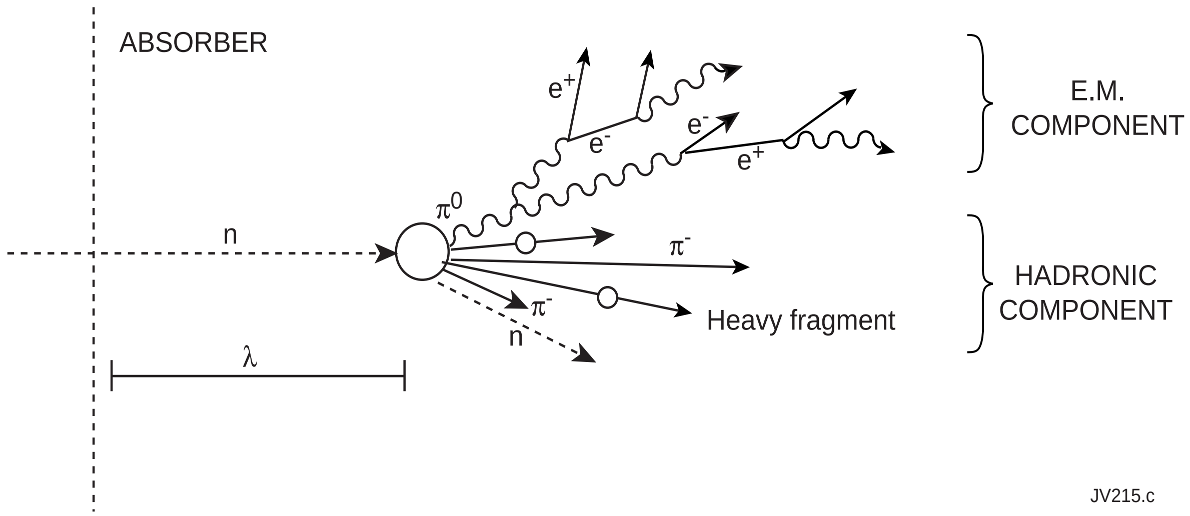

Simple model treats interaction on a black disc of rafius R

$$\sigma_{int} = \pi R^2 \; \alpha \; A^{2/3}$$

Infact $\sigma_{inel} = \sigma_0 \; A^{0.7}$ where σ_0 = 35 mb

the nuclear interaction length $\lambda_{int} = \dfrac{A}{N_A \sigma_{int}} \propto A^{1/3}$

Total multiplicity, $n \; \alpha \; \ln E$

c.m. energy goes into KE of secondaries rather than straight particle production which would imply $n \; \alpha \; \sqrt{s}$

The secondaries are produced with a limited transverse momentum

$$\langle p_T \rangle \approx 300\text{-}400 \text{ MeV}$$

Hadr. Cascade -Intrinsic Fluctuation

- Hadron showers contain em component due to π^0, η.
- Size of the em component (F_0) is essentially determined by the 1st interaction.
- Considerable event to event fluctuation in F_0.

On average 1/3 of mesons ($\pi^0/\pi^+ + \pi^- + \pi^0$) produced in the first interaction will be π^0's.

The 2nd generation $\pi^\pm$,'s also produce π^0's if sufficiently energetic.

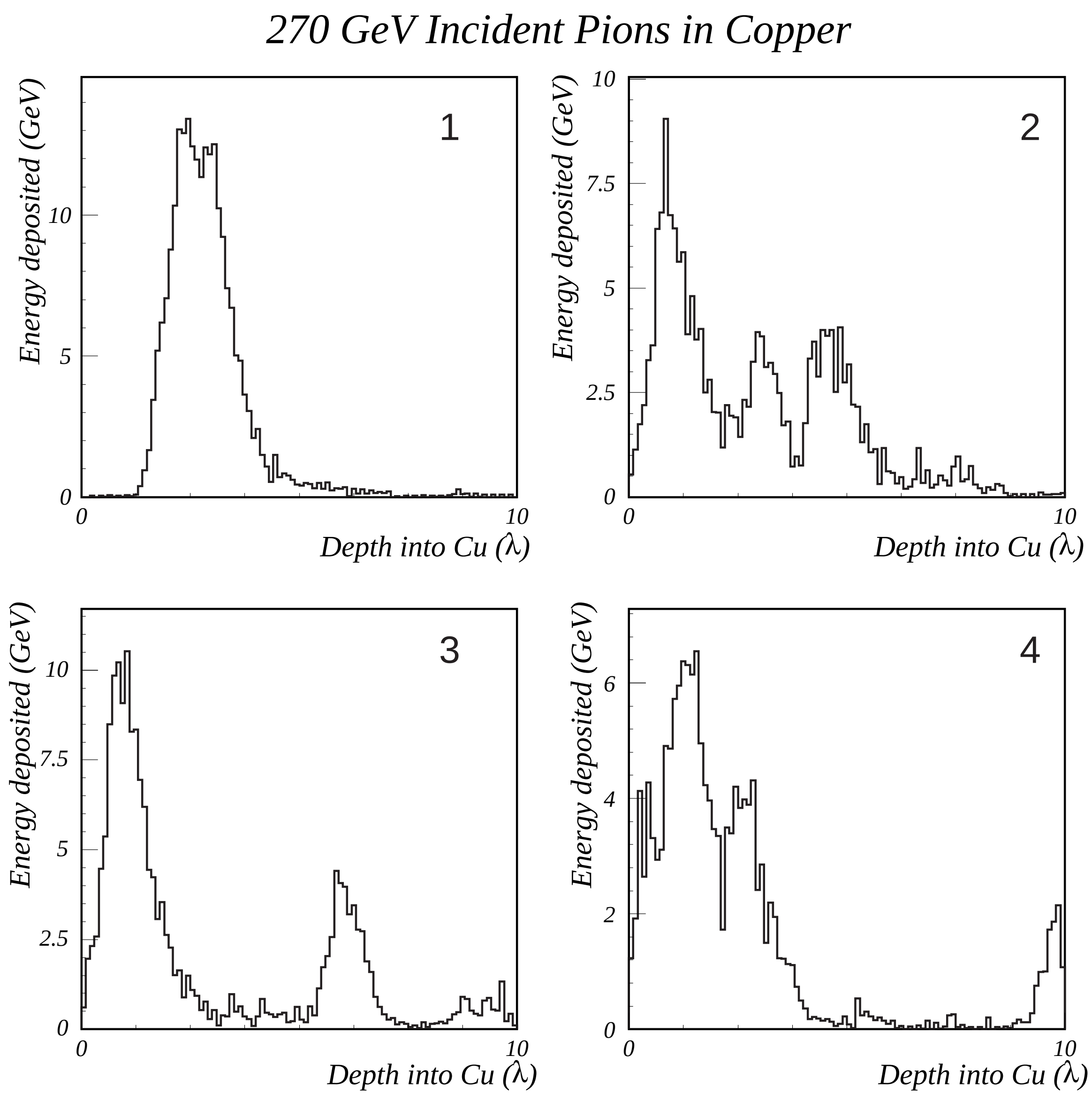

Hadronic Cascade Longitudinal Development

- It is convenient to describe the hadron shower development using scaled variables

  $\nu = x / \lambda$ and $E_{th} \sim 2\, m_\pi = 0.28$ GeV

λ, the nuclear interaction length, is the scale appropriate for longitudinal and lateral development of hadronic showers

  $\lambda \sim 35\, A^{1/3}$ g cm^{-2}

Consider a simplified model of hadronic shower development. The generation length can be taken to be λ. Assume that for each generation <n> secondaries/primary are produced. The cascade continues until no more pions can be produced.

in generation ν $\quad e(\nu) = \dfrac{E}{\langle n \rangle^{\nu}}$

at shower max $\quad e(\nu_{\max}) = E_{th} \quad \therefore \; E_{th} = \dfrac{E}{\langle n \rangle^{\nu_{\max}}}$

$$n^{\nu_{\max}} = \frac{E}{E_{th}} \Rightarrow \nu_{\max} = \ln(E / E_{th}) / \ln\langle n \rangle$$

- Mean Longitudinal energy deposition profiles are characterized by a sharp peak near the 1st interaction point (from π^0's produced in the 1st interaction) followed by a more gradual falloff with a characteristic scale of λ. The maximum, as measured from the front, occurs at

  $x / \lambda = \nu_{max} \sim 0.2 \ln E + 0.7$ (E in GeV)

Total "path length" for hadronic showers is shorter by E_{th}/ε

hence $\quad \dfrac{a^{\pi}_{\text{intr}}}{a^{em}_{\text{intr}}} \approx \sqrt{\dfrac{E_{th}}{\varepsilon}} \approx 6$

Hadronic Cascade - Profiles

Hadron shower profiles for single $\pi^{\pm}$

Longitudinal

- sharp peak from π^0's produced in the 1st interaction
- followed by a more gradual falloff with a characteristic scale of λ.

WA78 : 5.4λ of 10mm U / 5mm Scint + 8λ of 25mm Fe / 5mm Scint

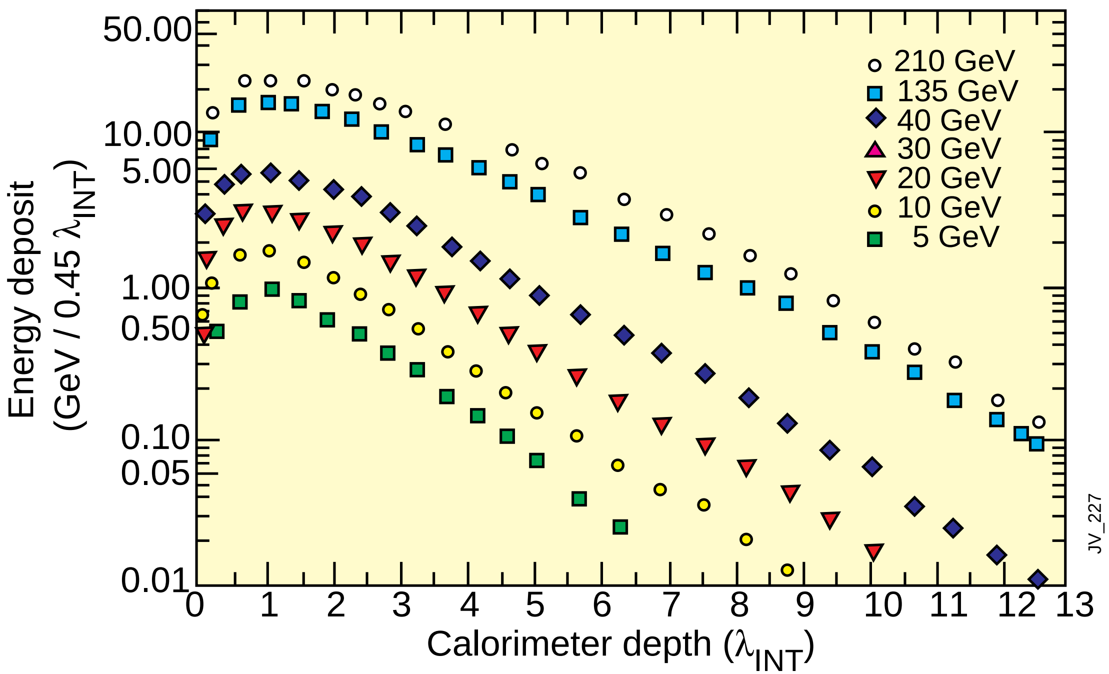

Approx. 10 λ required to contain 99% of the energy of $\approx$ 200 GeV pions

Lateral

- Secondaries produced with $\langle p_t \rangle$ ~ 300 MeV
-approx. energy lost in $\approx$ 1 λ in most materials.
- Characteristic transverse scale is $r_\pi \approx \lambda$.
- Pronounced core, caused by the π^0 component, .

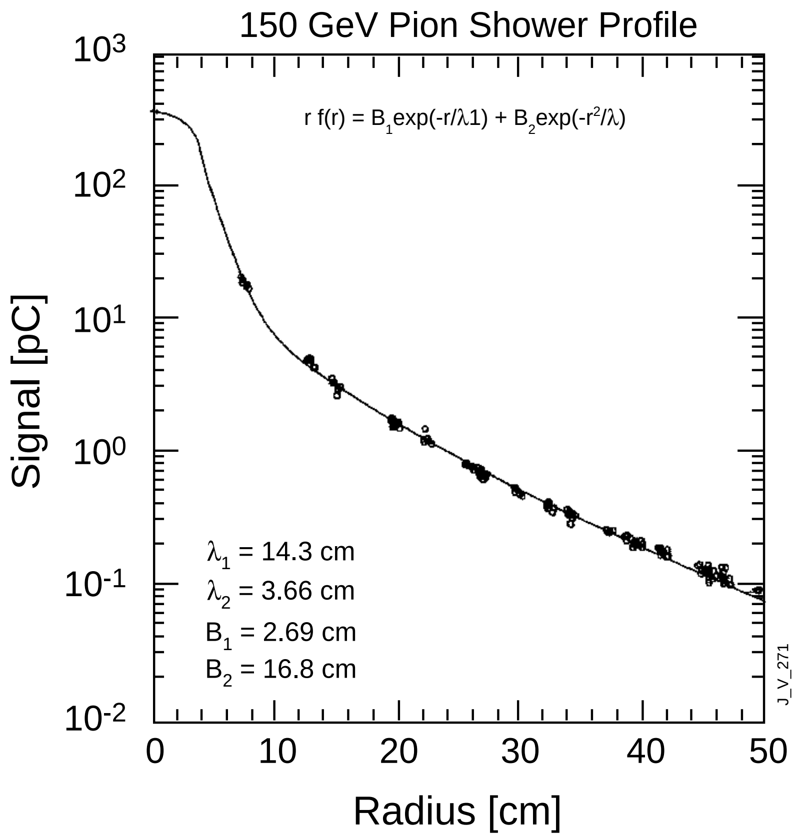

Transverse radius for 95% containment is $R_{0.95} \approx 1\ \lambda$

Energy Resolution

The energy resolution of calorimeters is usually parameterised as:

$$\frac{\sigma}{E} = \frac{a}{\sqrt{E}} \otimes \frac{b}{E} \otimes c$$

symbol ⊕ implies the quadratic sum of the three terms on rhs

'stochastic or sampling' term (coeff. a) accounts for
- the statistical fluctuation in the number of primary and independent signal generating processes, or any further process that limits this number e.g. conversion of light into photo-electrons by a photodevice

'noise' term (coeff. b) includes
- the energy equivalent of the electronics noise and
- pileup - the fluctuation of energy carried by particles, other than the one(s) of interest, entering the measurement area

'constant' term (coeff. c) accounts for
- non-uniformity of signal generation and/or collection
- the cell to cell inter-calibration error
- the fluctuation in the amount of energy deposited in dead materials in front or inside the calorimeter
- the fluctuation in the amount of energy leakage from the front, the rear and the sides of the volume used for energy measurement.
- for hadronic showers contribution from the fluctuation in the e.m. component (dependent logarithmically on energy)

There may be a correlation with the 'a' term

- The tolerable size of these three terms depends on the energy range involved in the experiment.
- Such parametrisations allow the identification of the causes of resolution degradation.
- Quadratic summation implies independent contributions which may not be the case.

em. Energy Resolution

- Intrinsic e.m. Energy Resolution
- Energy Resolution of e.m. Sampling Calorimeters
- Energy Resolution of e.m. Sampling Calorimeters
- Longitudinal Non-Uniformity
- Inter-Calibration Error

Intrinsic e.m. Energy Resolution

- It is instructive to look at homogeneous calorimeters in which all the energy is deposited in the active medium
- If shower is fully contained then the only fluctuation is one due to the produced no. of ion-pairs or photons, n.
- If W is mean energy required to produce an ion pair (or a photon) then

$$n = \frac{E}{W} \quad \text{and} \quad \frac{\sigma}{E} = \frac{\sqrt{n}}{n} = \sqrt{\frac{W}{E}}$$

Fluctuation is reduced as total energy deposited does not fluctuate

Improvement in resolutuion is characterised by the Fano factor, F,

$$\frac{\sigma}{E} = \sqrt{\frac{FW}{E}}$$

F is a function of all processes that lead to energy transfer in the detector including reactions that do not lead to ionisation e.g. phonon excitations

In Ge (77°K) measure σ = 178 eV for γ of 100 keV
Deduce $\sigma = \sqrt{(FWE)} = \sqrt{(0.13 \cdot 2.96 \cdot 10^5)} \approx 195$ eV

NB : Without Fano factor σ = 540 eV !
The difference between the band gap energy and the W-value goes into production of phonons.

Scintillating crystal/ homogeneous noble liquid calormeters can give excellent energy resolution at high energies

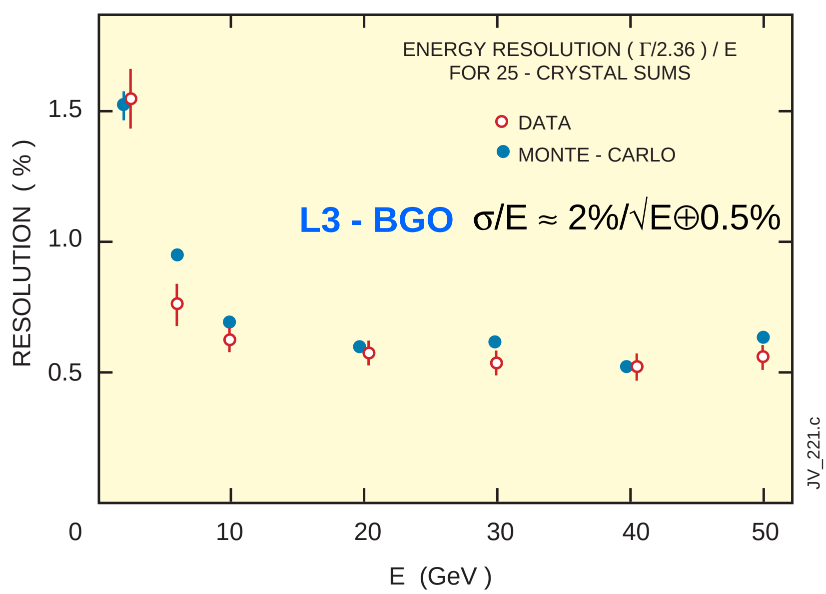

Energy Resolution of e.m. Sampling Calorimeters

• Shower develops in a sandwich of high-Z absorber and low-Z active layers
• only a fraction of the shower energy is dissipated in the active medium,
• the energy resolution is dominated by the fluctuation in the energy deposited in the active layers

Consider a picture of shower development where

$$\left.\frac{dE}{dx}\right|_{act} << \left.\frac{dE}{dx}\right|_{abs}$$

(act-active, abs-absorber)
then no. of charged particles 'crossing' an active layer is

$$n = \frac{E}{\Delta E_{abs}}$$

where ΔE_{abs} is energy lost by a m.i.p. in the absorber layer with a thickness t_{abs} measured in units of X_0:

$$\Delta E_{abs} = t_{abs}\frac{dE}{dx}$$

$$\frac{\sigma}{E} = \frac{\sqrt{n}}{n} = \frac{\sqrt{\Delta E_{abs}}}{\sqrt{E}}$$

$$\therefore \frac{\sigma}{E} \propto \frac{\sqrt{t_{abs}}}{\sqrt{E}}$$

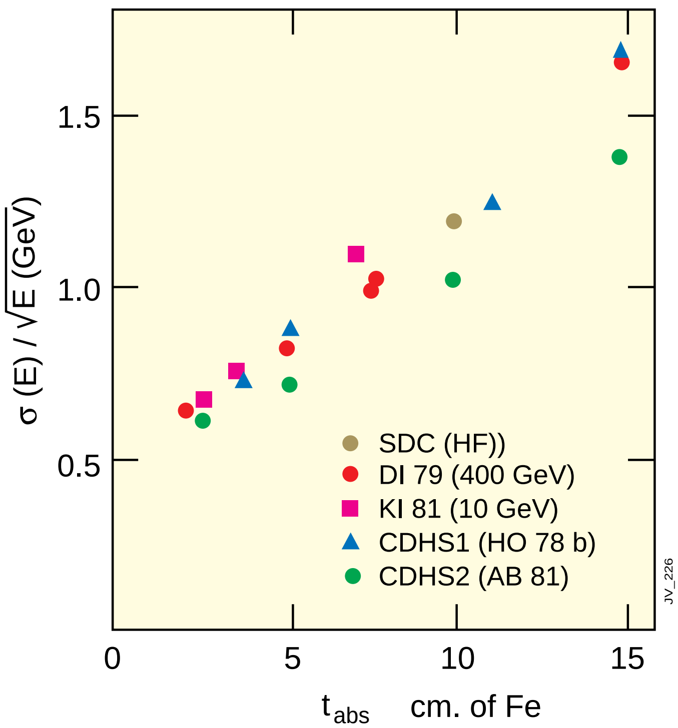

For fixed active layer thickness the energy resolution should improve with decreasing absorber thickness

e.m. Showers in Sampling Calorimeter

Two cloud-chamber photographs of e.m. showers developing in lead plates (thicknesses from top down 1.1, 1.1, 0.13 X0) exposed to cosmic radiation at sea-level. There are two views in each photo.

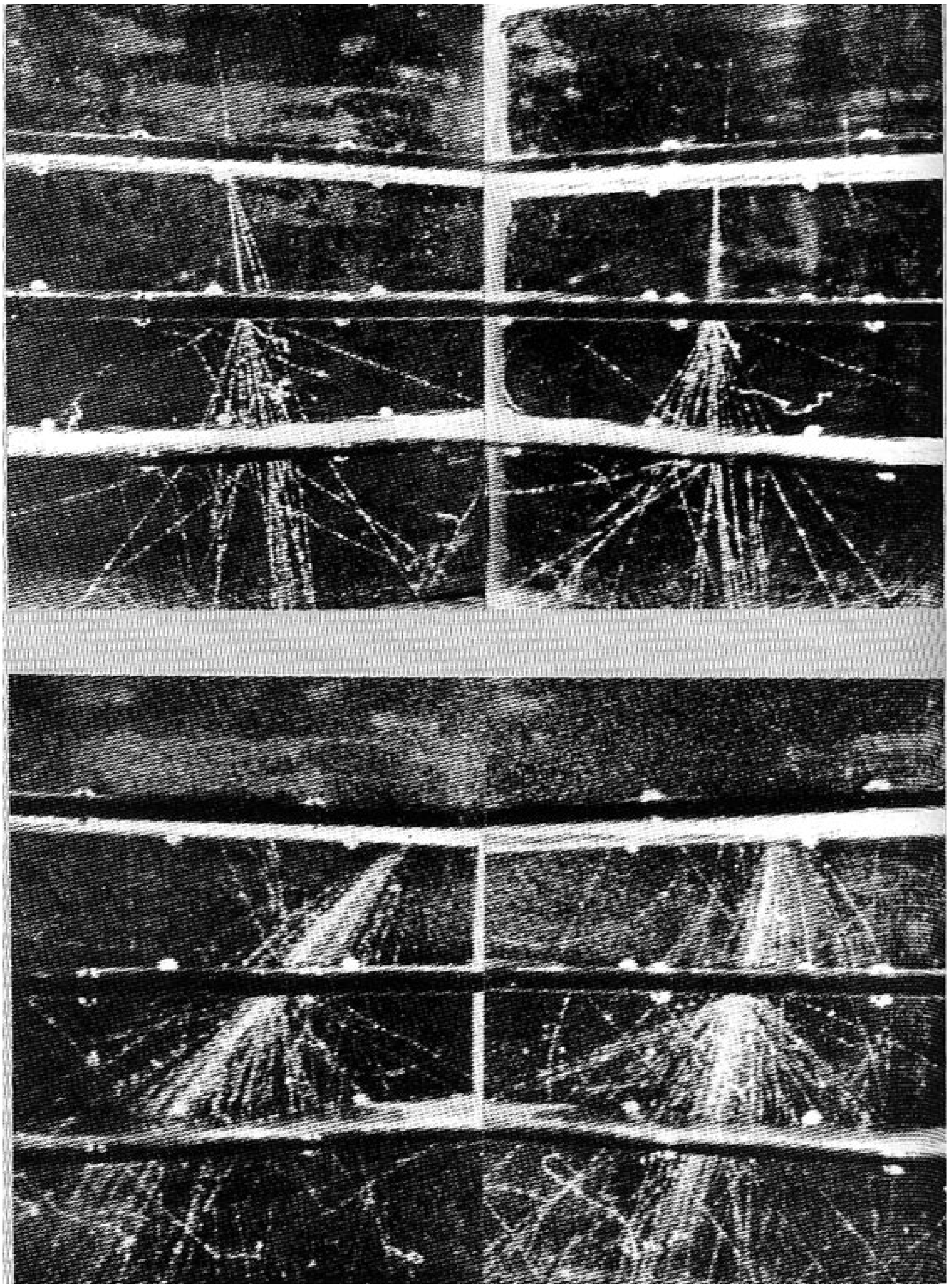

Energy Resolution of e.m. Sampling Calorimeters

If active layers become too thin (e.g. gas calorimeters) then energy resolution is degraded through path length and in gases through Landau fluctuations in addition.

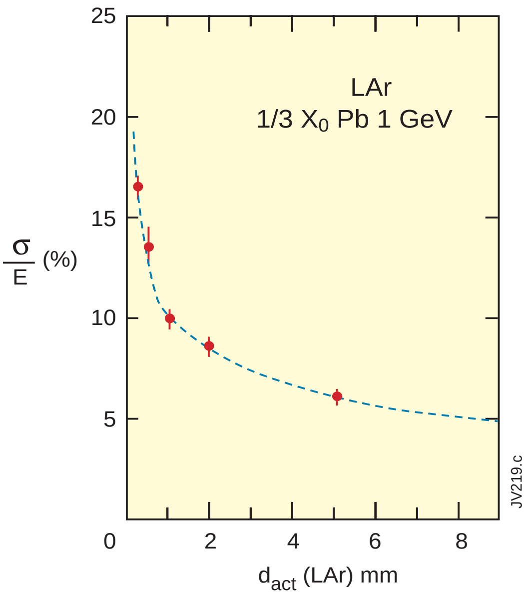

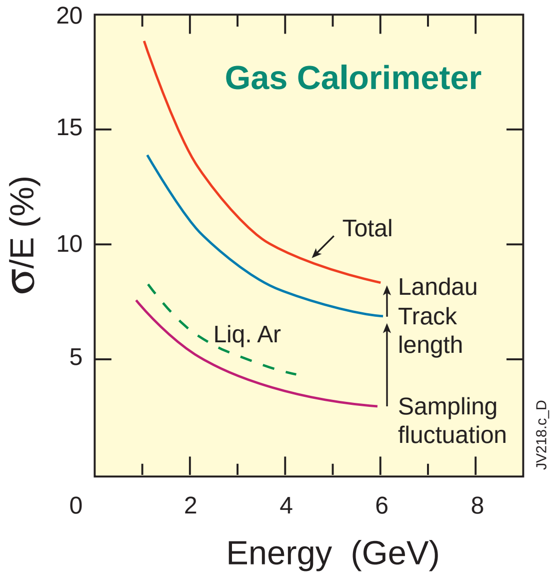

- large fraction of the energy is deposited by low energy electrons
- bremstrahlung photons emitted by electrons are soft (energies below 1 MeV)
- energy lost, mainly in absorber, by electrons produced via Compton or photoelectric effect.
- resulting electrons have a short range in the absorber layer

energy resolution can be improved by decreasing the absorber thickness (or increasing the sampling frequency)

A universal parametrisation for the energy resolution is

$$\frac{\sigma_s}{E} = \frac{5\%}{\sqrt{E}} \left(1 - f_{samp}\right) \; \Delta E_{cell}^{0.5\left(1 - f_{samp}\right)}$$

where ΔE_{cell} is the energy deposited in 1 absorber and 1 active layer and f_{samp} is the fraction of energy deposited in the active layers

$$f_{samp} = 0.6 f_{mip} = 0.6 \frac{d\left(\frac{dE}{dx}\right)_{act}}{\left[d\left(\frac{dE}{dx}\right)_{act} + t_{abs}\left(\frac{dE}{dx}\right)_{abs}\right]}$$

d - thickness of active layer
e.g. 1 cm Pb / 1 cm Scint
$f_{mip} \approx 2/(12.75+2) \approx 13.5\%$

Longitudinal Non-Uniformity

Longitudinal non-uniformity of signal generation and/or collection, either intrinsically or through radiation damage, when folded with the fluctuation in the longitudinal profile from one shower to another (at a fixed energy) leads to a loss of energy resolution (contribution to constant term)

At a given energy the shower max fluctuates with $\sigma \approx 1\ X_0$.

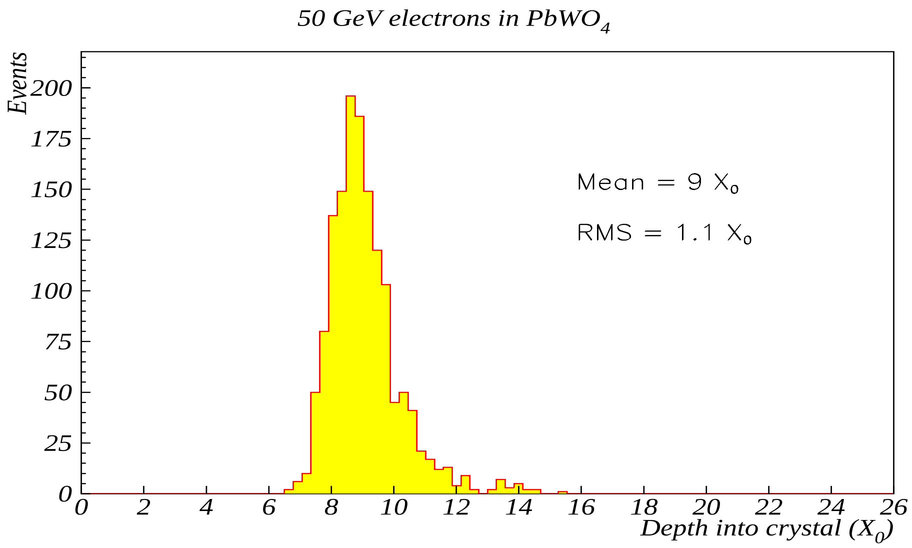

e.g. BGO crystals in L3 expt.

- scintillation light is generated isotropically and is detected by Si photodiodes mounted on the rear face
- efficiency of light collection from the front is much increased due to the taper of the crystals.

- non-uniformity is greatly reduced by coating the polished crystals with 40-50 μm thick layer of high reflectivity NE560 white paint.

B.Adeva et al. NIM A289 (1990) 35

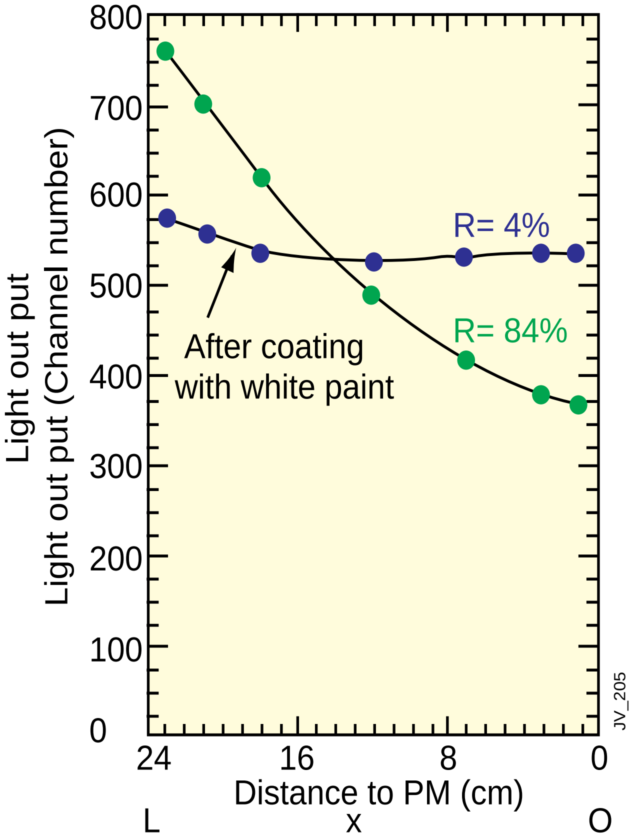

Inter-Calibration Error

• e.m. showers are narrow
usually central cell, or at most, central 4 cells contain ≈ 80 % of shower energy
• lateral shower shape is independent of energy
any effect on resolution will end up in constant term
• Measured energy is;

$$E = \Sigma \ g_i \ E_i$$

• if r.m.s. error on g_i is δ then $c \approx \delta_f / \sqrt{n}$ ranging from $\delta/2$ to δ

• cell to cell inter-calibration should be substantially better than the desired constant term

Energy Leakage

Degradation due to longitudinal and lateral leakage for a totally active LXe calorimeter

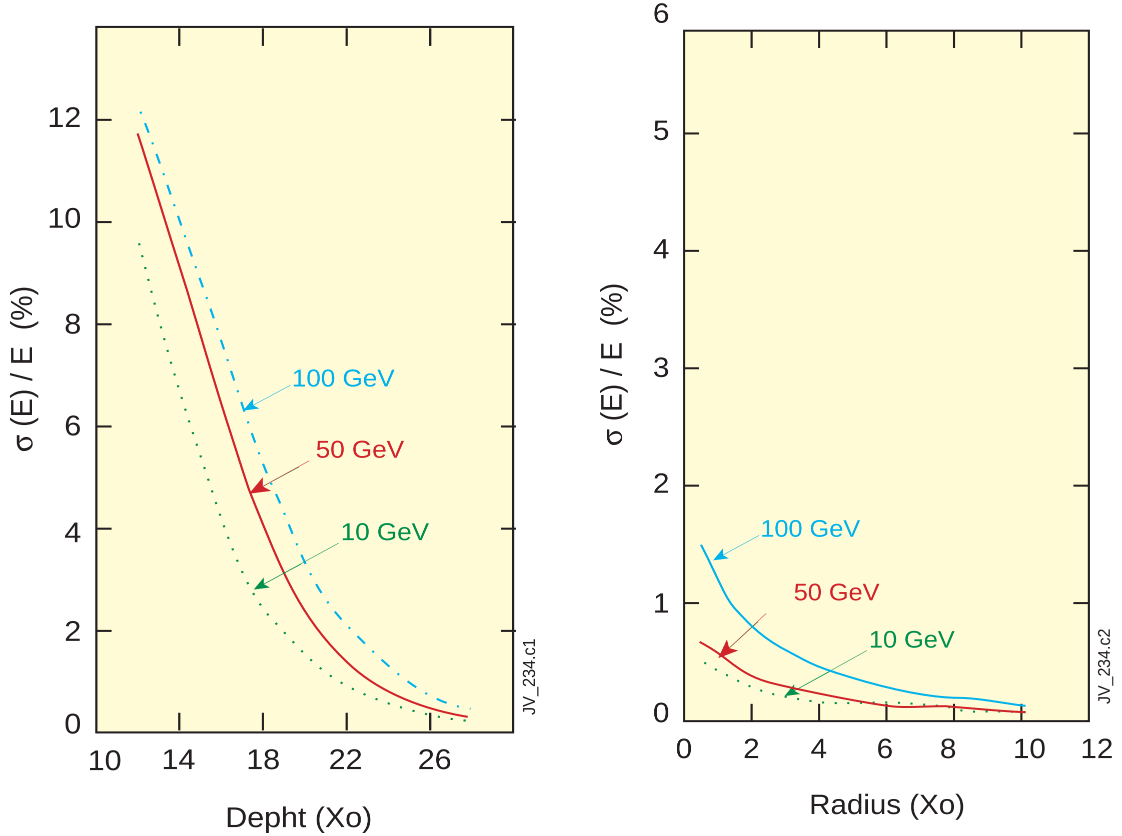

Longitudinal leakage has more serious consequences.
At fixed energy, profile of longitudinal energy deposition differs from one shower to another. For a fixed depth of calorimeter, fraction of energy leakage (f) and its fluctuation increases with energy

$$\frac{\sigma_{rms}}{\langle E_{dep} \rangle} = \frac{f}{2} \quad for \quad f < 20\%$$

Lateral profile of energy deposition differs much less from one shower to another and energy dependence is weak
Lateral shape is almost independent of energy especially at high energies

Energy Resolution of Hadronic Calorimeters

- Energy Resolution of Hadronic Calorimeters
- Hadr. Cascade - em Component
- Energy Resolution of Hadronic Calorimeters
- Hadr. Cascade - Role of e/h
- Compensation
- Sampling and Intrinsic Fluctuations

Energy Resolution of Hadronic Calorimeters

Hadronic calorimeters, because of large depth required ($\sim 10\lambda$) are by necessity sampling calorimeters

Response of em sampling calorimeter is $E_{vis} = e\,E$
where E, E_{vis} are incident and visible energies resp. and $e = f^{e}_{samp}$

Response of a hadronic sampling calo is

$$E = E_{em} + E_{ch} + E_{n} + E_{nucl}$$

where E_i is energy deposited by ith component
E_{em} - em component (π^0s)
E_{ch} - charged pions or protons
E_n - low energy neutrons
E_{nucl} -energy lost in breaking nuclei (binding energy) sometimes labelled 'invisible' energy

Each component has its own sampling fraction

$$E_{vis} = eE_{em} + \pi E_{ch} + nE_{n} + NE_{nucl}$$

N is normally v. small but E_{nucl} can be large (~ 40 % in Pb) and hence e/h > 1 for non-compensating calorimeters

Fluctuations in the visible energy have two sources

- sampling fluctuation as in em case. Can be reduced by finer absorber plates
- intrinsic fluctuation in shower components (δE_{em}, δE_{ch} etc.)

∴ stochastic term

$$a_h = \frac{a}{\sqrt{E}} \oplus \left(\frac{a_{\rm intr}}{\sqrt{E}} + c \right)$$

c, the constant term, depends on e/h and vanishes for compensating calo.

Hadr. Cascade - em Component

- Hadron showers contain an electromagnetic component

(due to π^0, η).

- Size of the em component (F_0) is essentially determined by the 1st interaction.

- Considerable event to event fluctuation in F_0. On average 1/3 of mesons ($\pi^0/\pi^+ + \pi^- + \pi^0$) produced in the first interaction will be π^0's. The 2nd generation $\pi^\pm$,'s may also produce π^0's if sufficiently energetic.

Assume that for each generation <n> secondaries/primary are produced with a fraction $f_0 = 1/3$.

At shower max an energy fraction F_0 has been depositied by neutrals

$$\nu=1, \quad F_0 = f_0$$
$$\nu=2 \quad F_0 = f_0 + f_0 (1-f_0)$$
$$\nu=3 \quad F_0 = f_0 + f_0 (1-f_0) + f_0 (1-f_0)^2$$

....

$$\Rightarrow \quad F_0 = f_0 \ \Sigma_1 (1-f_0)^{\nu-1}$$
$$\Rightarrow \quad F_0 = [1 - (1-f_0)^\nu]$$

- at low energies $F_0 \rightarrow f_0$ whereas
- at very high energies ν_{max} is large and hence $F_0 \rightarrow 1$.

Neutral pions , developing as em showers, do not produce any hadronic interactions and hence drop out of the hadronic cascade.

Energy Resolution of Hadronic Calorimeters

It usually turns out that the response of the calorimeter to electrons and photons i.e. em component (labelled as e) may differ from that of charged hadrons i.e. non-em (labelled h).

Hence response to electrons (E_e) and charged pions (E_π) is

$E_\pi = e\,F_0 + h\,(1-F_0)$
$E_e = e$

$$\frac{e}{\pi} = \frac{(e/h)}{[(e/h)F_0 + (1-F_0)]}$$

If e/h = 1 the calorimeter is said to be compensating.

If |e/h| ≥ 10% calorimeter performance is compromised :

i) measured energy distribution is non-Gaussian

ii) an e/π ratio different from unity and dependent on energy

iii) a non-linear energy response to hadrons

iv) an additional contribution to the relative energy resolution (σ/E)* due to fluctuation in f_0.

σ/E does not improve as 1/√E with increasing energy.

---

* $dE_\pi = (e - h)\,dF_0$

$$\frac{dE}{E} = \frac{dF_0\,|(e/h) - 1|}{[(e/h)F_0 + (1-F_0)]}$$

Hence the fractional error depends on e/h, F_0 and dF_0.
If e/h = 1, then there is no contribution due to the fluctuation dF_0.
Assuming $dF_0/F_0 = df_0/f_0 \sim 1/\sqrt{(f_0\langle n\rangle)}$
⇒ for a 200 GeV hadron with $\langle n\rangle \approx 9$,
$dF_0 \approx 0.6 \Rightarrow (dE/E)_{comp} \approx 3.5\%$

$(dE/E)_{comp} \sim 1/\sqrt{\ln E}$, and → 0 as E→ ∞ since $\langle n\rangle \propto \ln E$.

Hadr. Cascade - Role of e/h

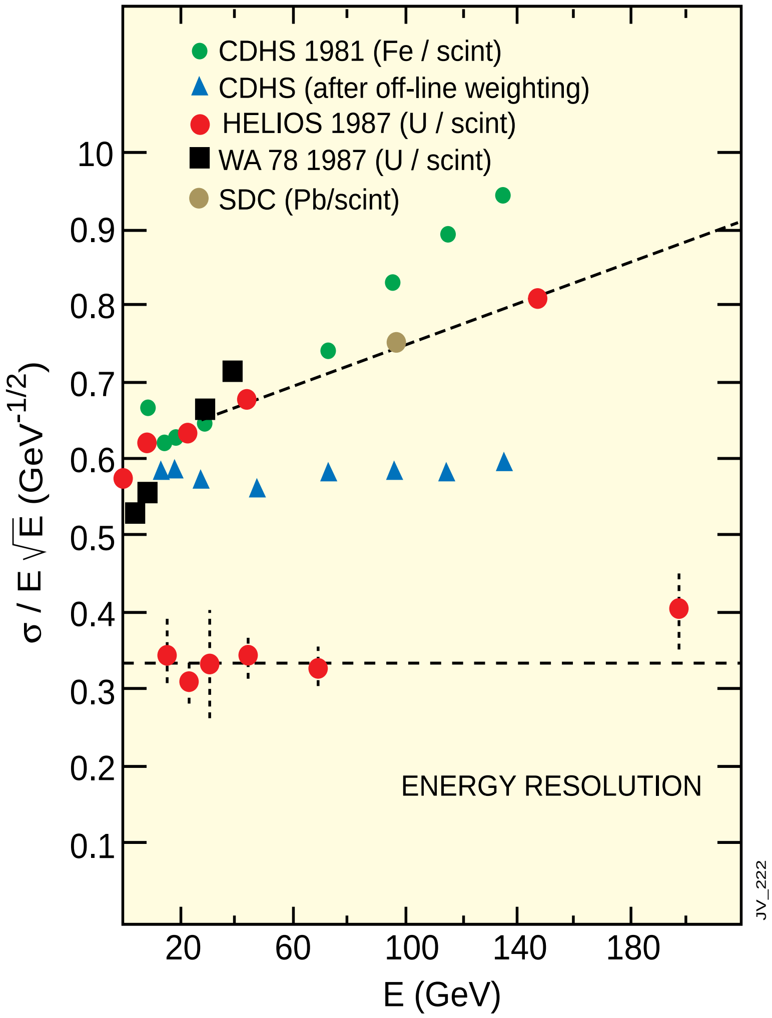

Compensation

• Degree of (non-)compensation is given by the energy independent e/h ratio
• e/h cannot be measured directly but can be inferred from the energy dependent e/π signal ratios.
• Two relations between the signal ratio e/π (E) and e/h

$$\frac{e}{\pi} = \frac{e/h}{1+(e/h-1)F_0}$$

$$F_0 = 1 - (E/0.76)^{-0.13} \qquad D.\ Groom$$

$$and \quad F_0 = 0.11 \ln E \qquad R.\ Wigmans$$

It is instructive to see how the energy is dissipated by a hadron in a Pb absorber. The breakdown is as follows :

42 % invisible energy (nuclear breakup)
43% charged particles
12% neutrons with KE ~ 1MeV
3% γ's with 1 MeV

The sizeable amount of invisible energy loss means that hadronic calorimeters tend to be undercompensating (e/h>1).

Compensation can be achieved in three ways :

i) boost the non-em response by using depleted uranium.
ii) suppress e.m. response
ii) boost the response to low-energy neutrons

Sampling and Intrinsic Fluctuations

Use the technique of 'interleaved calorimeters'

2 independent calorimeters - L (R) - sum of odd (even) numbered scintillator layers

NIM A277(1989)42

	Pb	U
absorber thickness (mm)	10	3.2
Scint. thickness (mm)	2.5	3.0
lateral segmentn. (cm^2)	20×20	5×60
no. of towers	9	12
total lateral size (cm^2)	60×60	60×60
long. segmentn.	1λ+4λ	4×1.5 λ
total depth	5λ	6λ

1 λ deep tail catcher to veto late starting showers

Deduce for showers

hadrons	Pb calo.	$\sigma_{samp} = 41.2 \pm 0.9\%/\sqrt{E}$	$\sigma_{intr} = 13.4 \pm 4.7\%/\sqrt{E}$
	U calo.	$\sigma_{samp} = 31.1 \pm 0.9\%/\sqrt{E}$	$\sigma_{intr} = 20.4 \pm 2.4\%/\sqrt{E}$
electrons	Pb calo.	$\sigma_{samp} = 23.5 \pm 0.5\%/\sqrt{E}$	$\sigma_{intr} = 0.3 \pm 5.1\%/\sqrt{E}$
	U calo	$\sigma_{samp} = 16.5 \pm 0.5\%/\sqrt{E}$	$\sigma_{intr} = 2.2 \pm 4.8\%/\sqrt{E}$

Conclude for compensating Pb and U calorimeters

- energy resolution is dominated by sampling fluctuations

$$\sigma_{samp} = \frac{11.5\% \sqrt{\Delta E_{cell}(MeV)}}{\sqrt{E(GeV)}}$$

- sampling fluctuations for hadrons are larger than those for e's by a factor of 2

very good e.m. energy resolution is incompatible with e/h=1

Energy Measurement of Jets

- Jet Energy Measurement
- Jet Energy Resolution
- Di-jet Mass Resolution

  v/s Calorimeter Segmentation

Jet Energy Measurement

Factors that determine the required performance of hadronic calorimetry are

jet energy resolution and linearity
missing transverse energy resolution

Jet energy resolution is limited by effects from

jet algorithms (cone radius, lateral segmentation)
fluctuation in fragmentation
underlying event and energy pileup at high luminosity
magnetic field

Figure of Merit : di-jet mass resolution

Use results from study in context of an LHC experiment

A. Beretvas et al., CMS TN/94-326

Physics input		
	low p_T di-jets	$50 < p_T < 60$ GeV
	high p_T di-jets	$500 < p_T < 600$ GeV
	high mass di-jets	$3 < m_{Z'} < 4$ TeV
	minbias	QCD di-jets, $2 < p_T < 500$ GeV
Typical Calorimeter parameters		
	geometric coverage	$\lvert\eta\rvert < 1.5$
	magnetic field	4T
	compensation	$e/h = 1$
	e.m. resolution	$\sigma/E = 3\%/\sqrt{E} \oplus 0.5\%$
	had. resolution	$\sigma/E = 60\%/\sqrt{E} \oplus 3\%$
	had. lateral segmentation	$\Delta\eta\times\Delta\phi = 0.1\times0.1$
	tower thresholds	low p_T events - $E_T > 0.3$ GeV
		high p_T events - $E_T > 1$ GeV

Jet Energy Resolution

Stochastic Term for Jets

$$\frac{\sigma(E)}{E} = \frac{a}{\sqrt{E}} \oplus c$$

$$\sum_i z_i = 1, \quad \sum_i k_i = E \qquad \frac{dk_i}{k_i} = \frac{a}{\sqrt{k_i}} \oplus c$$

If stochastic errors dominate

$$dk_i = a\sqrt{k_i}$$

$$dE_J = \sqrt{\sum_i (dk_i)^2} = \sqrt{\sum_i a^2 k_i} = a\sqrt{E}$$

$$\therefore \frac{dE}{E} = \frac{a}{\sqrt{E}}$$

an ensemble of particles act, w.r.t. errors, as a single particle

Constant Term for Jets

in high energy regime where constant term dominates

$$dE_J \approx \sqrt{(cz_iE)^2} = cE\sqrt{z_i^2}$$

assuming that there is a leading particle, l, with fraction z_l, then

$$\frac{dE_J}{E} \approx c\ E\ z_l$$

For fragmentation function

$$zD(z) = (1-z)^2 \qquad \langle z_l \rangle \approx 0.23$$

$\Rightarrow$ constant term is reduced
e.g. for a calorimeter with a=0.3 and c=0.05, in which a 1 TeV jet fragments into 4 hadrons of equal energy the error on the energy decreases from 50 GeV to 25 GeV

Di-jet Mass Resolution v/s Cone Size

Assume perfect calorimeter, no magnetic field, no underlying event

Low and High p_T and High Mass Di-jets

Fractional Mass Resolution (%) v/s Cone Radius

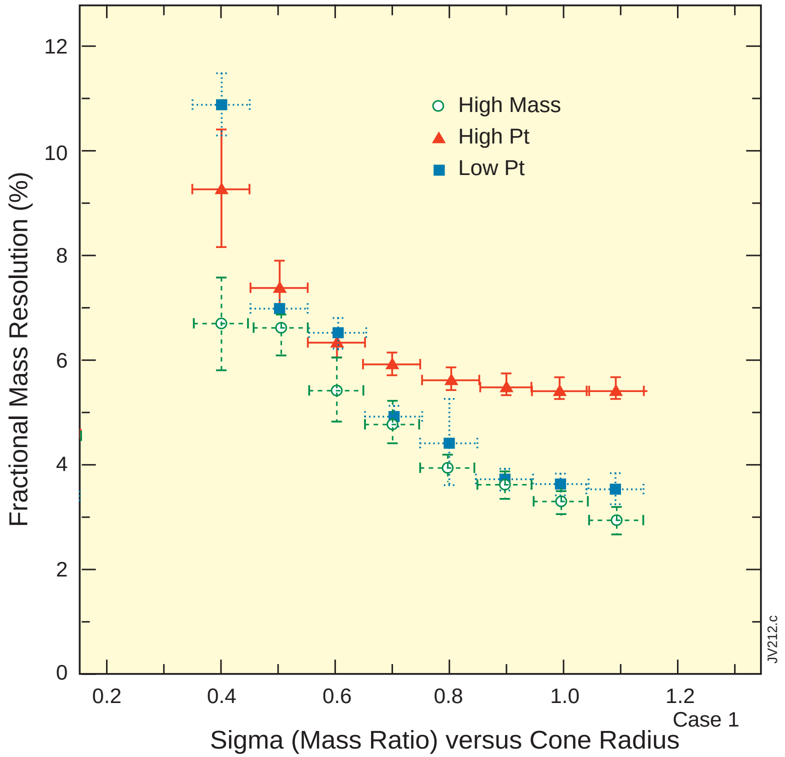

Low p_T di-jets

perfect calorimeter +overlapping minbias

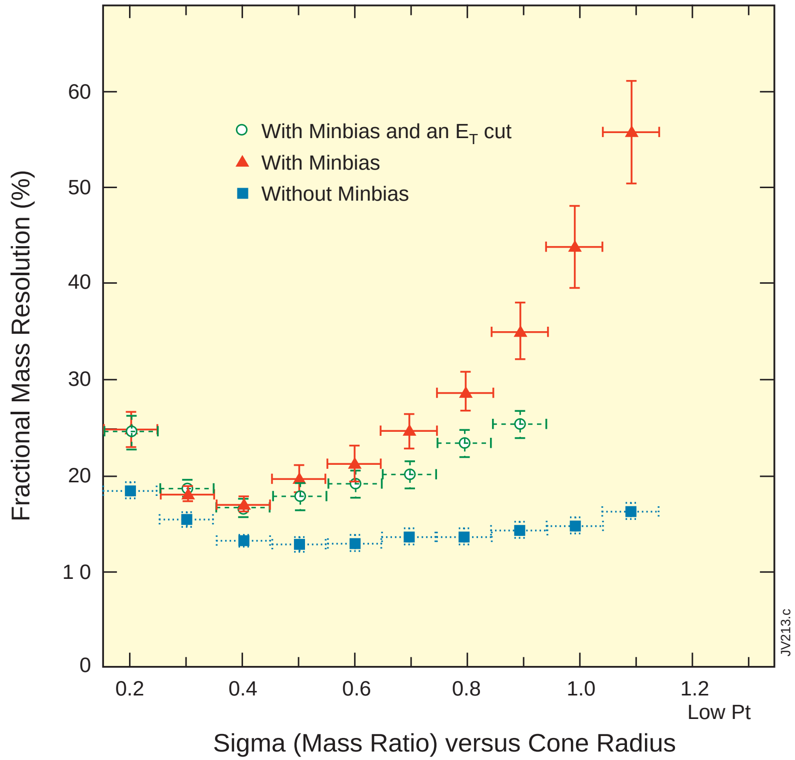

mass resolution decreases with increasing cone size

worsened mass resolution for

- a smaller cone size - exludes some signal energy
- a larger cone - pick up significant pileup energy

optimize cone size to obtain best mass resolution for each physics process and instantaneous luminosit

Di-jet Mass Resolution v/s Calorimeter Segmentation

Mass Resolution due to angular error dθ is given by

$$\frac{dM}{M} = \frac{p_T}{M} d\theta$$

only highly boosted and low mass di-jets (eg. boosted Zs from H → ZZ) will have a significant contribution from angular error

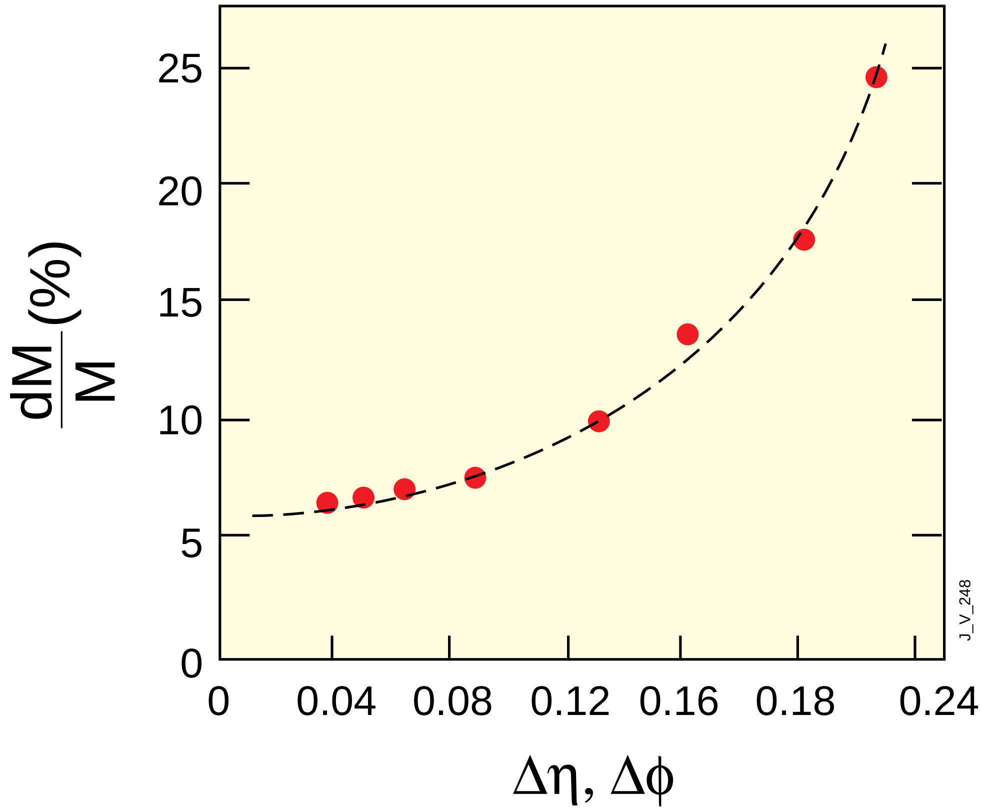

dM/M worsens dramatically when Δη, Δϕ > 0.1

Experimental Measurements

Measurement of Momentum

- Charged particle in a magnetic field
- Multiple scattering

Measurement of Energy

- characteristics of e.m. cascades
- characteristics of hadronic cascades
- e.m energy resolution
  - homogeneous calorimeters
  - sampling calorimeters
- hadronic energy resolution
- energy measurement of jets

Identification of Particles

- electrons, photons -using calorimeters, inner tracker, TRDs
- pions / kaons / protons using Cherenkovs
- b-jets
- neutrinos (and jets)
- muons

e / h± Separation

Exploit the differences in longitudinal and lateral development of showers initiated by electrons and hadrons

- preshower detector placed between ≈ 1.5 - 4 X_0
- lateral segmentation and longitudinal segmentation (veto on HCAL)
- energy-momentum matching

An appropriate combination of these can lead to rejection power of ≈ 10^4 at high energies Ultimate rejection power is limited by

- charge exchange processes eg. $\pi^+ n \rightarrow \pi^0 p$, $\pi^- p \rightarrow \pi^0 n$
- first hadronic interaction leading to anomalously large π^0 multiplicity or energy

UA1 U/TMP Calorimeter R. Apsimon et al NIM A305(1991)331

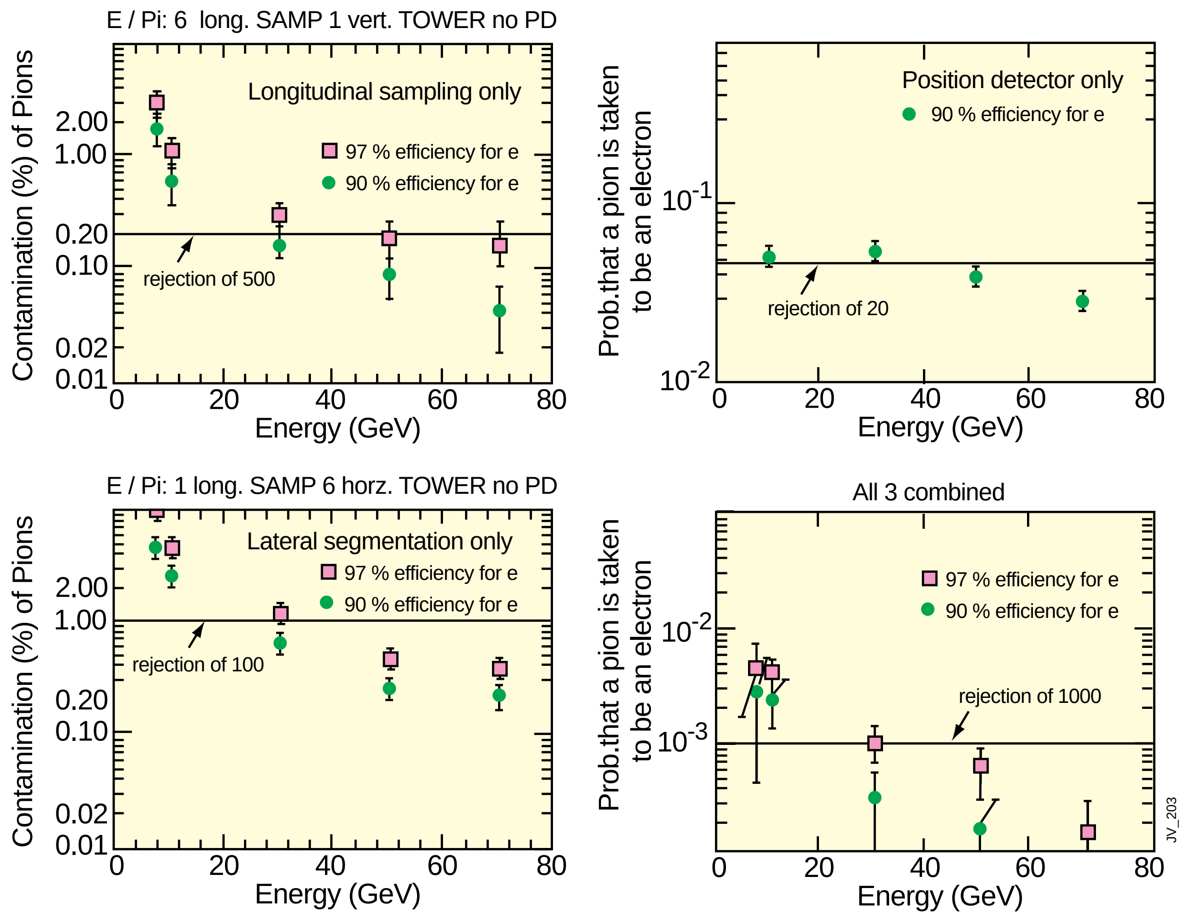

Lateral Segmentation	towers of 11×11 cm² (≈14×14 X_0)
Longit. Segmentation	3, 6, 10, 7 X_0 / 2×0.7λ / 2×2.5λ)
Preshower Detector	at 3X_0 with orthogonal strips of pitch 9mm

γ / jet Separation

γ/jet separation

Physics motivation - observation of $H \rightarrow \gamma\gamma$ signal in range

$80 < m_H < 150$ GeV. Look for single isolated γ's. σ is small and backgrounds are large. Large uncertainties in jet production and fragmentation

$$\frac{jet - jet}{\gamma\gamma_{irreducible}} \approx 2.10^6 \qquad \frac{\gamma - jet}{\gamma\gamma_{irreducible}} \approx 8.10^2$$

Rejection of $\approx$ 5000 against jets is needed

Use isolation cuts and fine lateral and/or longitudinal segmentation

γ/jet separation in ATLAS

E_{HCAL} ($\Delta\eta \times \Delta\phi = 0.2 \times 0.2$) $\leq$ 0.5 GeV

EM isolation $\frac{E_{3\times5}}{E_{7\times7}} > 90\%$

Lateral shower profile - look for an em core : 4 towers contain > 65% of cluster energy

Shower width in η

For a photon efficiency of > 90%, $R_{jet} \geq 1500$

γ / π^0 Separation

Isolated π^0's which take a large fraction of the jet energy can be rejected by detecting presence of 2 em showers.

<u>CMS Barrel</u>

- use fine transverse crystal granularity (2.18×2.18 cm^2)
- γs from π^0 with p_T=25 GeV have a minimum separation of 15 mm
- Neural net algorithm compares energy deposited in signal containing 3×3 crystal array - variables are constructed from 9-energies, x and y position, and a pair measuring the shower width

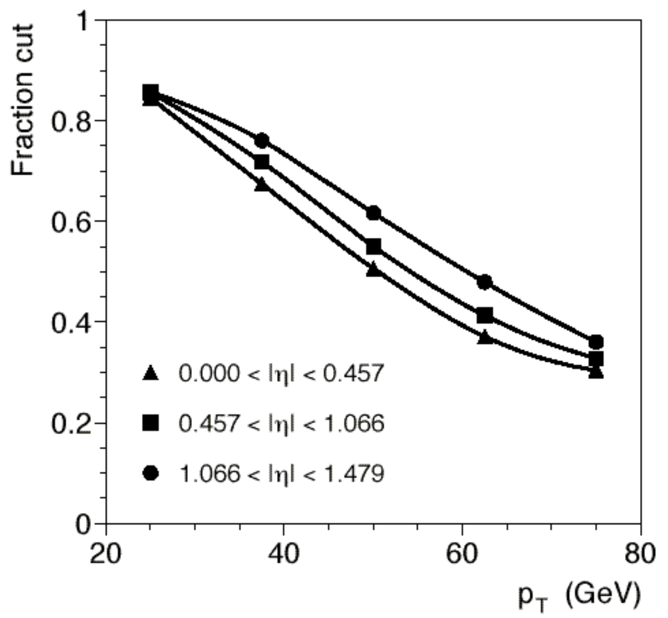

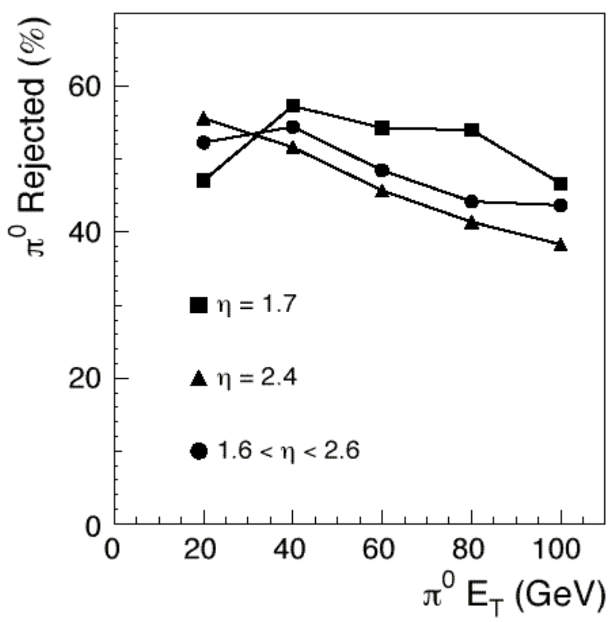

<u>CMS Endcap</u>

- use preshower - two planes of Si strips with fine pitch (≈2mm)

compare signal (summed in 1,2 or 3 adjacent strips with the total signal in 21 adjacent strips centred on strip with highest signal

Use variable

$$F = \frac{\sum S_N}{\sum_{j=-m}^{m} S_{j_{\max}+j}}$$

F for E_T=60 GeV: 2nd Si plane

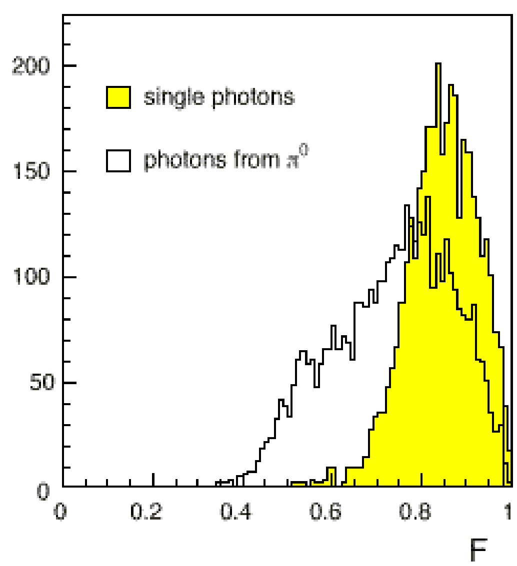

Electron Identification - Transition Radiation

Predicted by Ginzburg and Franck in 1946

$$p = \gamma m v \Rightarrow m = \frac{1}{\beta c \gamma} p$$

$$\therefore \left(\frac{\Delta m}{m}\right)^2 = \frac{1}{\beta^2 c^2}\left(\frac{\Delta\gamma}{\gamma}\right)^2 + \left(\frac{\Delta p}{p}\right)^2$$

If $\Delta p/p$ is small, mass resolution at high momenta is $\alpha\ \gamma$

Transition radiation is emitted when a charged particle moves from a medium of refractive index n_1 to a medium of a different index n_2

This may be thought of as an apparent acceleration

- Radiated energy /boundary to vacuum

$$W = \frac{1}{3}\alpha\ \hbar\omega_p\ \gamma \quad i.e.\ W \propto \gamma$$

$$where\ \ \hbar\omega_p\ \ is\ the\ plasma\ frequency\ (\approx 20\ eV\ \ for\ \ polyethylene)$$

Hence can use it for particle identification

- X-rays are emitted at small angle ($\theta \approx 1/\gamma$). TR stays close to the charge particle track

$$E_{ph} = \frac{\gamma}{3}\hbar\omega_p$$

- Number of emitted photon/boundary is small

$$N_{ph} \approx \frac{W}{\hbar\omega_p} \propto \alpha \approx \frac{1}{137}\ !$$

- Need many transitions → build a stack of many thin foils with high Z gas to absorb the X-rays

- Particle must traverse a minimum distance to efficiently emit TR. (typically 20μm for polyethylene)

Transition Radiation Detector

ATLAS Transition Radiation Tracker

Straw tube proportional chambers embedded in polyethylene fibres

Diameter of staws 4mm

Gas 70% Xe + 20% CF_4 + 10%CO_2

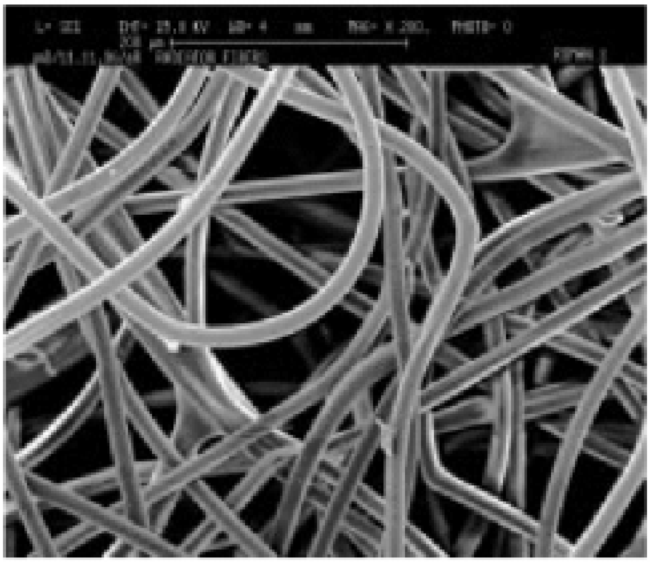

Figure 12-38 Micro-photograph of a sample of polyethylene fibre radiator (scale: 70 µm per 1 cm).

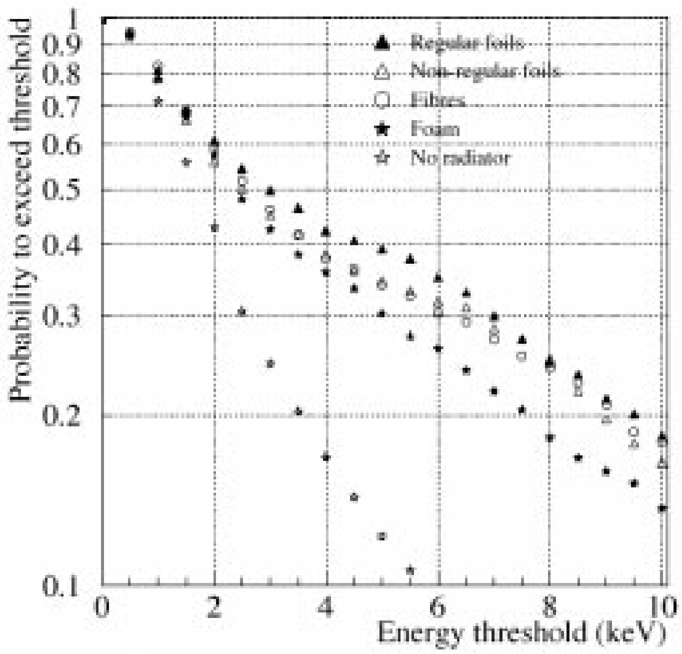

Figure 12-39 For 200 GeV electrons and for different types of radiators, probability per straw to observe an energy deposition above a given threshold.

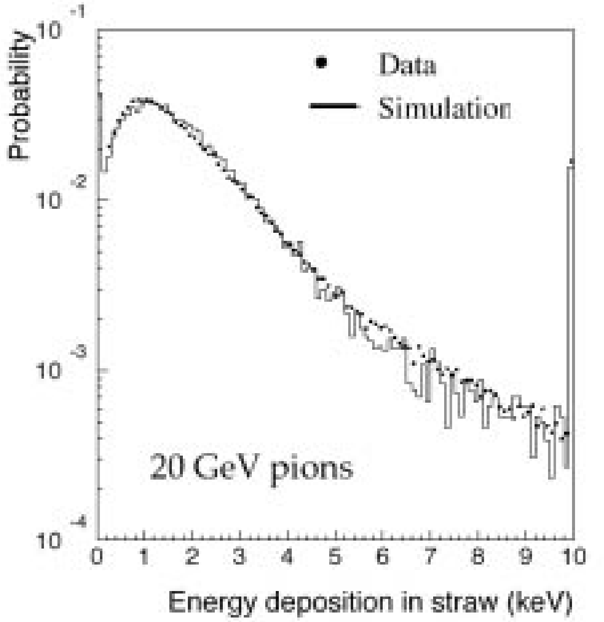

Figure 12-41 Normalised dE/dx spectra for 20 GeV pions for data and simulation.

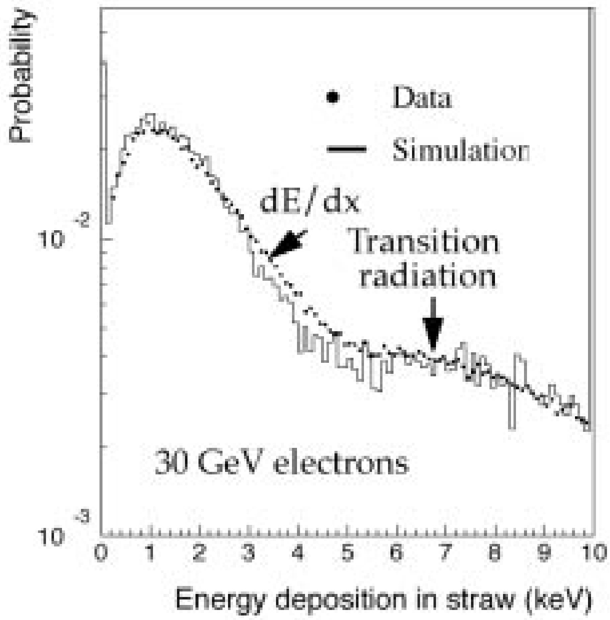

Figure 12-42 Normalised dE/dx and transition-radiation spectra for 30 GeV electrons for data and simulation.

Data from Test Beams

ATLAS TRD Test

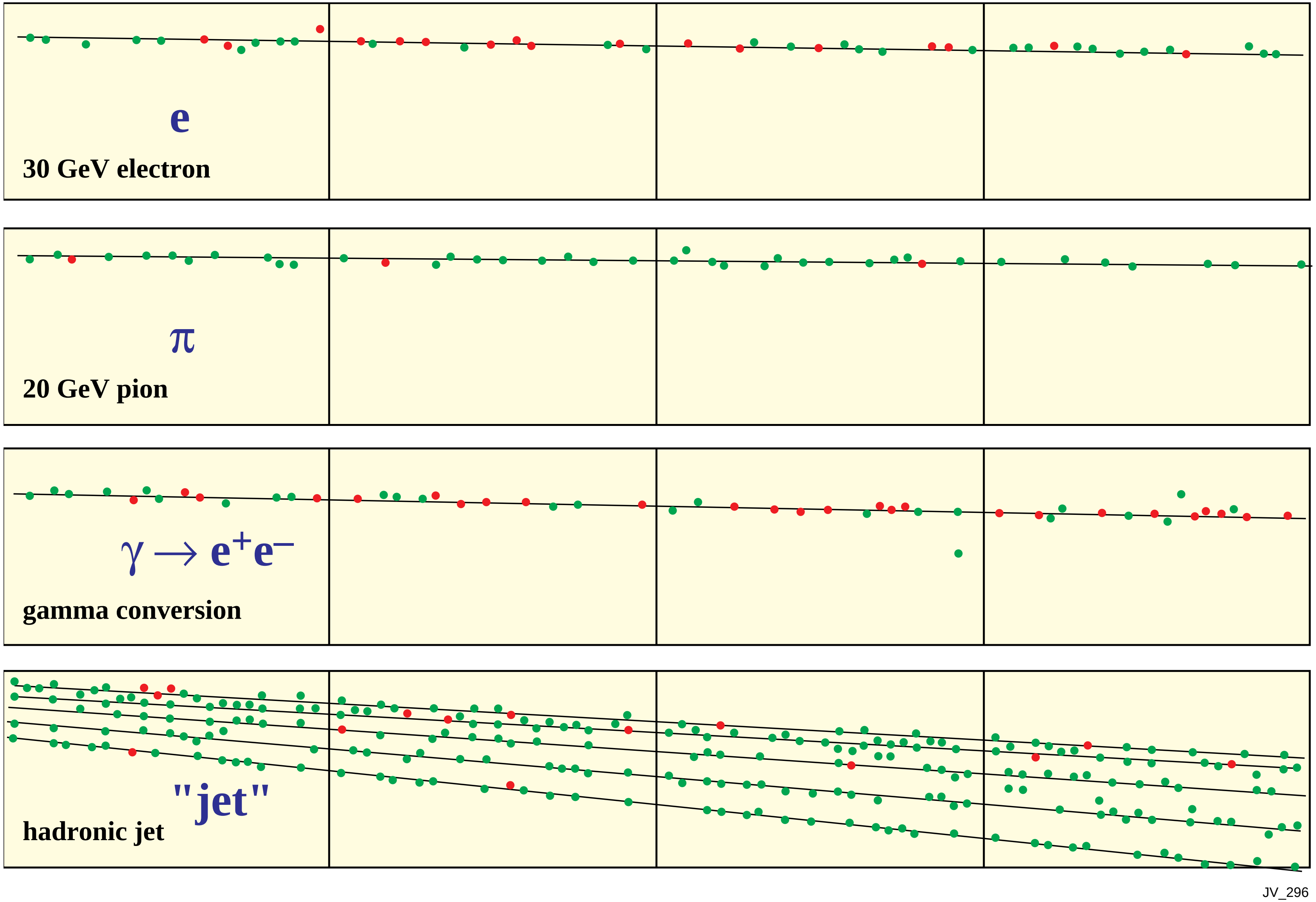

Identification of Particles using Cherenkov Radiation

Charged particle emits Cherenkov radiation when

$$v_{particle} > \frac{c}{n} \quad or \quad \beta \geq \beta_{thr} = \frac{1}{n}$$

(= sonic shock wave induced by supersonic aircraft)

"Huygen's" wavelets add constructively along line defined by C^v angle

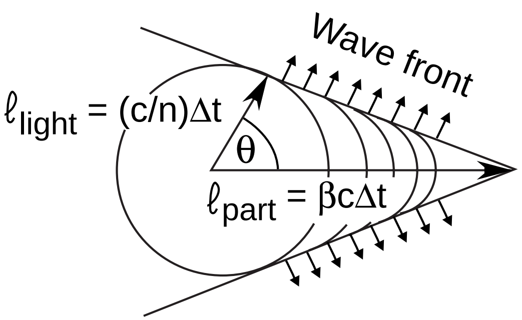

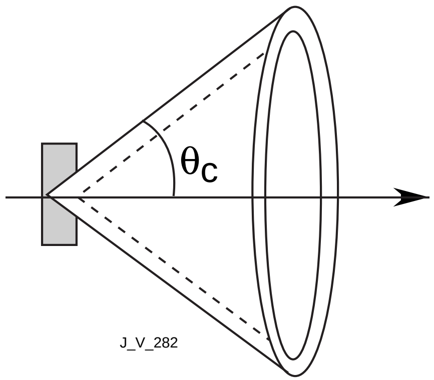

$$\cos\theta_C = \frac{1}{n\beta} \quad \text{with} \quad n = n(\lambda) \geq 1$$

$$\theta_{\max} = \cos^{-1}(1/n)$$

No. of γ's emitted/unit length/ unit energy interval is:

$$\frac{d^2N}{dxdE} = \frac{\alpha}{\hbar c}\sin^2\theta_C \approx 365\ \sin^2\theta_C \quad eV^{-1}cm^{-1}$$

Energy loss by Cherenkov radiation is small compared to loss due to ionization (≈ 1%)

Usually Cv radiation is detected by photomultipliers (sensitivity range 350-550 nm). Then

$$\frac{dN}{dx} \approx 475\ \sin^2\theta_C \quad photons/cm \quad for \quad Z = 1$$

Cherenkov Detectors

Detectors can exploit :

$N_{ph}(\beta)$ threshold detector (do not measure θ_C)

$\theta(\beta)$ Ring Imaging Cherenkov (RICH)

Principle of Operation of Ring Imaging Cherenkovs

Optimal configuration - spherical mirror and spherical detector at $R_M = 2\ R_D$

All photons emitted at the same angle are focused onto the same point i.e. no emission point error

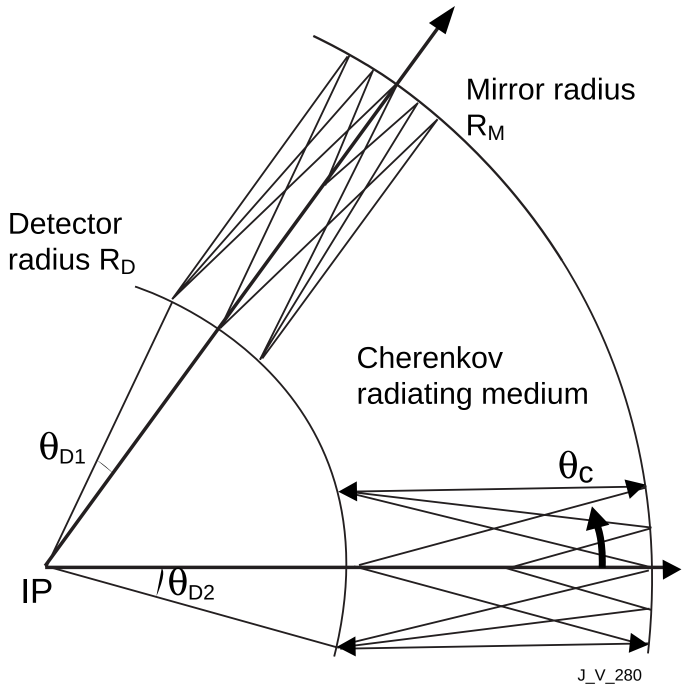

Parameters for some selected Cherenkov radiators.

Medium	n-1	θ_{max}	$\pi_{thr}(p)$ GeV/c	N_γ ($eV^{-1}cm^{-1}$)
Air	1.000283	1.36°	5.9	0.21
Isobutane	1.00217	3.77°	2.12	0.94
Aerogel	1.0065	6,51°	1.23	4.7
Aerogel	1.055	18.6°	0.42	37.1
Water	1.33	41.2°	0.16	160.8
Quartz	1.46	46.7°	0.13	196.4

Threshold Cherenkov Detectors

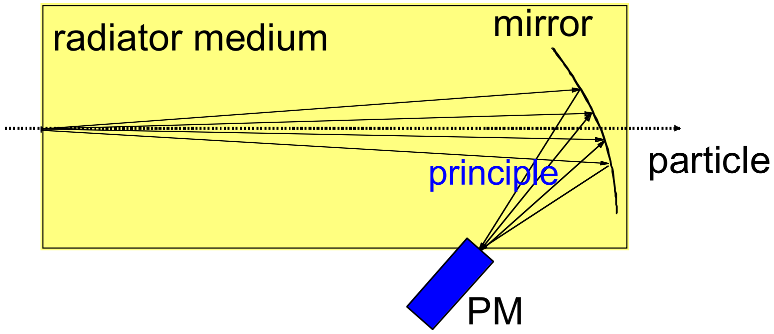

e.g. Aerogel threshold Cherenkov detectors in BaBar

A1: n = 1.055 and A2: n = 1.0065

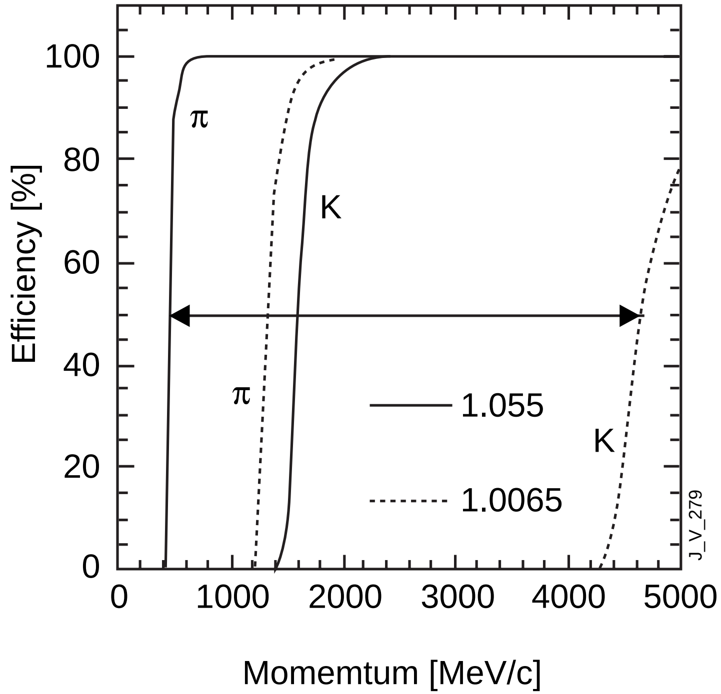

Threshold Cherenkov detectors

- a simple yes/no decision based on whether a particle is above/below a threshold velocity ($\beta = 1/n$)

The no. of photons emitted depends on velocity and is:

$$N_\gamma \propto \sin^2\theta_C = 1 - \frac{1}{\beta^2 n^2} = 1 - \frac{1}{n^2}\left(1 + \frac{m^2}{p^2}\right)$$

p > 0.4 GeV/c	π in A1 gives light
p > 1.2 GeV/c	π in A1 and A2 gives light
p > 1.4 GeV/c	K in A1 gives light
p > 4.2 GeV/c	K in A1 and A2 gives light

π/K separation between 0.4 and 4.2 GeV/c

Ring Imaging Cherenkovs

Ring Imaging Cherenkov (RICH) detectors determine identity of particles by measuring Cherenkov angle (θ_C) given by

$$\theta_C = \cos^{-1}\left(\frac{1}{\beta n}\right) = \cos^{-1}\left(\frac{E}{pc}\frac{1}{n}\right) = \cos^{-1}\left(\frac{\sqrt{p^2+m^2}}{pc}\frac{1}{n}\right) \qquad p = \frac{1}{\sqrt{n_\sigma}}\sqrt{\frac{\left(m_2^2-m_1^2\right)\sqrt{N_{pe}}}{2\tan\theta\times\sigma_\theta^{pe}}}$$

Two particles with masses m_1 and m_2 can be distinguished by n_σ up to a momentum p

e.g. LHCb use 2 RICHs, Photodetector : HPD

A1: combined gas (C_4F_{10}) and aerogel A2: gas

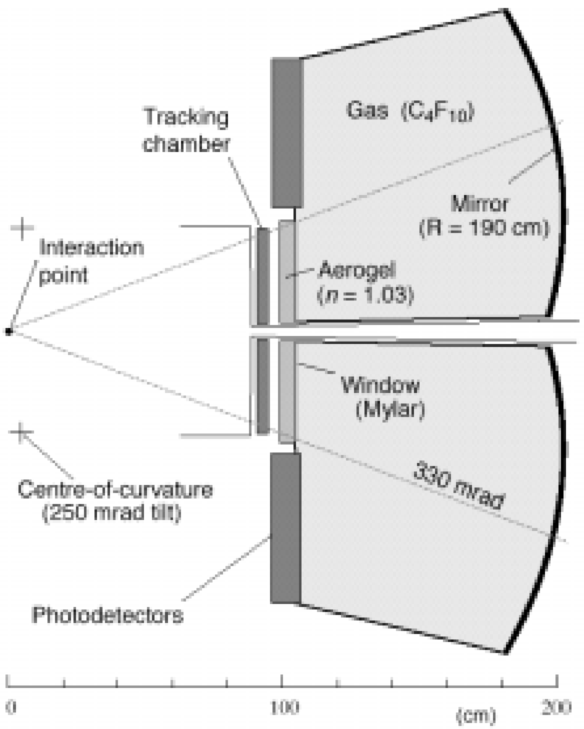

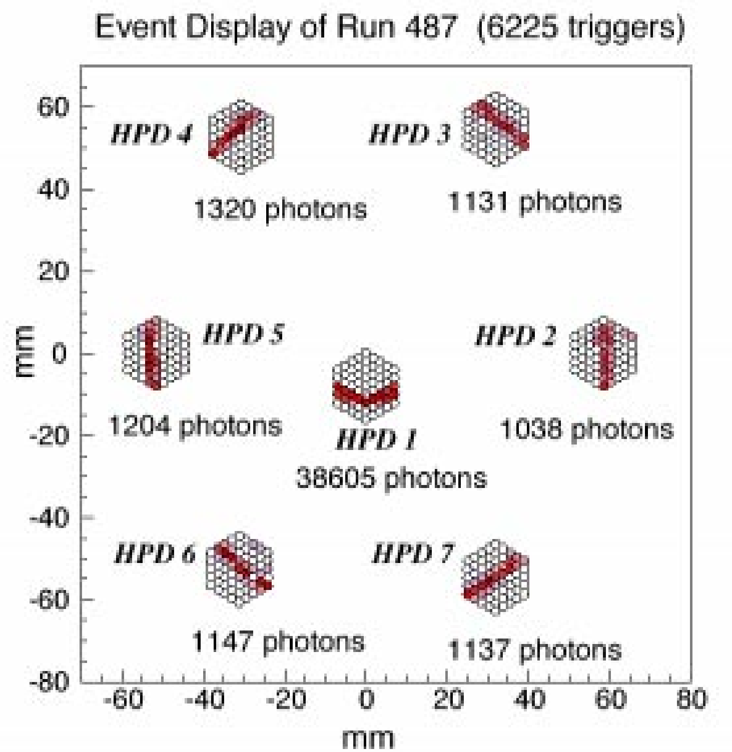

π/K can be distinguished (3σ) up to 75 GeV/c

N=20 p.e. and σ_e = 1 mrad and ω =31 mrad (CF_4)

Identification of b-jets

b-jets can be tagged using

- electrons within a jet from the semi-leptonic decay of a b-quark
- looking for one or more tracks within a jet having a significant impact parameter
- reconstructing a secondary vertex consistent with the flight path of a B-meson

b-jets Tagging using Impact Parameter Measurement

Important parameters

- distance of first measuring layer from interaction vertex
- spatial resolution
- number of points close to the interaction vertex
- low multiple scattering

e.g. using pixel detectors

in CMS pixel barrel layers placed at r=4.5 and r=7 cm at low luminosity

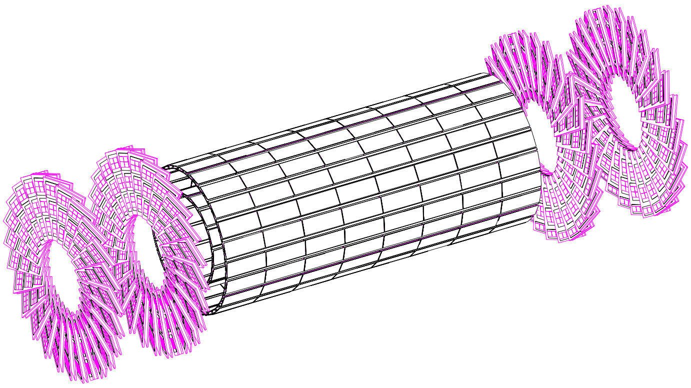

b-tagging efficency v/s mistagging rate

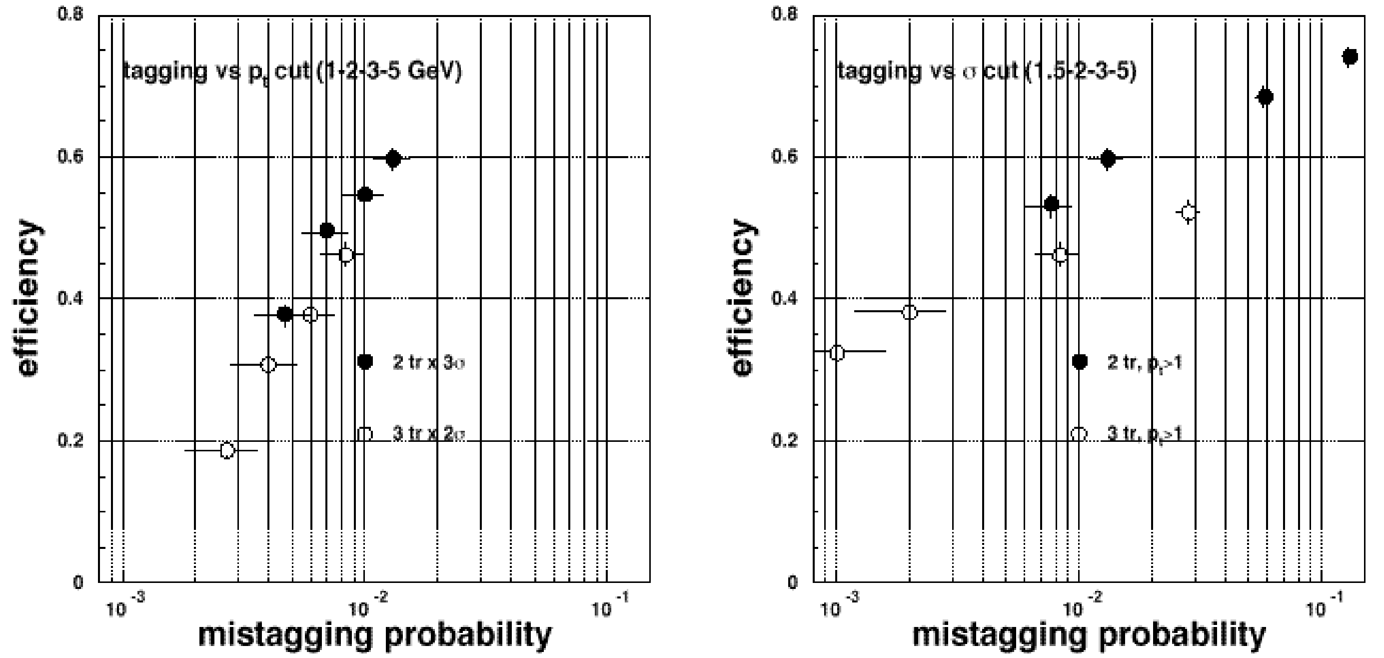

Identification of b-jets

b-jets can be tagged using

- electrons within a jet from the semi-leptonic decay of a b-quark
- looking for one or more tracks within a jet having a significant impact parameter
- reconstructing a secondary vertex consistent with the flight path of a B-meson

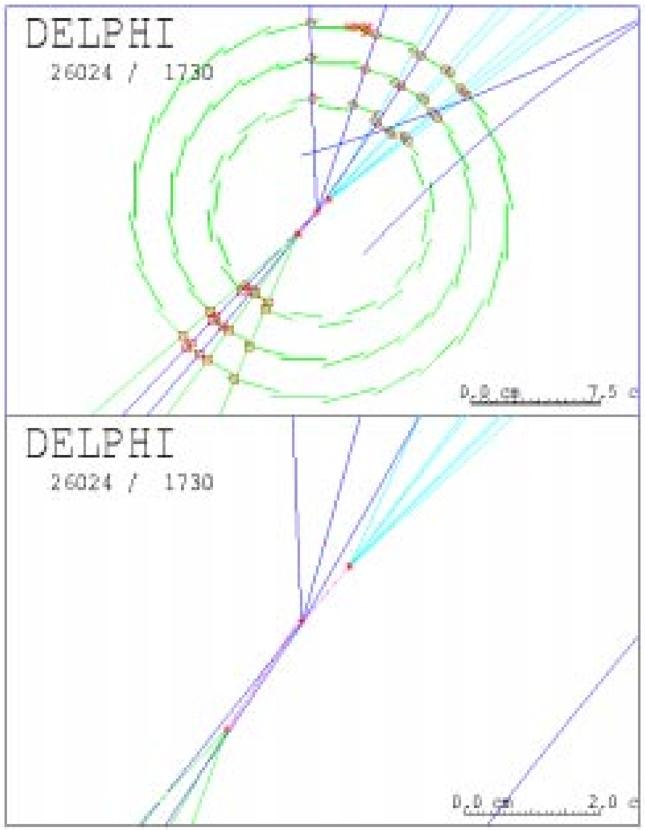

b-jets Tagging using Impact Parameter Measurement

Important parameters

- distance of first measuring layer from interaction vertex
- spatial resolution
- number of points close to the interaction vertex
- low multiple scattering

Typically can get a rejection against u, d, and s quarks of a factor of 100 for an efficiency of ≈ 50%

Identification of Neutrinos

The presence of neutrinos is deduced from theimbalance in the transverse energy

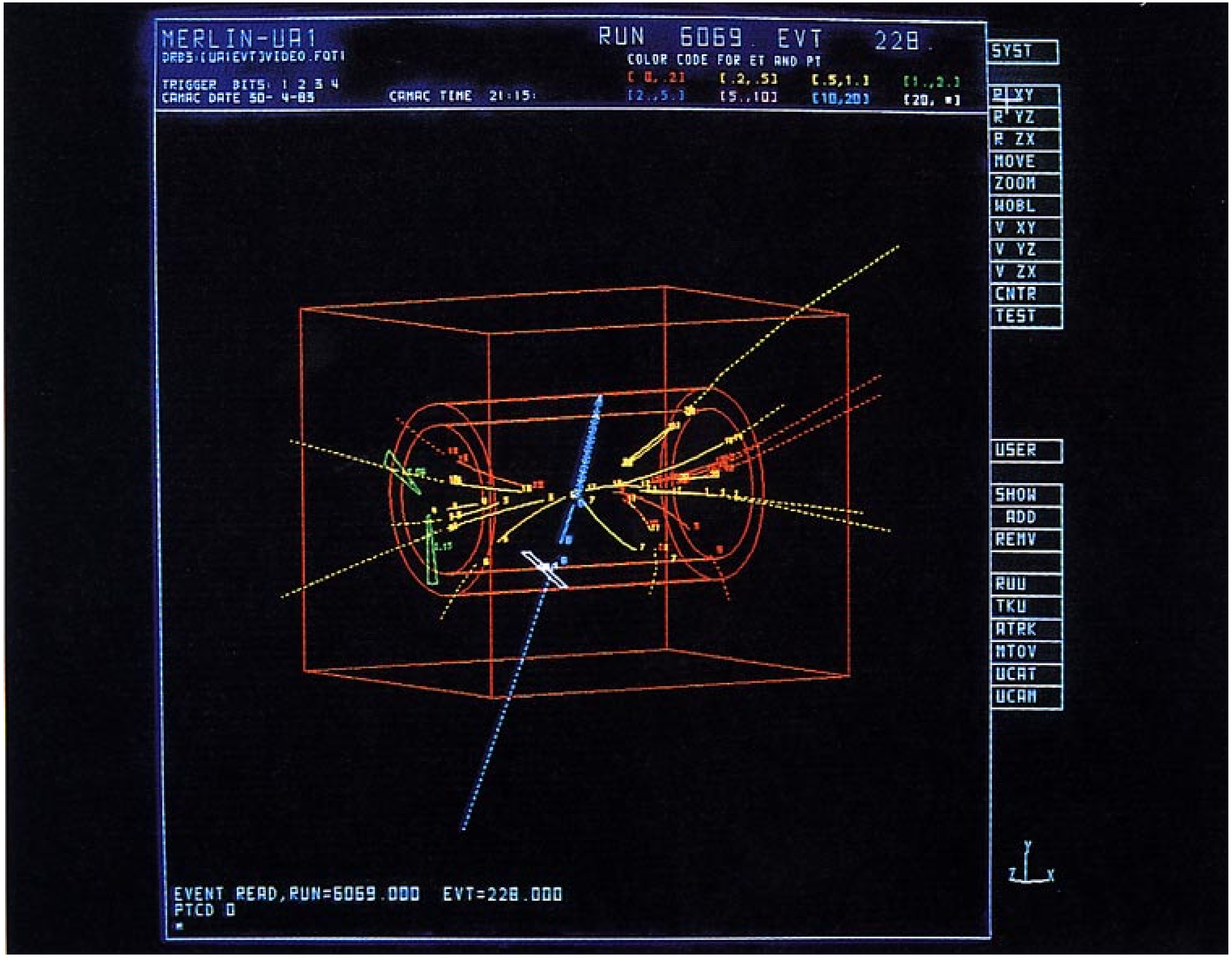

Identification of Muons

Muons identified by their penetration through about 10 λ of calorimeter material
The material of calorimeters absorbs the e's, γ's and $h^{\pm}$.

Hadron Punchthough

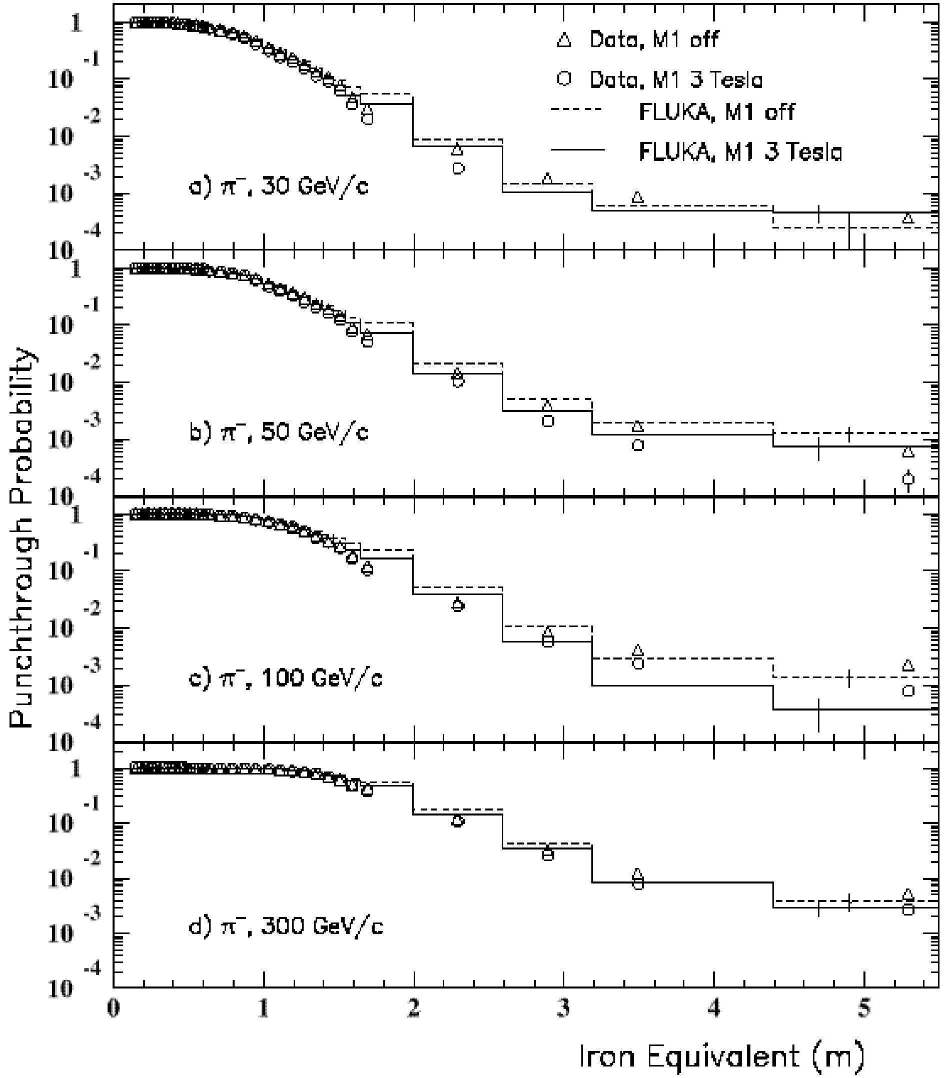

Energy Loss in Absorber

- for $E_{\mu} \leq$ 20-30 GeV - energy loss fluctuations dominate
- high energy muons generate their own background.

Hard bremstrahlung (catastrophic energy loss) can spoil μ-tracking. The critical energy for μ in Fe is $E_c \approx$ 350 GeV.

Hadron Punch-through

Debris from hadronic showers can accompany muons leading to:

- mis-identification of hadron as μ
- confusion and difficulty in matching μ-tracks (in jets)
- increase in μ trigger rate

Punchthrough and Radiation

Examples of particles trversing calorimeters and magnetiized Fe

RD5

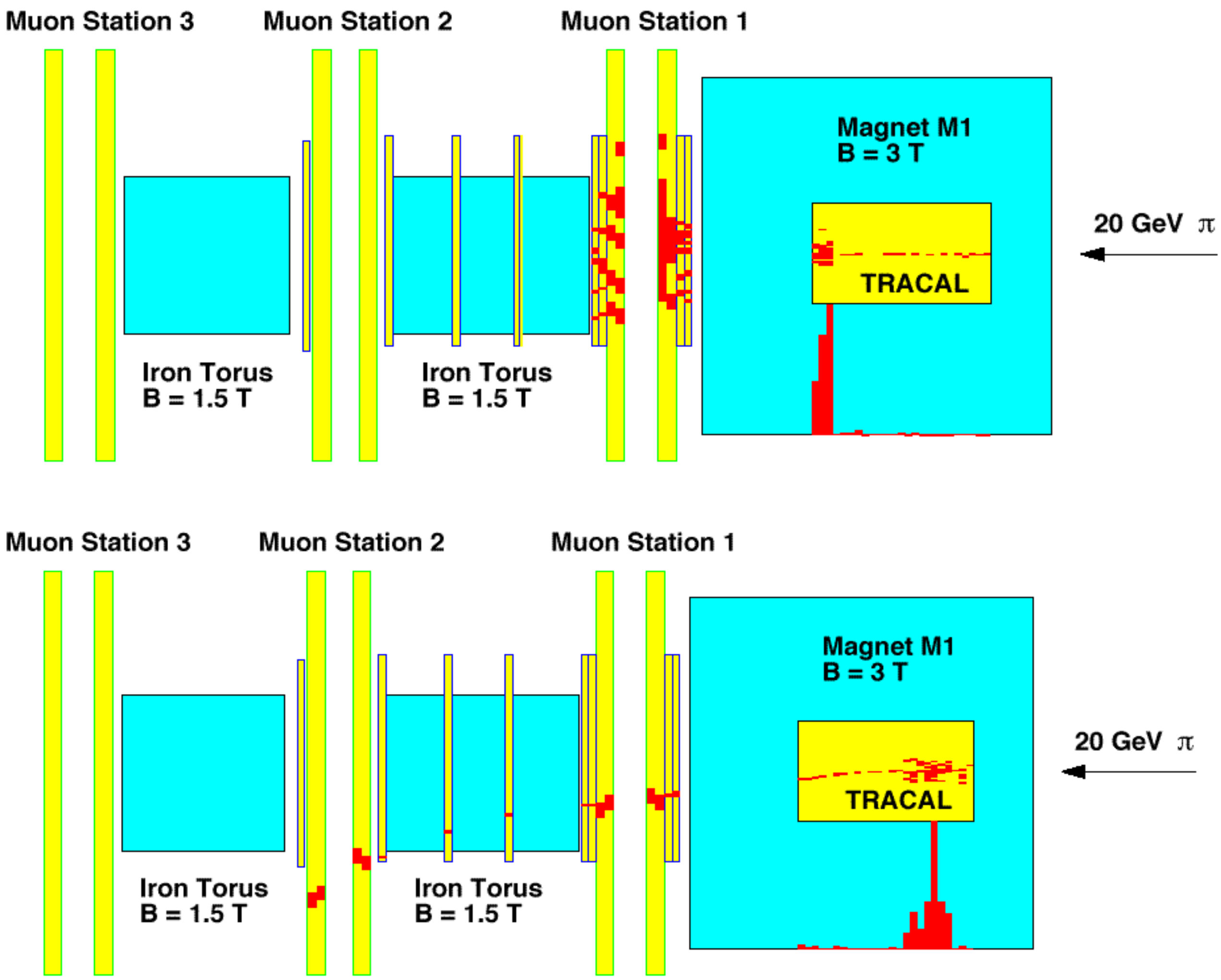

Simulation

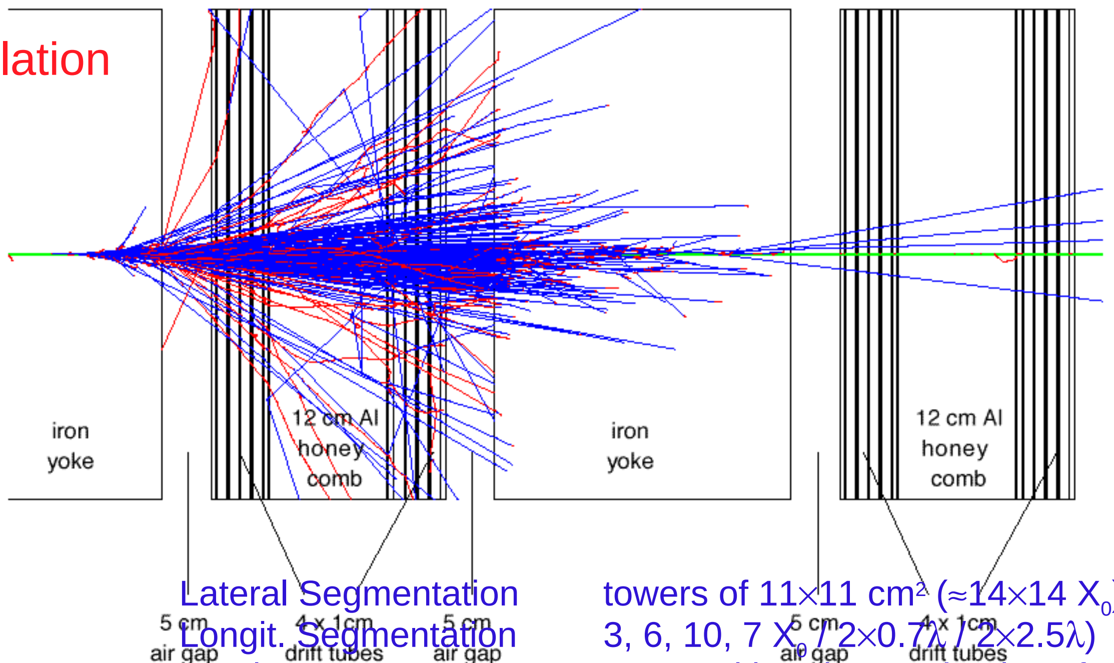

Lateral Segmentation
Longit. Segmentation
Preshower Detector

towers of 11×11 cm² (≈14×14 X_0)
3, 6, 10, 7 X_0 / 2×0.7λ / 2×2.5λ)
at 3X_0 with orthogonal strips of pitch 9mm

LHC Experimental Challenge

LHC Machine Parameters

pp collisions at	$\sqrt{s}$ = 14 TeV
design luminosity	L = 10^{34} $cm^{-2}s^{-1}$
bunch crossing interval	25 ns
pp interaction rate	10^9 interactions/s

High Interaction Rate

data for only ~100 out of the 40 10^6 crossings can be recorded per second

1st level trigger decision will take ~2-3 μs

⇒ front-end electronics needs pipelining

Large Particle Multiplicity

~ <20> superposed minimum bias events in each crossing at design luminosity

~ 1000 tracks emerge from the interaction region every 25ns

need highly ganular detectors with good time resolution for low occupancy

⇒ large number of channels

High Radiation Levels

⇒ radiation hard detectors and electronics

Muon System at LHC (pp)

Muon identification should be 'easy' at L > 10^{34} cm^{-2}s^{-1}

Muons can be identified inside jets

b-tagging

control efficiency of isolation cuts

Can trigger on and identify muons down to $p_t \approx 4$ GeV

acceptance for $H \to ZZ^* \to 4l$

CP Violation, top physics

Factors that Determine Performance

1st Level Trigger

rate from genuine muons ($b, c \to \mu X$) is very high

must make a p_t cut with v. high efficiency

large geometric acceptance ($|\eta| \geq 2$)

flexible threshold (p_t in the range 5 - 75 GeV)

Pattern Recognition

hits can be spoilt by

correlated backgrounds : δ's, e.m. showers, punchthrough

un-correlated : neutrons and associated photons

Momentum Resolution

high momenta : large $\int B.dl$,

good chamber resolution (< 100μm) & alignment

low momenta : inner tracking measurement is better than best stand alone measurement

Magnetic Field Configurations Layout of Muon System

1. Measure μ momentum in Inner Tracker and Identify μ in calorimeter and a backing calorimeter / filter
ALEPH, DELPHI, OPAL

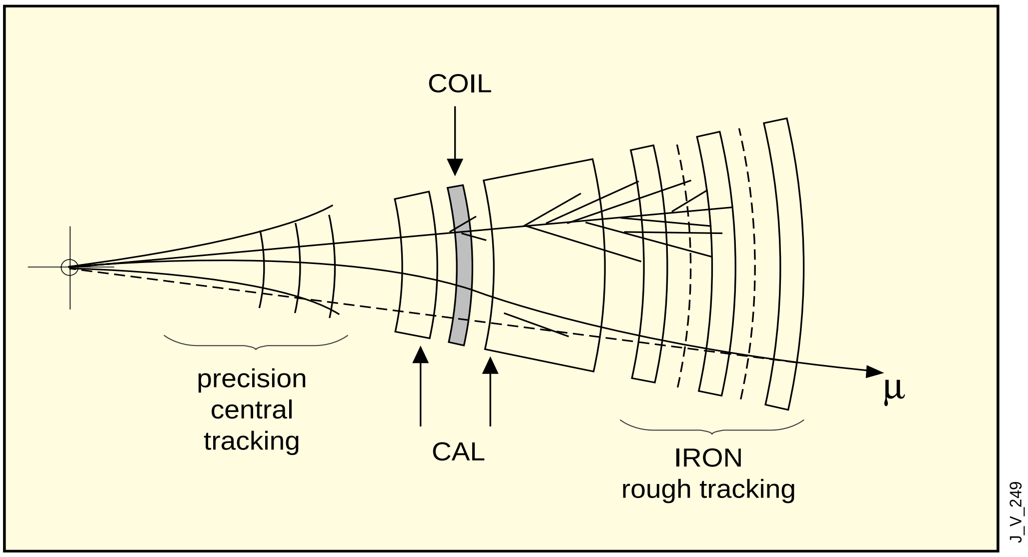

Cheap, but limited to low multiplicity, low rate

2. Identification and Measurement of muons after full absorption of hadrons
Absorb almost all hadrons in calorimeters. Measure μ momentum in relatively clean environ ment.
L3, ATLAS with a Toroid

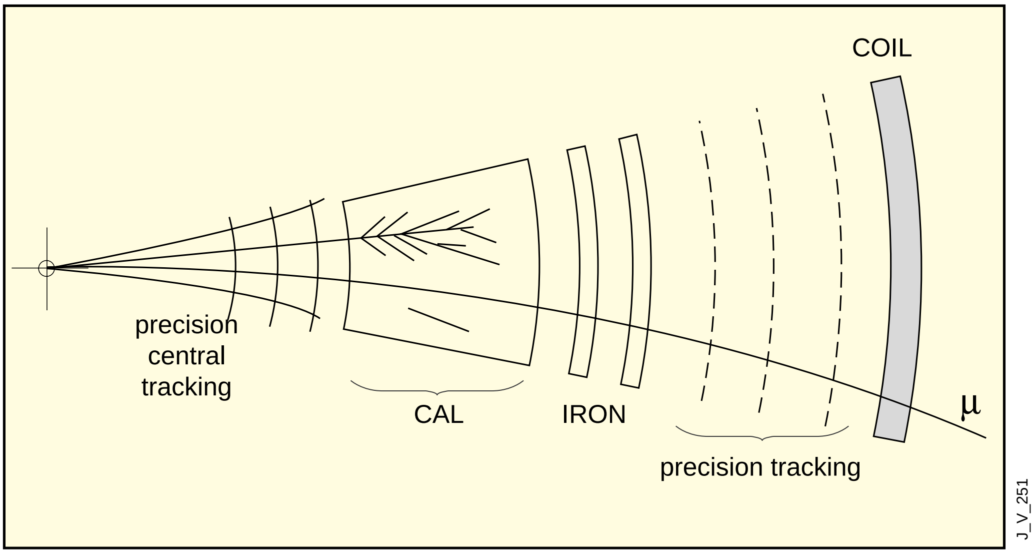

Safe for high multiplicities, need high $BL^2 \rightarrow$ expensive, good stand-alone measurement
+ solenod for inner tracking and precision measurement of low momentum muons

Magnetic Field Configurations
Layout of Muon System

3. Combined measurement of μ momentum in Tracker and Flux Return - Identify μ after full absorption of hadrons

High field solenoid after calorimetry. μ momentum precisely measured in inner tracking and after ≈10λ of calorimetry.

CMS

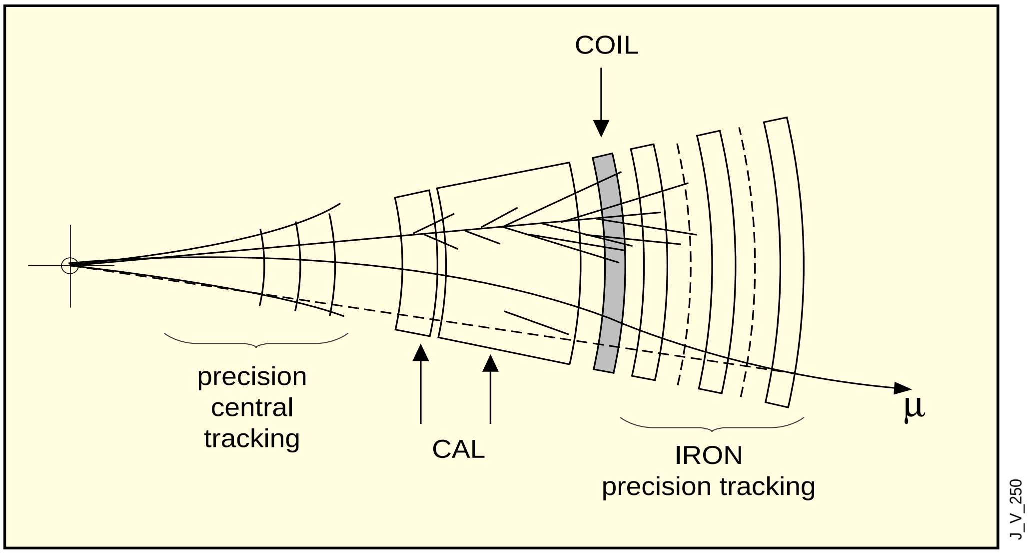

combination of the two momentum measurements gives a resolution better than weighted sum of the two

property of a solenoid
high momentum μ tracks point back to vertex after flux return

Air-Core Toroids

Advantages

- Constant resolution in p_t over wide η range (field decreases as 1/R)
- $\int B.dl \approx 1/\sin\theta$ compensating the Lorentz boost in forward direction
- good stand alone resolution - large BL^2
- reduce impact of muon radiation and soft hadron punchthrough

Drawbacks

- Bending not in transverse plane
- Need a solenoid to provide field for central tracker $\Rightarrow$ 4 magnets
- Solenoid coil before or after ECAL ?

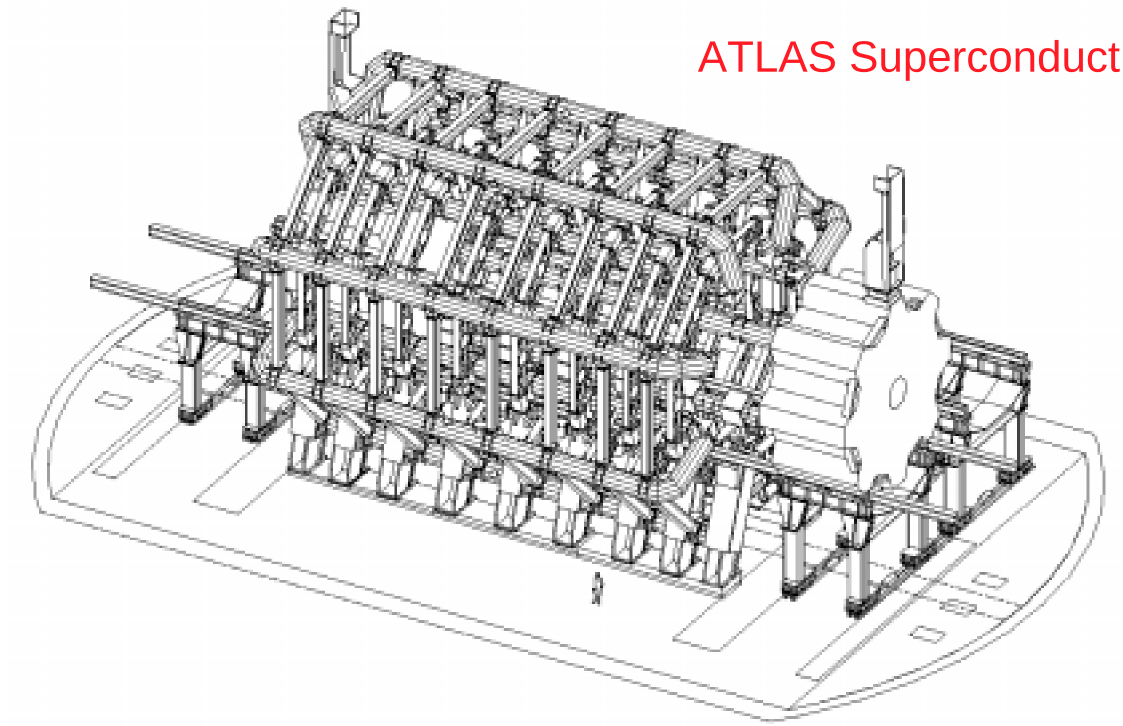
ATLAS Superconducting Toroids

For unambiguous sign measurement $\Delta p/p \leq 10\%$ measurement ,
$\langle B \rangle \approx 0.6$T over ≈ 4.5 m
$\Rightarrow$ sagitta of 0.5 mm for p_t=1 TeV $\mu \Rightarrow$ measure sagitta to 50 µm

Ampére's Theorem : $2\pi RB = \mu_0 nI \Rightarrow nI \approx 20 \times 10^6$ At
$\Rightarrow 2.5\ 10^6$ At for 8 coils, 2 x 2 x 30 turns
$\Rightarrow$ **I $\approx$ 20 kA $\Rightarrow$ superconducting coils**

Challenge

- Design of structure capable of holding the magnetic forces
- How to dissipate energy (1.5 GJ) in case of a quench?
- Spatial and alignment precision over large surface area.

Muon Momentum Measurement

Tracking in air-core magnetic field (e.g. ATLAS)

$$\frac{\Delta p}{p} = 26.7\ \sigma \sqrt{\left(\frac{1}{2N_1}+\frac{1}{N_2}\right)}\ \frac{p}{BL^2} \quad (\%)$$

p in GeV, B in T, σ and L in m

ATLAS : σ≈70 µm, $N_i \approx 6$, B≈0.6 T, L ≈ 4.5 m

→ Δp/p ≈ 0.8% at 100GeV

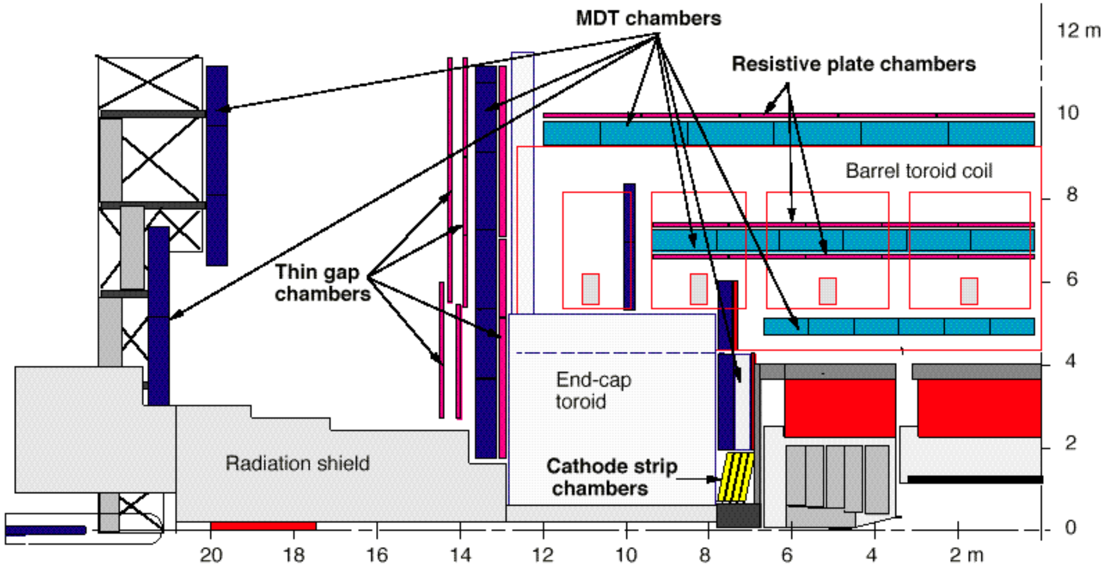

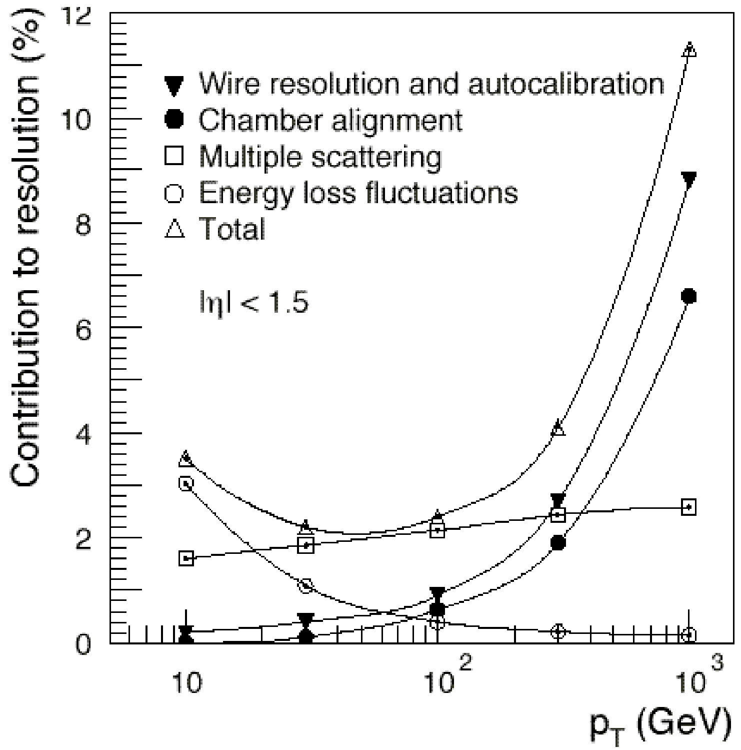

Figure 1-24 Contributions to the momentum resolution of the muon spectrometer, averaged over |η| < 1.5 and azimuthal angle, in a standard sector

Superconducting Solenoids

Advantages

- Large $\int B.dl$ for modest size
- bending in transverse plane ($r/\phi_{beam} \approx 20\ \mu m$!) and starts at primary vertex

Drawbacks

- Momentum resolution worsens as $L_c.\tan\theta/r_c$
- Large stored energy
- Conductor design for large fields

CMS Superconducting Solenoid

Field	4 T
Inner Bore	$\phi \approx 6$ m
Length, L	13 m
Current	19.5 kA
Stored Energy	2.7 GJ
Hoop Force	$\approx$ 64 atm

$B = \mu_0 n I$

n- no. of turns/m = 2168

$\Rightarrow I \approx 20$ kA

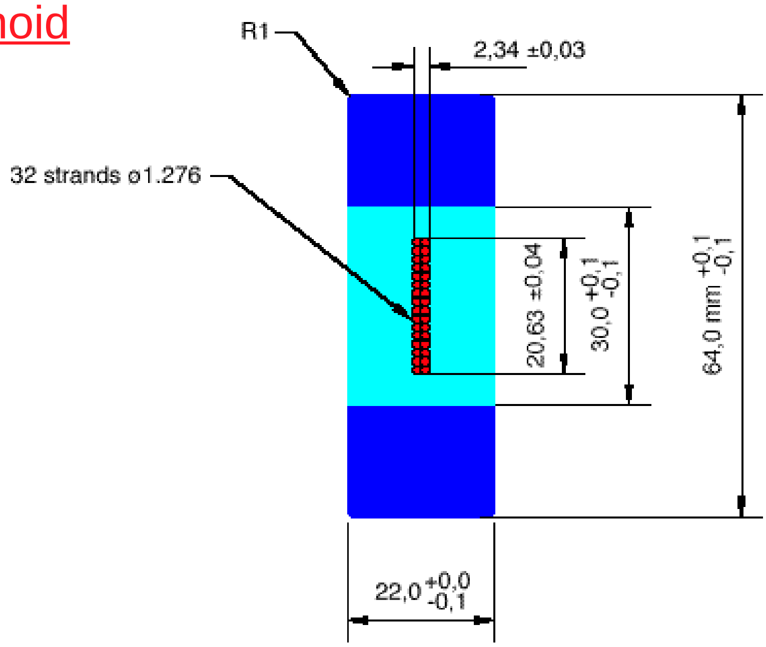

Challenge

- 4-layer winding needed to carry enough current to generate 4T
- Design of reinforced superconducting cable

CMS Solenoid

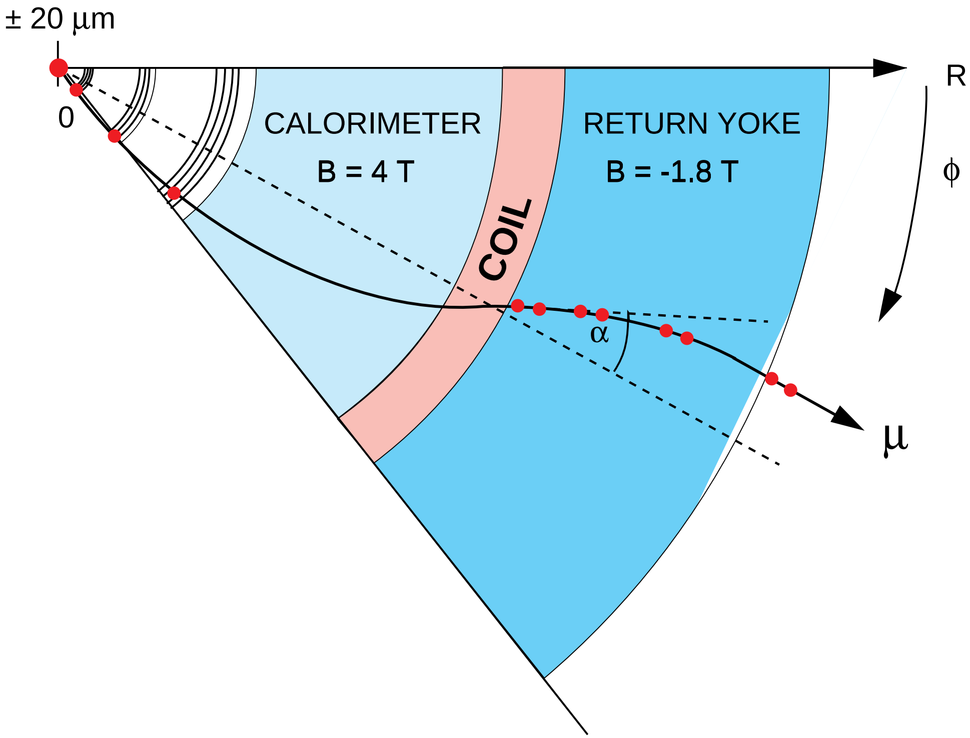

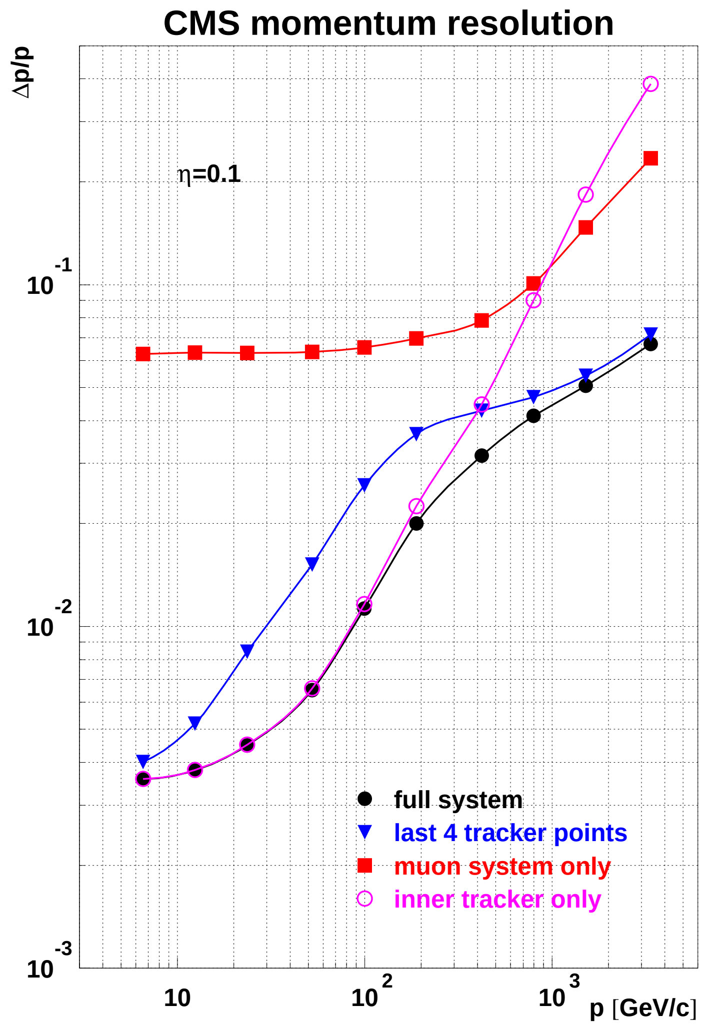

Tracking in Magnetized Iron (CMS)

(in multiple scattering dominated regime)

$$\frac{\Delta p}{p} \approx \frac{40\%}{B\sqrt{L}}$$

B~1.8T, and L ≈ 1.5 m

BUT stand-alone measurement is much better !

Rates in Muon System

Single muon rates for |η| ≤ 2.4

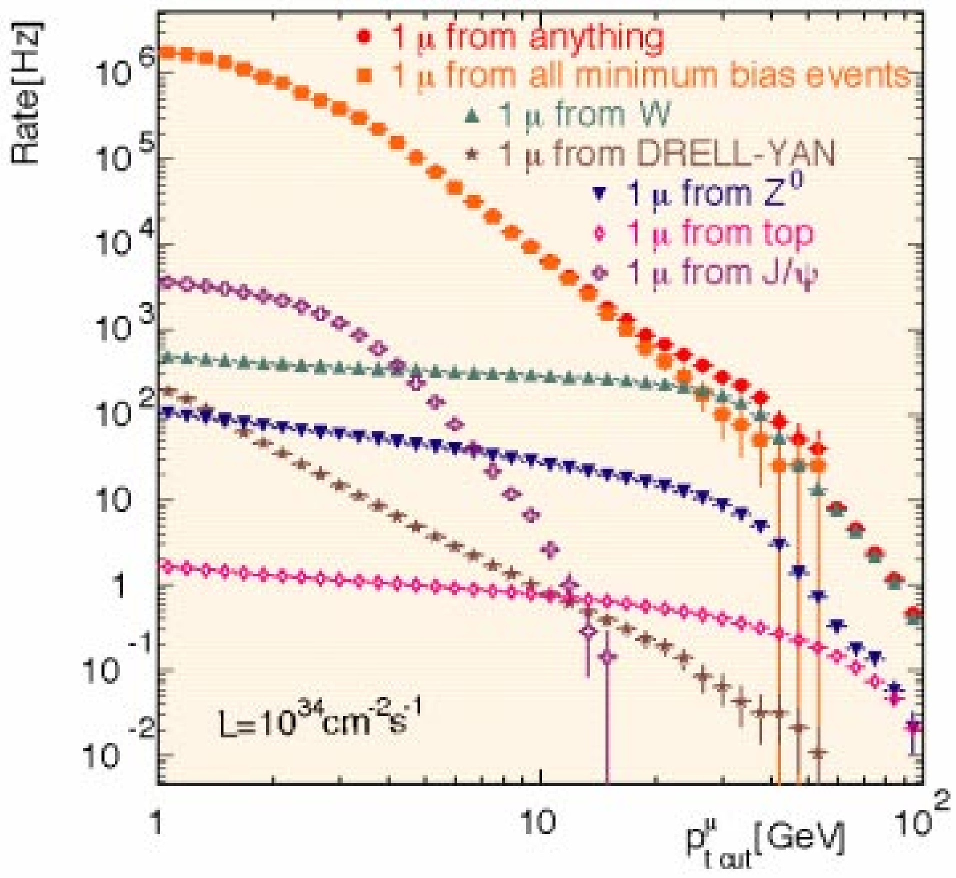

Hit rates from various sources in CMS Muon System

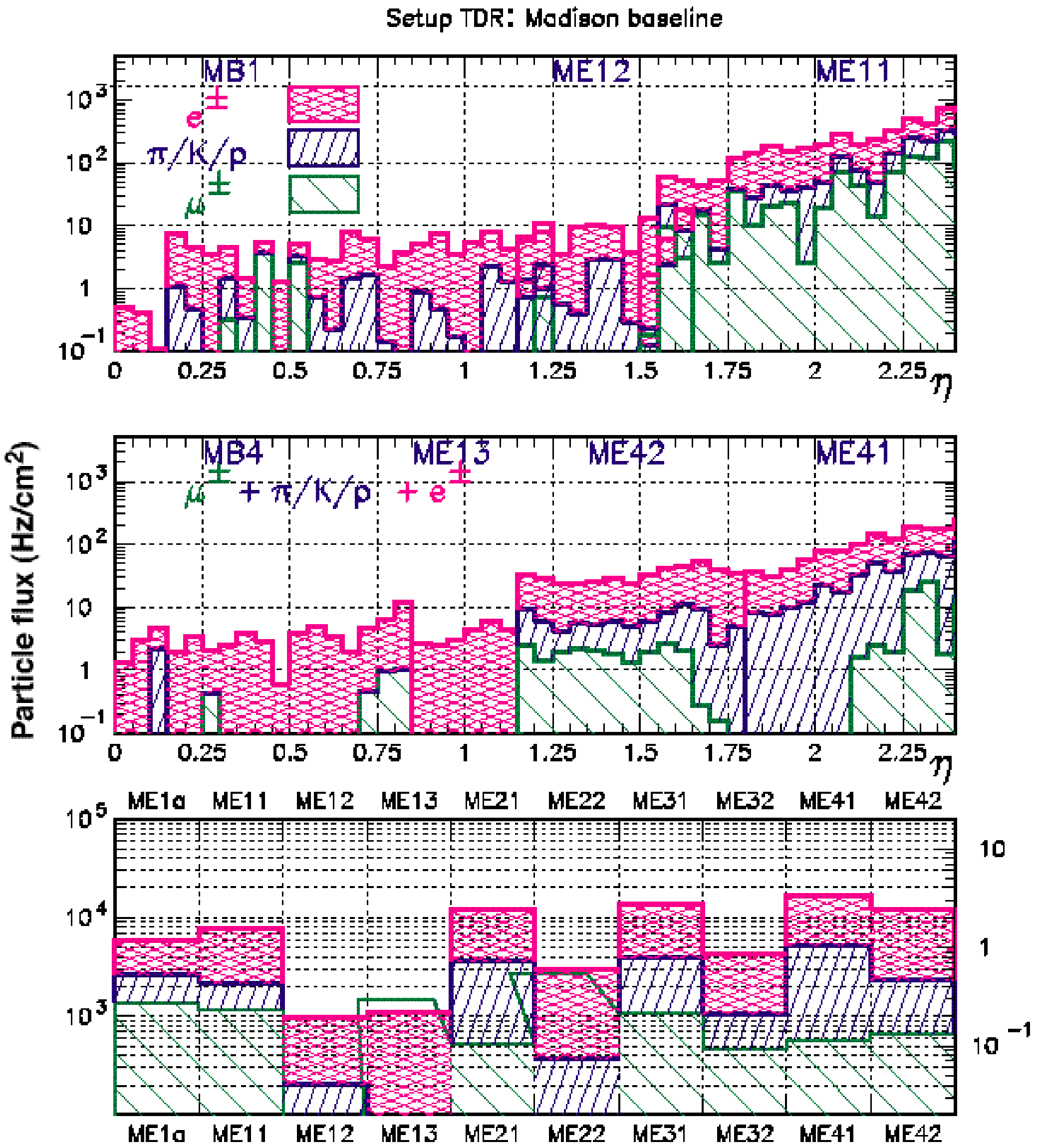

Muon Detectors

Two kinds of chambers - complementary functions

Accurate position measusurement for momentum determination
Level-1 Trigger

Drift Chambers - Low rate environment - Barrel ($t_{drift} \approx 400$ ns)

Cathode Strip Chambers - High rate environment - Endcaps (fast)

Less accurate position measurement but fast response (< 25ns)

Level-1 Trigger

Resistive Plate Chambers / Thin Gap Chambers

ATLAS Muon Monitored Drift Tubes

Principle of Operation

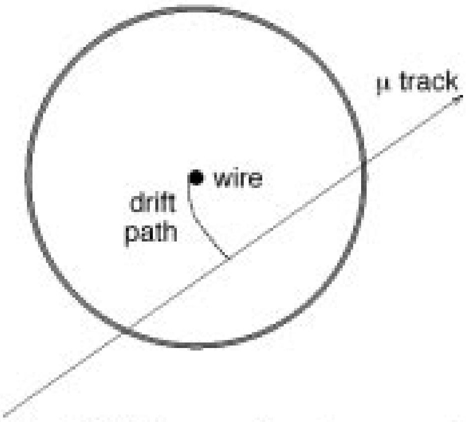

Figure 5-2 Drift tube operation in a magnetic field with curved drift path.

$\phi_{cathode}$ = 30 μm
ϕ_{wire} = 50 μm (W-Re)

Operating Parameters

Parameter	**Design value**
Gas mixture	$Ar/N_2/CH_4$ (91%/4%/5%)
Gas pressure	3 bar absolute
Track ionization	330 / cm
Gas gain	2×10^4
Wire potential	3270 V
Electric field at the wire	205×10^3 V/cm
Electric field at the wall	340 V/cm
Maximal drift time	500 ns
Averaged drift velocity	30 μm/ns
Effective threshold	22^{nd} electron
Resolution	80 μm

Drift Time-Distance Measurement

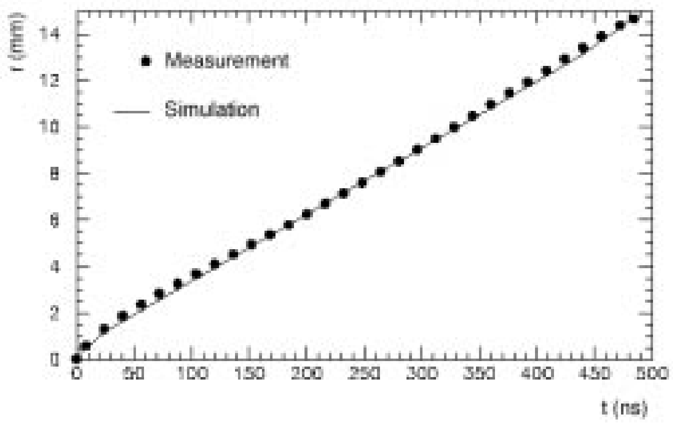

Figure 5-1 Relation between measured drift time and corresponding drift length in the absence of a magnetic field. $Ar/N_2/CH_4$ - 91 : 4 : 5 mixture.

Spatial Resolution as a function of drift distance

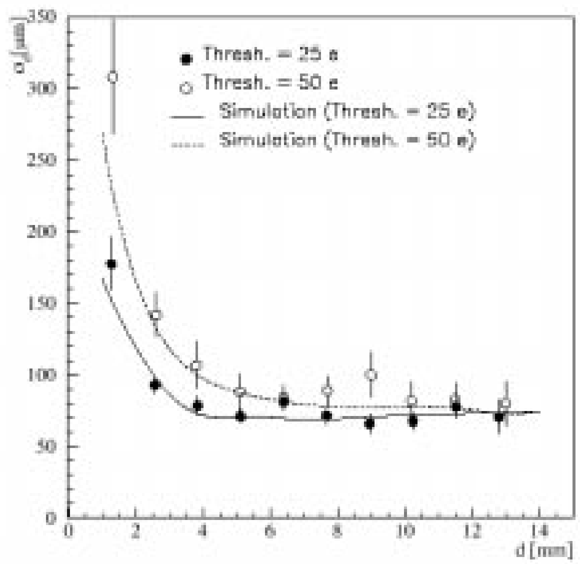

Figure 5-4 MDT resolution as a function of the drift distance, fo an Ar/N2/CH4 (91/4/5 mixture). The curves correspond to two discriminator threshold settings.

CMS Muon Drift Tubes

Drift Cell Layout

3 field shaping electrodes assure a linear space-time relationship

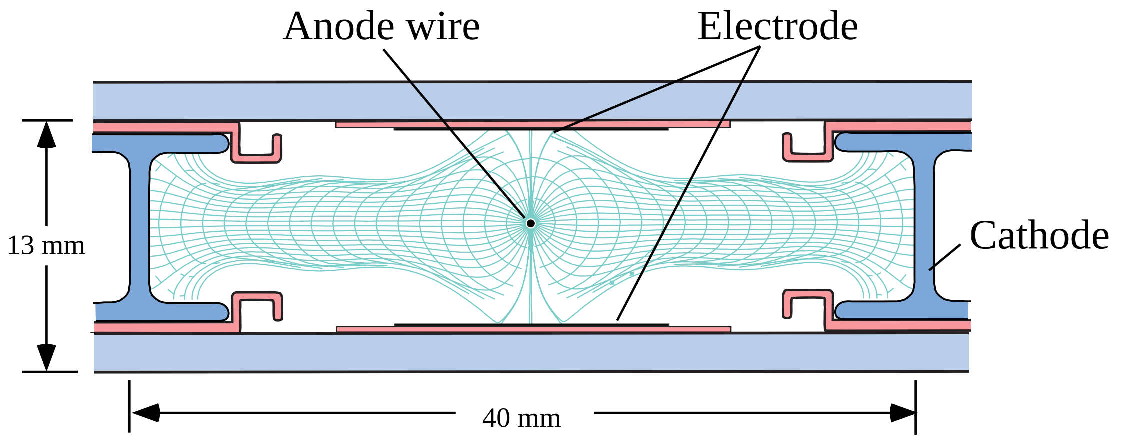

Operating Parameters

Nominal mixture	Ar - CO_2 (85% - 15%)
Nominal voltages	strips at 1800 V, wires at 3600, I-beams at -1800V
Gain (nominal setting)	9.10^4
Typical charge	1 pc
Cumulated charge	0.1 C/cm in 10 years of operation

Cathode Strip Chambers

Principle of Operation

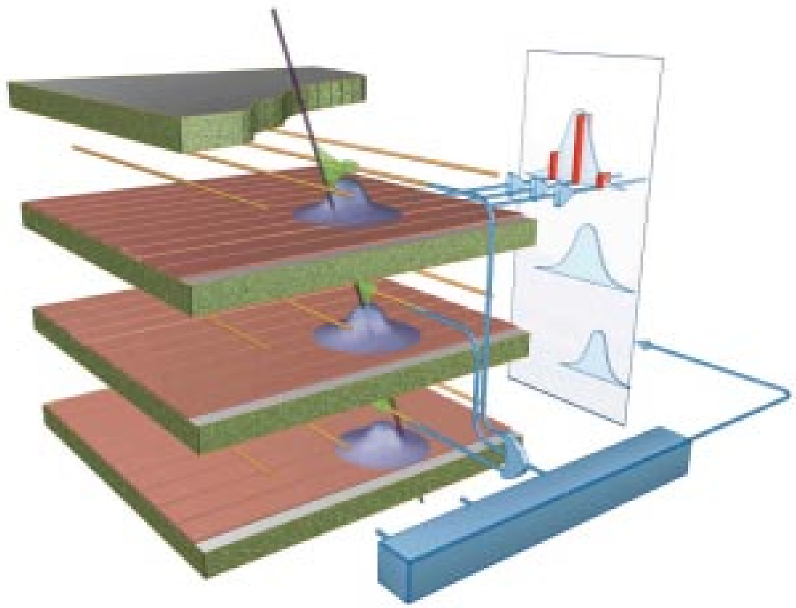

Spatial Resolution

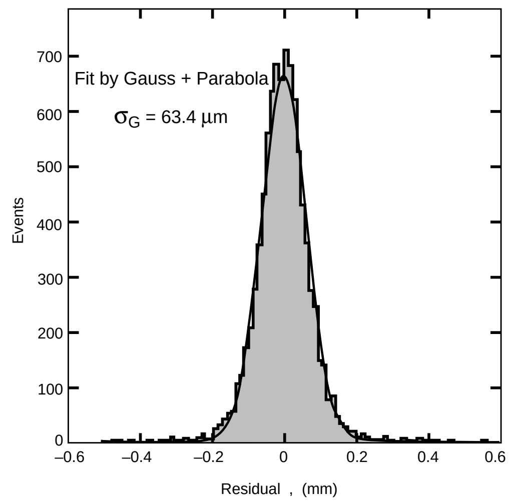

- Precise co-ord measured by interpolation of induced charge on strips
- Stereo coordinate is measured from signals on wires
- Closely spaced wires make CSC a fast detector

Operating Parameters

Nominal mixture	Ar-CO_2- CF_4 (30:50: 20)
Nominal voltage	3-4 kV
Gain	7.10^3

Muon Stations

ATLAS : Station comprising 6 layers of MDT Tubes

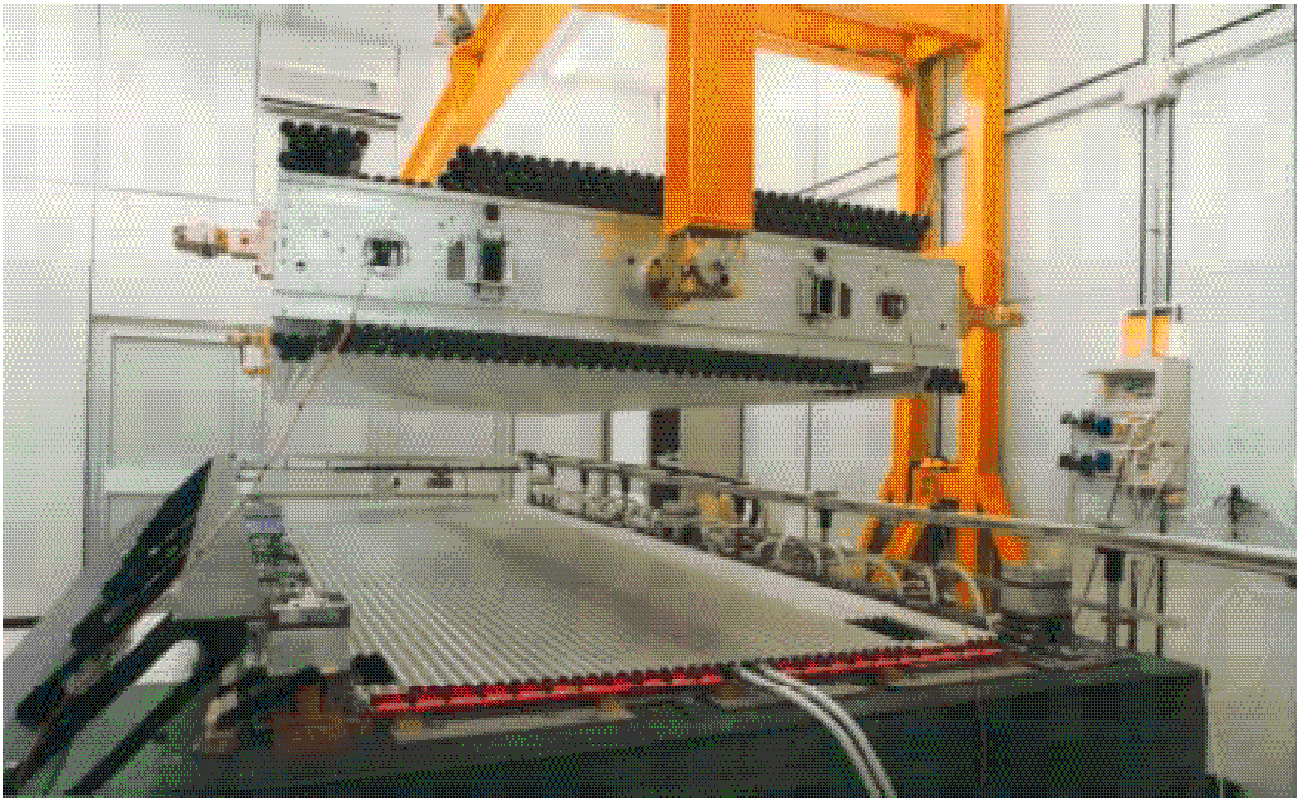

CMS : Station comprising Barrel Drift Tubes

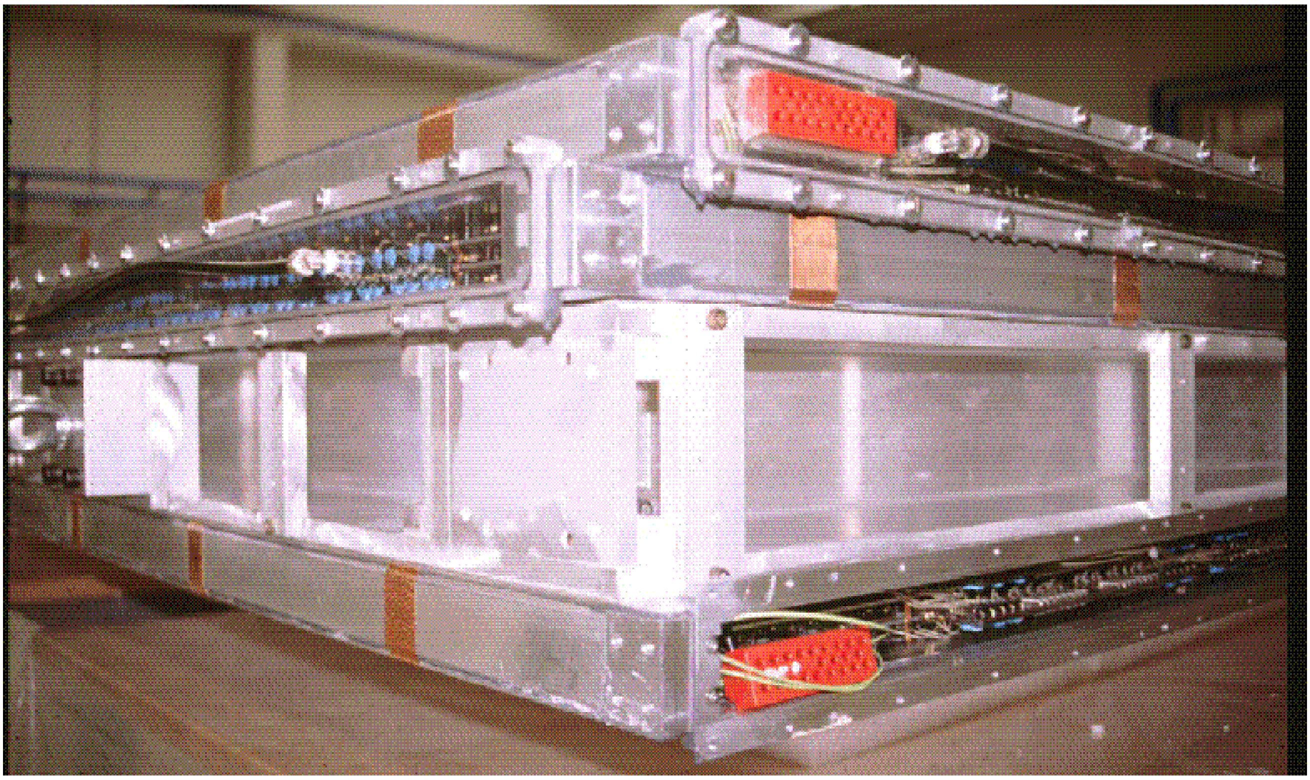

Inner Tracking

Role of a Tracker

measure the momentum and impact parameter of charged tracks with minimal disturbance

Factors that determine Performance

track finding efficiency - occupancy

momentum resolution

secondary vertex reconstruction

Benefits

precise momentum measurement

electron, τ and b-jet identification

secondary vertex and impact parameter measurement

isolation using charged tracks (p_t > 2 GeV)

ECAL calibration using p-E matching

only way to "SEE" the event (topological information)

CMS : isolation using charged tracks

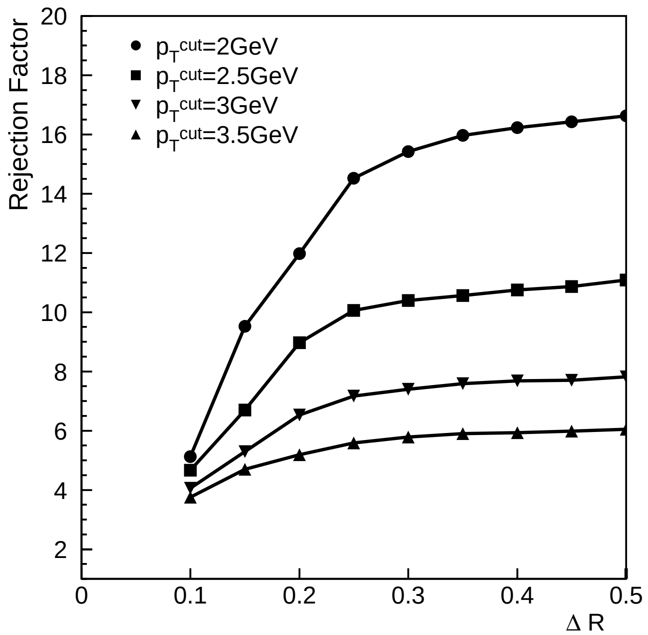

CMS: Isolation - E(3x3)/E(7x11) > 0.92

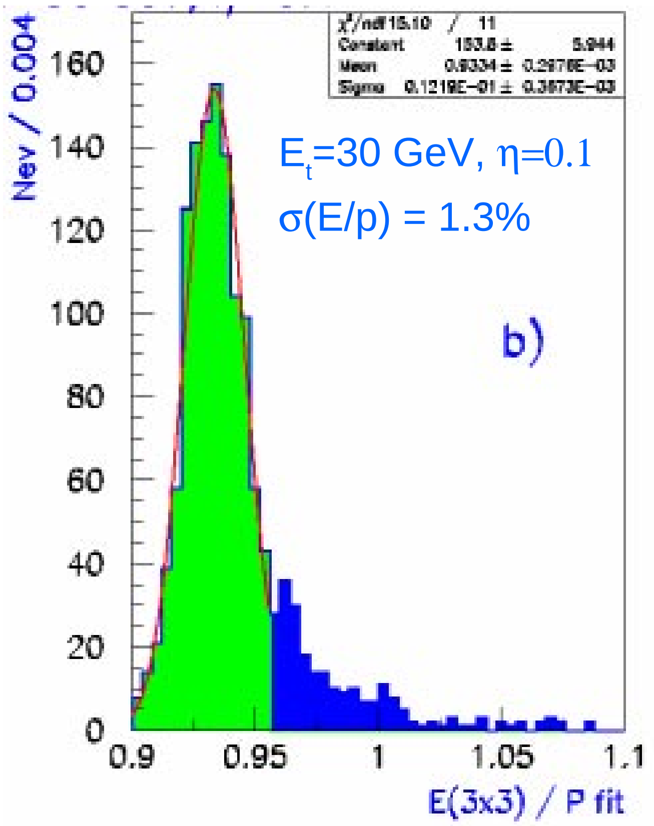

Radiation Levels in Inner Tracking

Radiation Levels in CMS Inner Tracker

(integrated over 10 years of operation i.e. 5.10^5 pb^{-1})

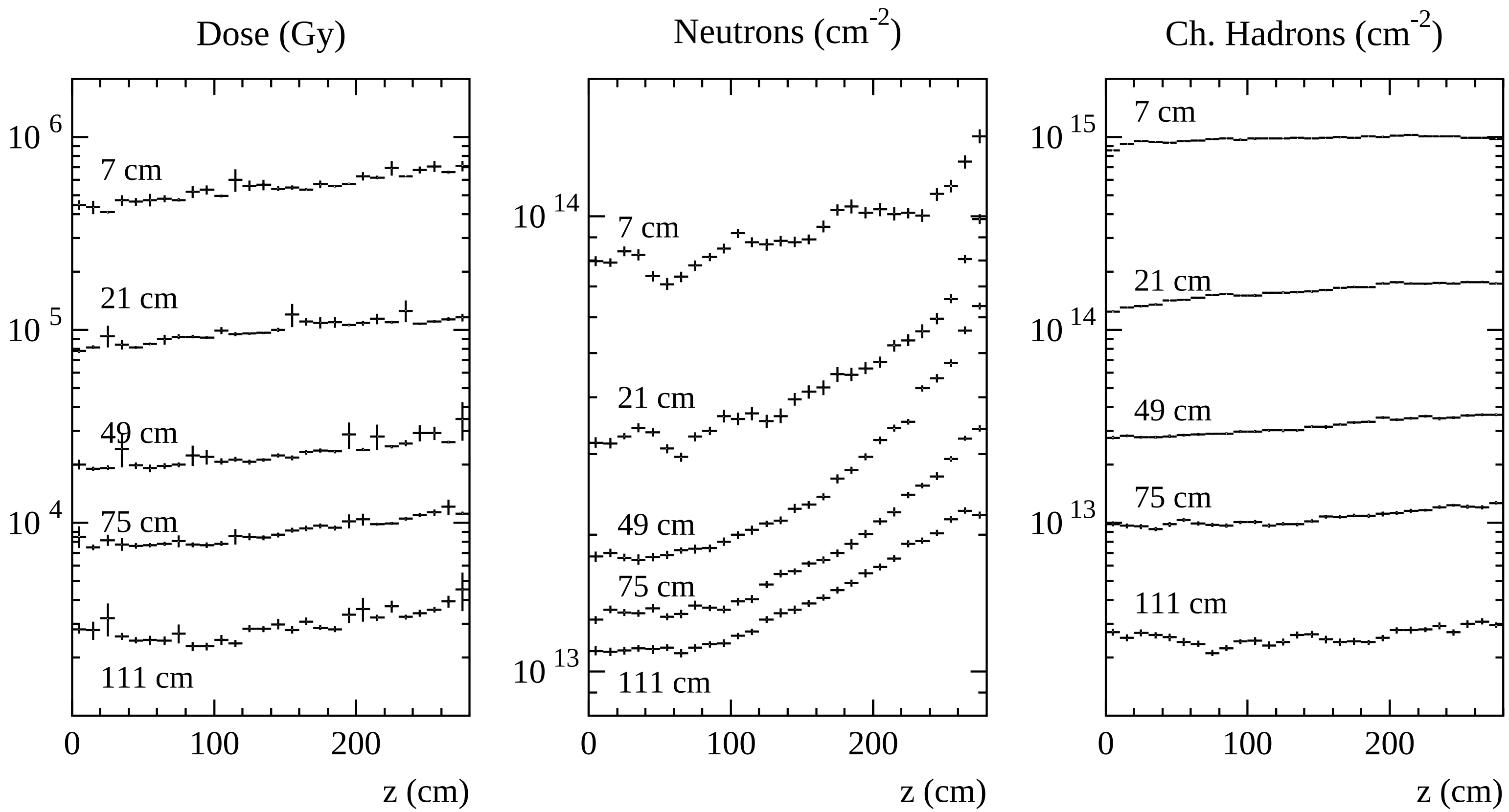

$\leq 4.10^7$ $h^{\pm}/cm^2/s$
pixels ($\approx 10^4$ μm^2)
occupancy $\approx 10^{-4}$

$\leq 4.10^6$ $h^{\pm}/cm^2/s$
Si μ-strip det.
($\approx$10 mm^2)
occupancy $\approx$ 1%

$\leq 4.10^5$ $h^{\pm}/cm^2/s$
Gas detectors.
($\approx$1 cm^2)
occupancy $\approx$ 1%

Charged Particle Tracking Devices

Bubble Chambers

Many discoveries in the 60' and 70's

Now Obsolete

Low repetition rates (< 10 Hz)

HEP moved on to study of low σ processes

Lack of triggering capability

Electronic Bubble Chambers

Time Projection Chambers

3-D spatial information with high granularity

Some particle identification using dE/dx

Not used in pp experiments at LHC

Long drift times (25 - 45 μs)

Suitable for LEP - low event rate (+ long bunch crossing time)

Tracking Detectors for LHC

Search for rare processes

very high particle rates (4.10^{10} particles/s emerging from interaction region)

very short bunch crossing time (25 ns)

semi-conductor pixels, microstrip detectors

short drift time (< 50 ns) gaseous detectors (straws, MSGCs etc)

Proportional Wire Chambers

Fast charged particles ionise atoms of gas

if W = energy to create an e-ion pair then

total ionisation n_{total} = ΔE/W = (dE/dx)Δx/W

$n_{total} \approx$ 3-4 $n_{primary}$

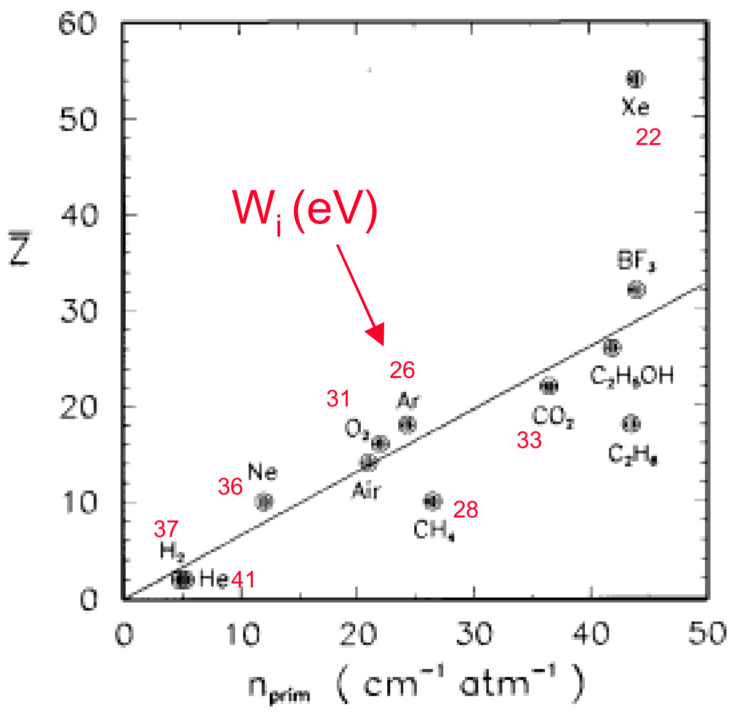

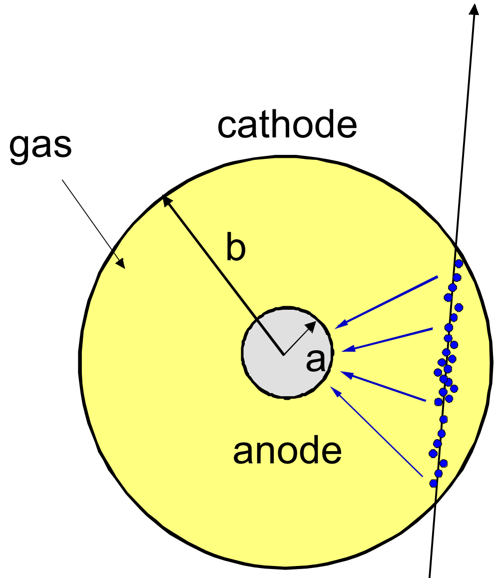

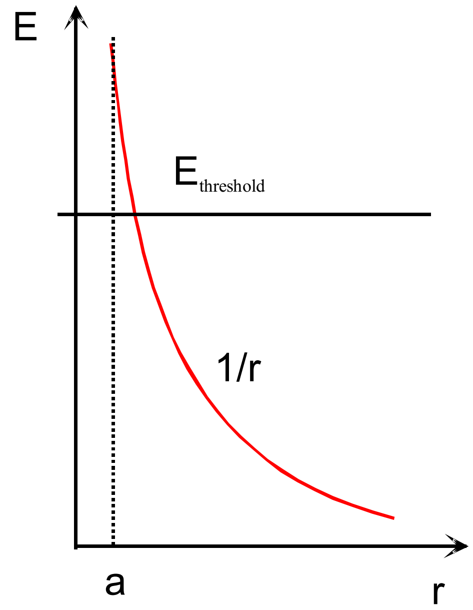

$$E(r) = \frac{CV_0}{2\pi\varepsilon_0} ? \frac{1}{r}$$

$$V(r) = \frac{CV_0}{2\pi\varepsilon_0} ? \ln\frac{r}{a}$$

C = capacitance / unit length

≈ 100 electron-ion pairs are not easy to detect

noise of a fast amplifier ENC ≈ 1000 e !

Need amplification in gas

Electric field close to the wire is sufficiently high for the electrons to gain enough energy to ionise further → exponential increses in e-ion pairs

Gain in Wire Chambers

Prob. an electron will produce an ionising collision with an atom in distance dr is

$N_a \sigma_i dr$ where N_a = no. of atoms/unit volume

Increase in no. of electrons after dr is

$dn = n N_a \sigma_i dr$

Let $N_a \sigma_i = \alpha$ i.e. larger the value of α, the more the collisions per unit distance.

Define $\alpha = 1 / \lambda_{coll}$ λ - mean free path length

(a known as the 1st Townsend coeff. giving e-ion pairs/cm)

$dn = n \alpha(r) dr$

α is a function of r as it varies with electric field which usually varies with r

$$\therefore \; n = n_0 \exp \int_a^{r_c} \alpha(r) \; dr$$

where n_0 = no. of electrons present initially

$$Gain \;\; M = \frac{n}{n_0} = \exp \int_a^{r_c} \alpha(r) \; dr$$

$$\text{infact} \;\; M \;\alpha\; e^{CV_0}$$

Consider what happens near a anode wire

r (µm)	E (kV/cm)	α (ip/cm)	λ=1/α (µm)
10	200	4000	2.5
20	100	2000	5
100	20	80	125
200	10	≈1	1 cm

50% (90%) of electrons produced ≈ 2.5 (10) µm from anode wire !

Detector Gas Mixtures

Avalanche multiplication occurs in all gases

BUT desire low working voltage, stable operation at high gain, high rate capability, long lifetime, fast recovery

Principal component of a desirable gas - noble gas (e.g. argon)
- allows multiplication at relatively low E-field
- does not have molecules, produces only elastic scattering (little loss of energy)

Argon gives more primary ionization than He or Ne (Kr and Xe give even more but are expensive)

Counter full of argon does not give stable operation

- during avalanche process many excited Ar atoms decay emitting UV photons (e.g. 11.6 eV for Ar)
- UV γs strike cathode (usually Cu clad with inoization threshold of 7.7 eV) and eject photoelectrons which give rise to another avalanche

$\Rightarrow$ **positive feedback - continuous discharge**

Chamber filled with pure Ar suffers such breakdown at low gain

Polyatomic gases have many non-radiative vibrational and rotational excited states over a wide energy range

If chamber contains a fraction of such a gas, its molecules will absorb energy from excited argon atom by colliding with it or dissociating it into smaller molecules

Since $\tau_{emission} >> \tau_{collision}$ UV γ emission is 'quenched'

Presence of quenching gas can give enormous increase in stable obtainable gain e.g. isobutane (C_4H_{10}, Methane (CH_4)

common property of hydrocarbon, alcolhol families

Operation Modes of Chambers

At very low voltages, charges begin to be collected but recombination is still the dominant process

ionization mode - at higher voltage full charge collection begins

multiplication - at a certain voltage called the threshold voltage (V_T) the electric field close to the surface of the anode is large enough to begin process of multiplication

proportional mode - increasing V_0 above V_T results in gains > 10^4 with detected charge α primary deposited charge

limited proportionality - at even higher voltages proportionality is gradually lost - consequence of electric field distortions due to space charge around the anode

Geiger mode - the region of limited proportionality eventually ends in a region of saturated gain - same size of signal independent of orignal deposition

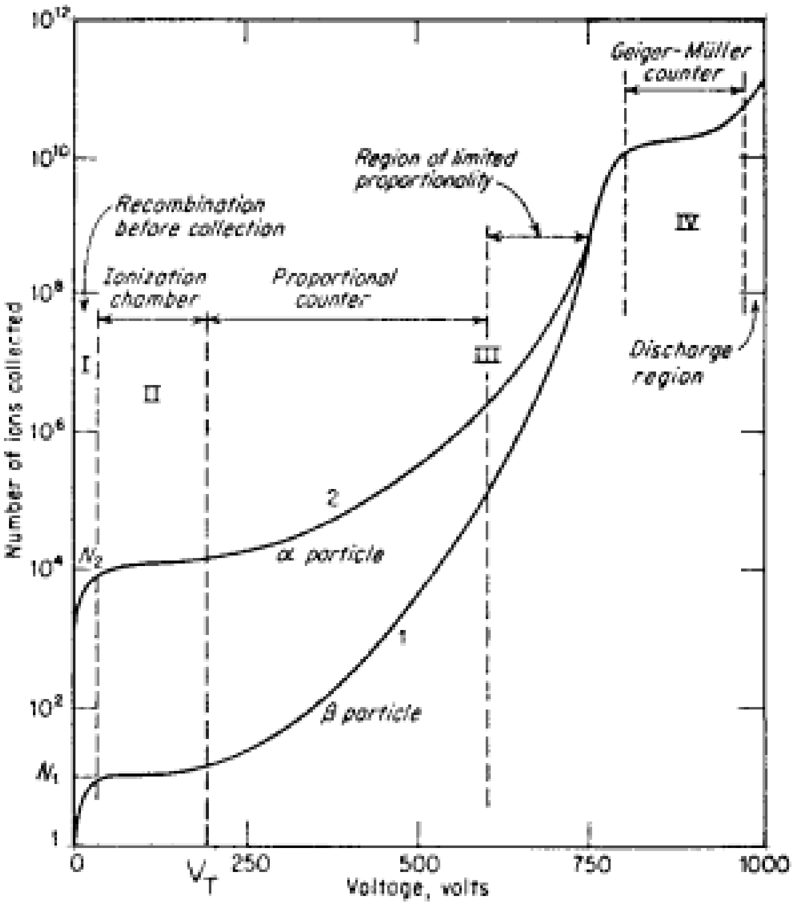

Time development of Signal

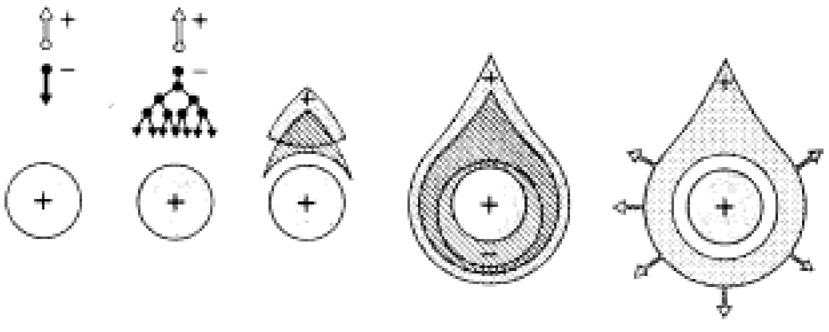

Consider a single primary electron drifting towards the anode (at ≈ 5 cm/µs) into region of increasingly high field

Typically at a radius of few wire radii, electric field is large enough and primary electron gains enough energy to cause ionisation

Due to lateral diffusion a drop-like avalanche surrounding the wire develops

Whole process of avalanche multiplication lasts ≈ 1 ns

Electrons are collected very fast (≈ 1 ns) as drift distance is few µm

+ve ions drift slowly towards the cathode.

signal on anode and cathode is induced by the moving charges
- electrons move v. short distance and induce very little signal
- ion drift determines the time development and size of induced signal

$$I(t) = \frac{Q}{2t_0 \ln(b/a)} \left(\frac{1}{1+t/t_0} \right)$$

t_0 - characteristic time

Total drift time of ions for Ar at NTP, a=10µm, b=8mm, C=8pF/cm, μ^+=1.7 cm^2 V^{-1}s$^-$, V_0=3 kV is **550 µs**.
Time growth is very fast (≈1/1000 if total drift time)
Normal practice to terminate counter with a resistor R such that signal is differentialted with a time constant RC allowing v. short pulses and high rate capability

Induced Charge

Suppose a charge q located at r from the wire moves a distance dr. Change in P.E. is

$$dU = q \frac{d\phi}{dr} dr$$

For a cylindrical capacitor, length l, capacitance C /unit length, electrostatic energy contained in electric field is

$$\frac{1}{2} l C V_0^2$$

$$dU = lCV_0 \, dV = q \frac{d\phi}{dr} dr$$

induced voltage change is $dV = \frac{q}{lCV_0} \frac{d\phi}{dr} dr$

Assume that <multiplication> occurs at a distance λ from the anode. Total induced voltage on anode by the electrons is (E=-dϕ/dr)

$$V^- = \frac{-q}{lCV_0} \int_{a+\lambda}^{a} \frac{d\phi}{dr} dr = \frac{-q}{2\pi\varepsilon l} \ln \frac{a+\lambda}{a}$$

while that by positive ions is :

$$V^+ = \frac{+q}{lCV_0} \int_{a+\lambda}^{b} \frac{d\phi}{dr} dr = \frac{-q}{2\pi\varepsilon l} \ln \frac{b}{a+\lambda}$$

For a = 10 µm, b= 3 mm and λ = 1 µm

$$\frac{V^-}{V^+} = \ln \frac{a+\lambda}{a} \Big/ \ln \frac{b}{a+\lambda} \approx \frac{0.095}{5.7} \approx 1.7\% \ !$$

The induced signal from electrons can be ignored. Then for total charge Q,

$$V(t) = -\frac{Q}{2\pi\varepsilon l} \ln \frac{r(t)}{a}$$

Time Development

Consider the drift of +ve ions with drift velocity

$$W^+ = \frac{dr}{dt} = \mu^+ \frac{E}{p} \qquad \frac{dr}{dt} = \mu^+ \frac{CV_0}{2\pi\varepsilon} \frac{1}{r} \frac{1}{P}$$

where μ⁺ the ion mobility (≈ 1 $cm^2 V^{-1} s^{-1}$, E is the electric field strength and P the pressure

Radius of shell at time t

$$\int_a^r r \; dr = \frac{r^2 - a^2}{2} = \int_0^t \mu^+ \frac{CV_0}{2\pi\varepsilon P} \, dt$$

$$r(t) = \sqrt{a^2 + \mu^+ \frac{CV_0}{\pi\varepsilon P} t} = a \sqrt{1 + \frac{t}{t_0}}$$

$$t_0 = \frac{a^2 \pi\varepsilon}{\mu^+ CV_0} = \frac{a^2}{\mu^+} \frac{\ln(b/a)}{V_0}$$

Combining with (a)

$$V(t) = -\frac{Q}{2\pi\varepsilon l} \ln\frac{r(t)}{a} = -\frac{Q}{4\pi\varepsilon l} \ln\left(1 + \frac{t}{t_0}\right)$$

If voltage acros counter is held constant, then charge must flow onto anode to provide a voltage across the capacitance lC which compenstaes the voltage between the anode and the +ve shell

$$Q(t) = -lC \; V(t) = l \frac{2\pi\varepsilon}{\ln(b/a)} V(t)$$

The induced current then is

$$I(t) = \frac{Q}{2t_0 \ln(b/a)} \left(\frac{1}{1 + t/t_0}\right)$$

Total drift time of ions

$$T = \frac{t_0}{a^2}(b^2 - a^2)$$

E.g. Ar at NTP, a=10µm, b=8mm, C=8pF/cm, µ+=1.7 $cm^2 V^{-1} s^{-}$, V_0=3 kV is **550 µs**.

Drift Chambers

Spatial information obtained by measuring time of drift of electrons

• need a trigger to signal the arrival of particles (bunch crossing or scintillator)

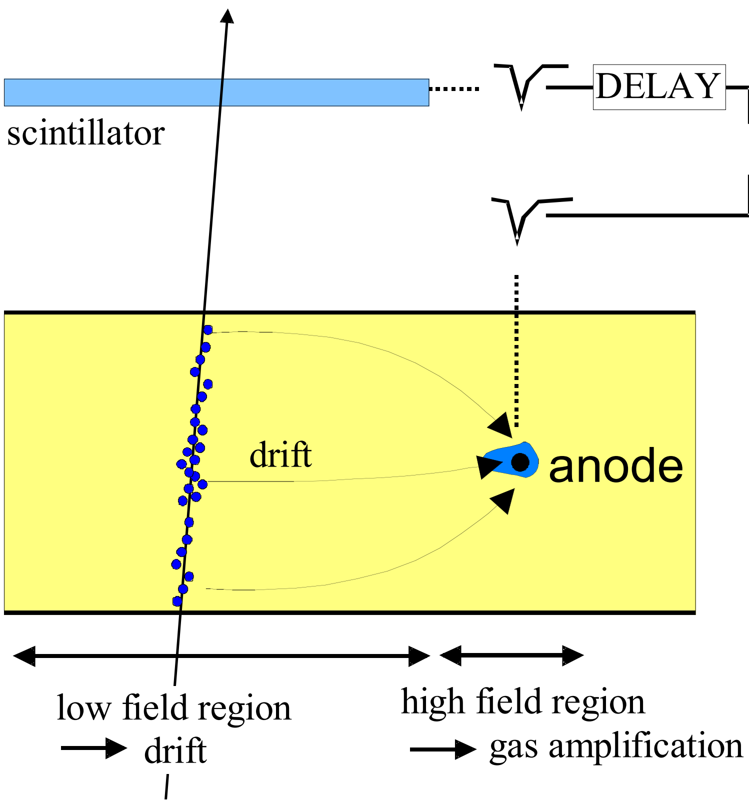

Measure arrival time of electrons at sense wire relative to a time t_0

Advantage

relatively small no. of wires and electronics needed

Choice of Gas

• high purity - electrons captured if electronegative impurity present
  the longer the drift path, the higher the required purity level
• gas exhibiting drift velocity saturation at not too high a field
  drift velocity less sensitive to field inhomogenieties, operating voltage, temperature etc.
• fast gas - for high counting rates
  max. counting rate limited by drift time (10^4 count/s/mm of wire)

Time Projection Chamber

TPC $\rightarrow$ 3-D imaging drift chamber - electronic bubble chamber

Basic Structure

- large gas filled cylinder with a thin HV electrode middle plane
- uniform axial parallel electric and magnetic fields (along axis)
- ends of cylinder covered by sector arrays of prop. anode wires
- parallel to each wire is a cathode strip cut in rectangular pads

e.g. ALEPH TPC

Dimensions : ϕ = 3.6 m, L = 4.4 m, (91%Ar:9%CH_4) at 1 atm

Electron drift time = 45 µs

r-ϕ interpolating signals induced on precisely located cathode pads

z from drift time

dE/dx information

diffusion significantly reduced by B-field

performance improved by laser calibration + p, T corrections

$\sigma_{R\phi} \approx 170$ µm, $\sigma_z \approx 740$ µm $\quad \frac{\sigma_{p_t}}{p_t} \approx 0.1\% \; p_t \oplus 0.3\% \; (GeV)$

Time Projection Chamber

1.2 T solenoidal field

Ar:CH_4 / 91%:9% at 1 atm
electron drift time ≈ 45 µs

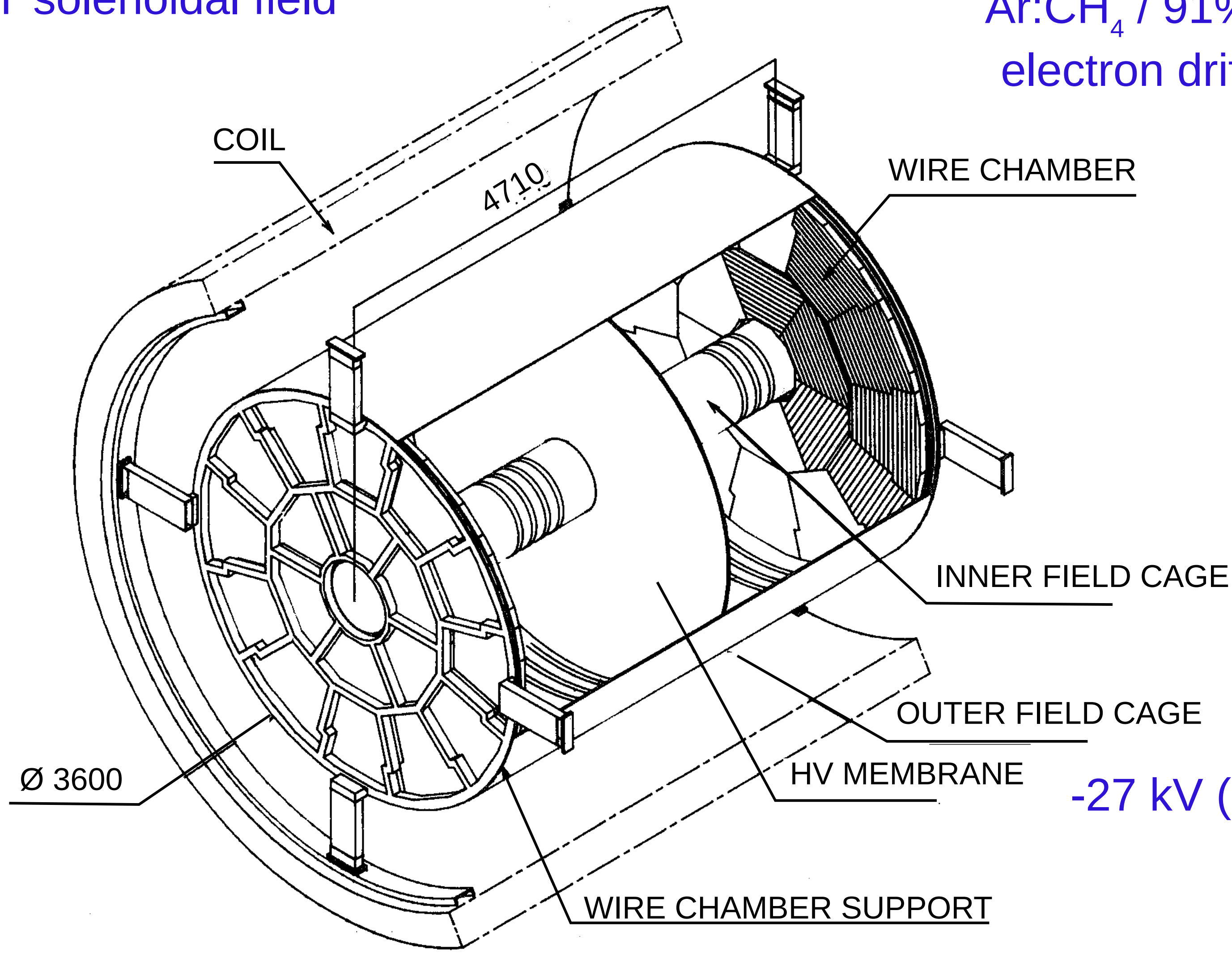

-27 kV (115 V/cm)

Microstrip Gas Chambers

MSGCs are made with micro-electronics technology
precision of lithographic techniques is ≈ 0.1 - 0.2 µm

Overcome two major limitations of MWPCs

- spatial resolution orthogonal to the wire limited by wire spacing (typically ≈ 1 mm)
- rate capability is limited by long ion collection time (typically ~ mm taking several tens of µs)

e.g. CMS : 225 m^2, 6.6 M ch., r-ϕ pitch 200 µm

Principle of Operation

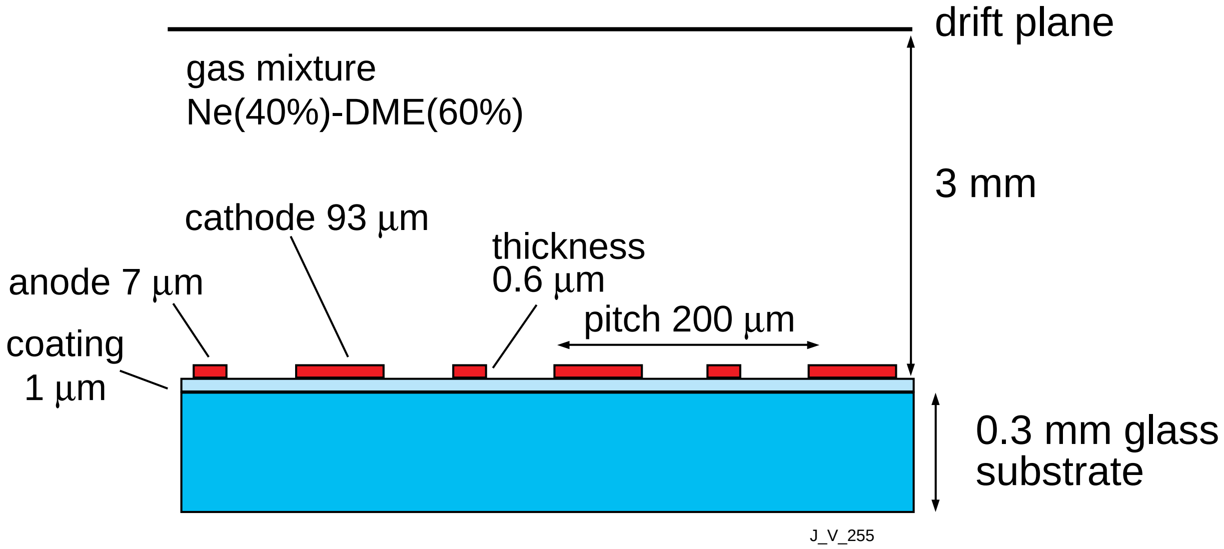

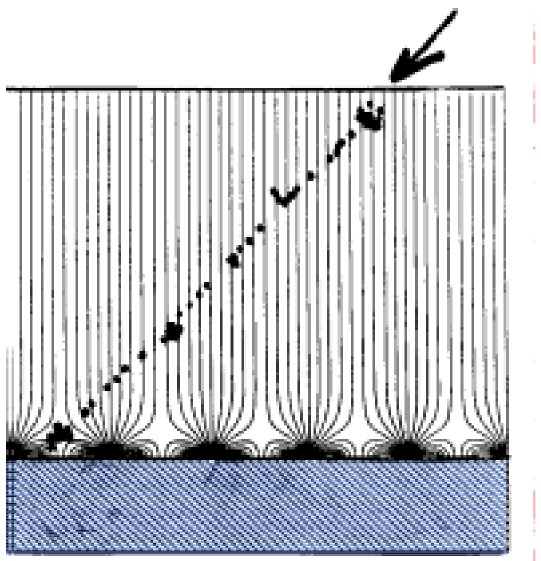

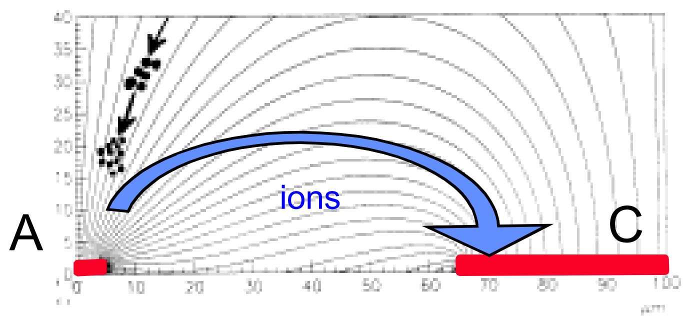

short ion drift distance - 60 µm !

CMS Microstrip Gas Chambers

Characteristics of CMS MSGCs

Substrate	300µm thick Desag 263 glass
Undercoating	allows stable gain and rate independence
Gold Strips	to slow ageing, no attenuation of collected charge along the strip

Advanced Passivation allows higher gain and robust operation

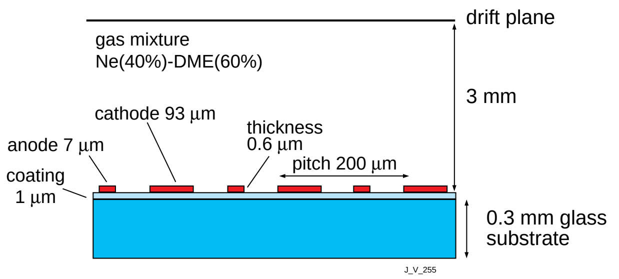

Nominal Operating Parameters

Mixture	Ne-DME (40%-60%)
Voltage	anode at ground cathode strips at -520 V drift cathode at -3500V
Gain	2000
Rates	~ 10^6 particles/mm^2/s

Detection Efficiency and Spatial Resolution

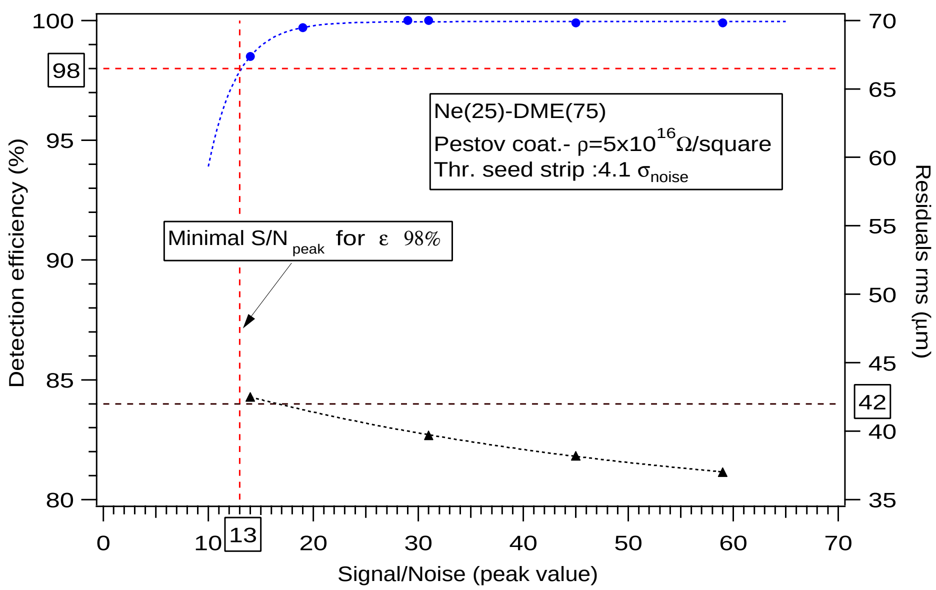

Robustness has been demonstrated on a few chambers in high intensity 400 MeV pion beam (10^4 Hz/mm^2) over 161 hour sat PSI
Further tests at PSI on pre-production prototypes in 1999

Micro-Gap Chambers

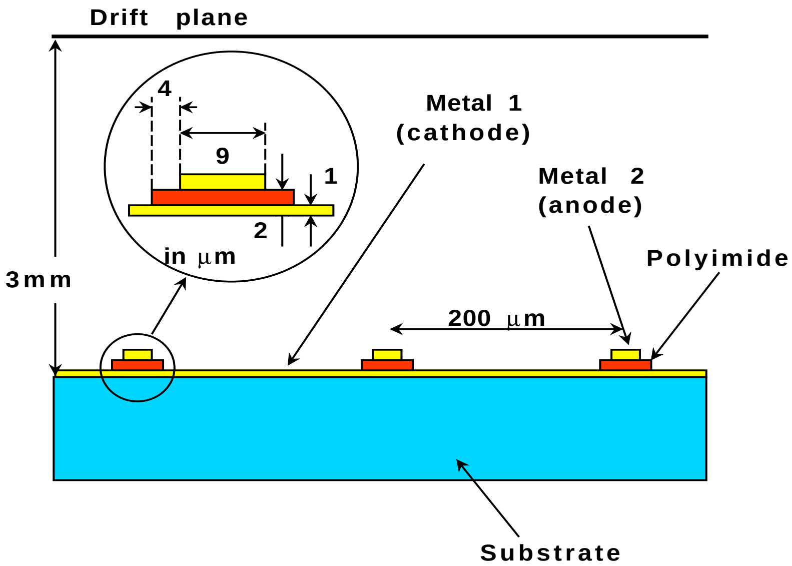

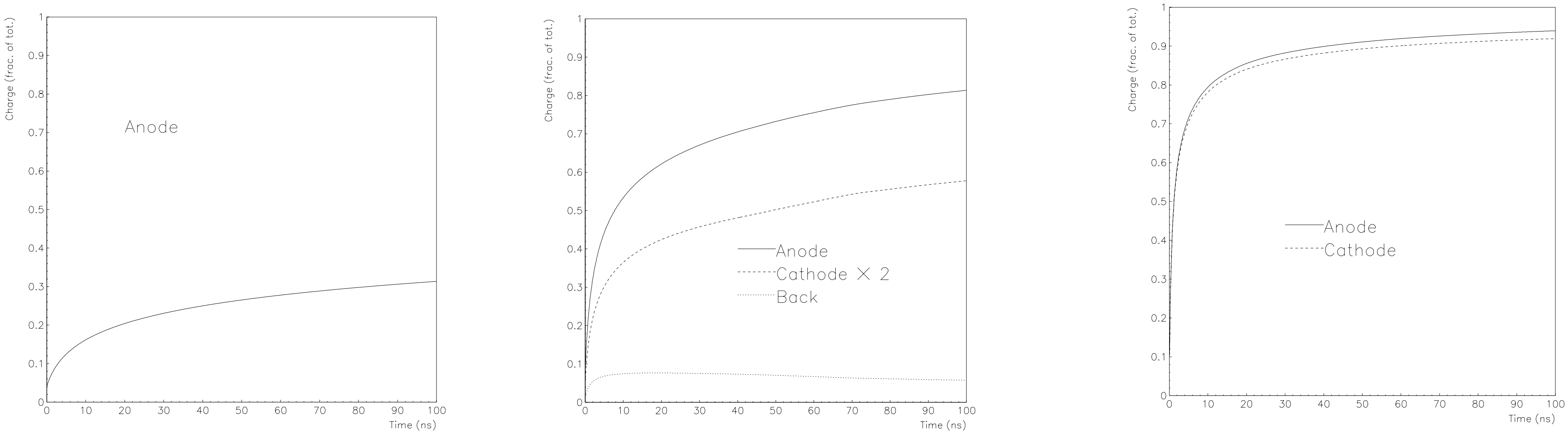

Time development of induced charge on the electrodes of a) MWPC, b) MSGC, c) MGC

Gas Electron Multiplier

R. Bouclier et al NIM A396 (1997)50.

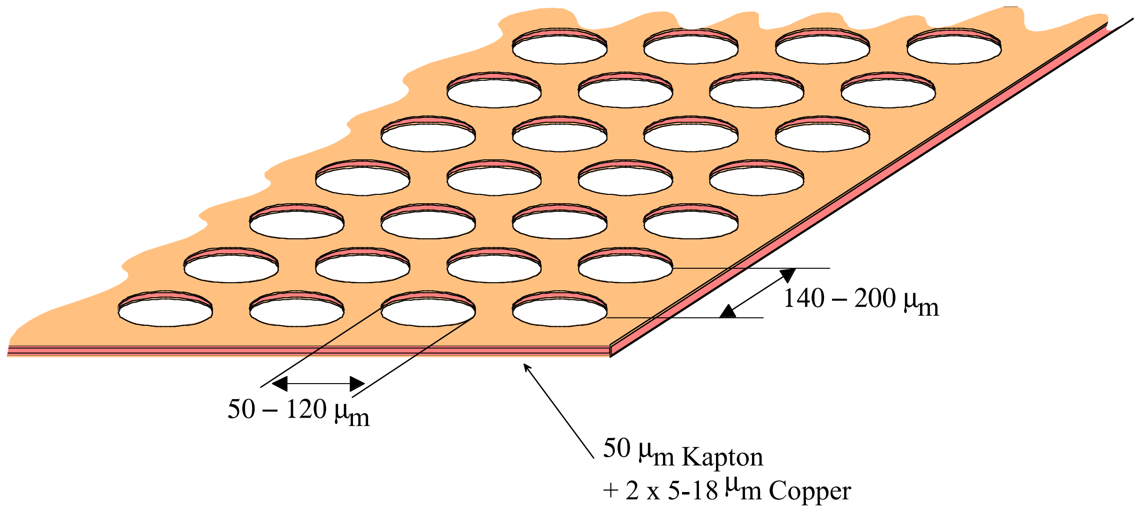

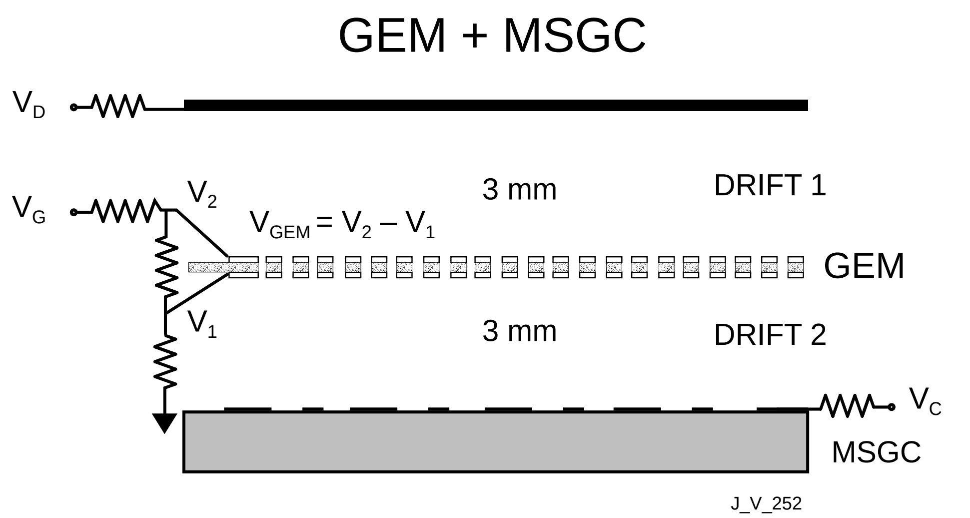

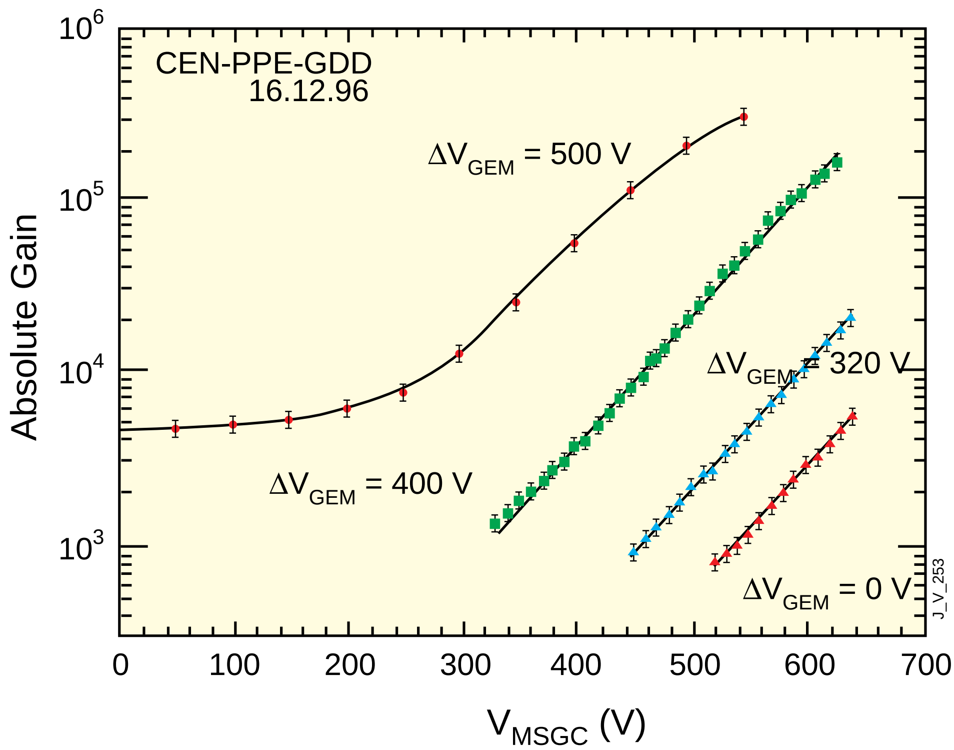

Silicon Detectors

Characteristics of Silicon

- Basic information carriers are electron-hole (e-h) pairs
- Band-gap: E_g = 1.2 eV
- Energy to create 1 e-h pair: W = 3.6 eV (NB ≈ 30eV in gas)
- High density (2.33 g/cm^3) - m.i.p. creates <30k> e-h pairs in 300 μm thick silicon
- High mobility: μ_e=1450, μ_h=450 cm^2/V.s ($V_d=\mu E$) - fast signal collection (≈ 10 ns in 300 μm thick silicon)
- Both electrons and holes contribute to the signal

No charge multiplication - require v. good amplifiers

Performance degrades with radiation damage

Detectors produced using micro-electronic techniques

fine pitch (≈ 50 μm) but short strip lengths (≈ 10 cm)

Signal in Silicon Detectors

Energy levels in atoms become energy bands in regular assembly of atoms e.g. in crystals

Valence and conduction bands are formed in crystals due to the periodic lattice structure

Valence band: electronc bound to specific lattice site

Conduction band: electrons are free to migrate through crystal

At $T \neq 0$, valence electrons can get enough thermal energy to get into conduction band

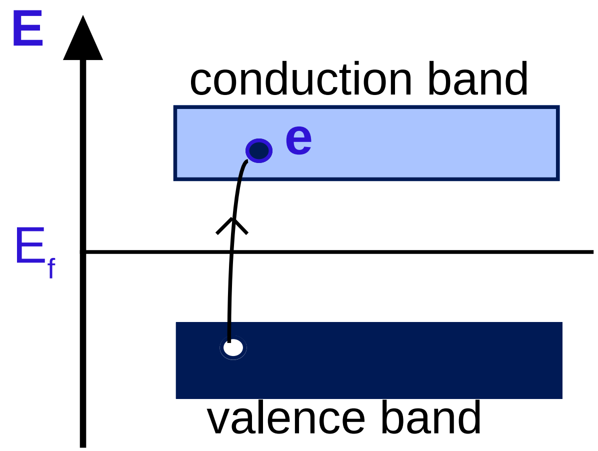

In a pure intrinsic (undoped) material the electron density, n, and hole density, p, are equal

$n_i = p_i$

For Si: $n_i = 1.45.10^{10}$ cm^{-3}

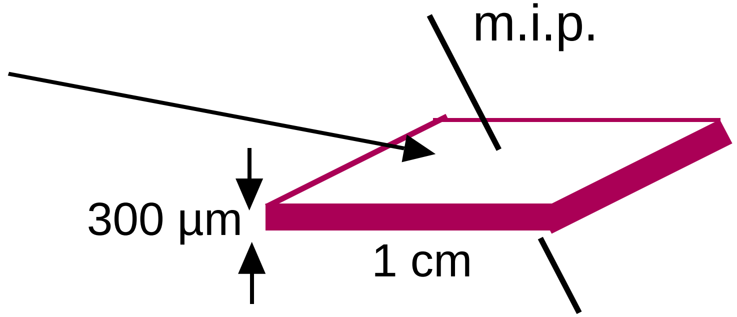

In this volume there are $4.5.10^8$ free charge carriers, but only <32,000> e-h pairs are produced by a m.i.p.

Must reduce the number of free charge carriers i.e. **deplete the detector** of charge carriers

Most detectors make use of reverse biased p-n junction

1 cm

n-type Semiconductor

Si sits in Group IV of the periodic table
i.e. it has 4 outer electrons and can form 4 covalent bonds

IF now a small concentration (few ppm) of pentavalent impurity is added (P, As)

• 1 valence electron left over after all covalent bonds formed
• It is very lightly bound and can easily be promoted to the conduction band without creating a corresponding hole

DONOR IMPURITY

• These electrons are not part of the regular lattice and can occupy a position in the normally forbidden gap (near top of gap)
• Thermal excitation is sufficient to ionize a large fraction of the donors (N_D)

$$n \approx N_D$$

Added concentration of electrons increases rate of e-h recombination, shifting equilibrium between electrons and holes. Concentration of holes decreased BUT

$$n\, p = n_i\, p_i$$

e.g. at room T, $n_i = p_i \approx 10^{10}$ cm^{-3}, if donor impurities $\approx 10^{17}$ atoms/cm^3,
n=10^{17} cm^{-3} and p = 10^3 cm^{-3}

$$n >> p$$

Charge neutrality is maintained by presence of ionized donor impurities which cannot migrate (fixed in the lattice)

electrons are majority carriers whereas holes are minority carriers

Donor & Acceptor Levels

$n\,p = n_i\,p_i$

e.g. at room T,

$n_i = p_i \approx 10^{10}\ cm^{-3}$,

if donor impurities

$\approx 10^{17}$ atoms/cm^3,

i.e. $p = 10^3\ cm^{-3}$

$n >> p$

n-type semiconductor

Donor site

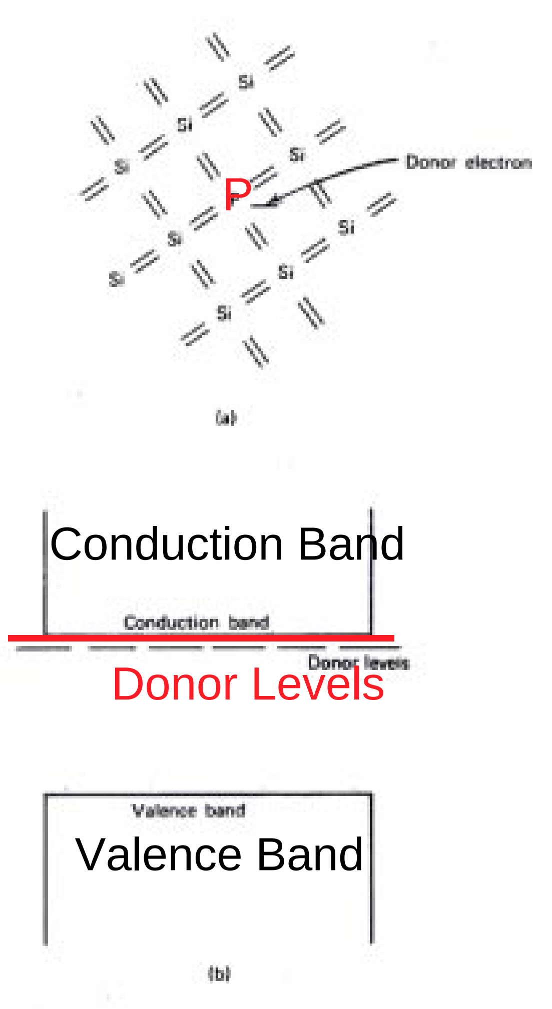

p-type semiconductor

Acceptor site

$p >> n$

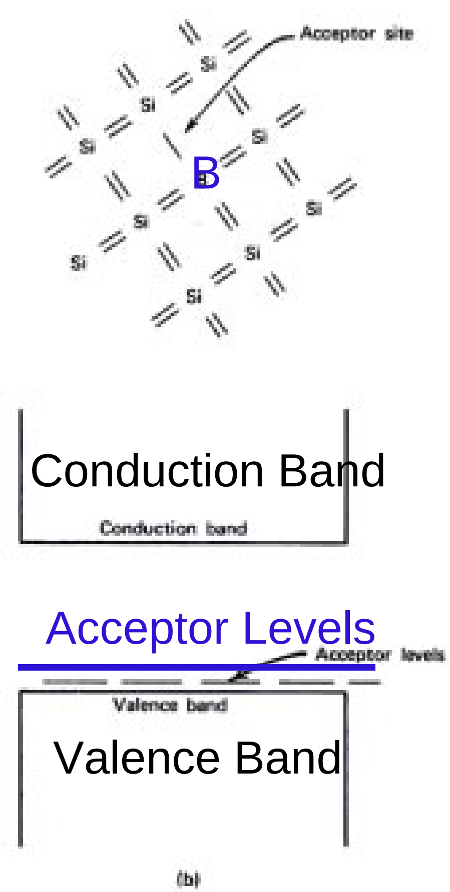

p-type Semiconductor

IF a small concentration (few ppm) of trivalent impurity is added (B)

• 1 fewer valence electron and 1 covalent bond left unsaturated
• vacancy represents a hole. Electrons can be captured to fill this vacancy
• electrons still bound to specific location but less firmly

ACCEPTOR IMPURITY

• These lie near bottom forbidden of gap - properties similar to sites occupied by normal valence electrons
• normal thermal excitation always assures electrons available to fill vacancies
• a large fraction of acceptor sites are filled

$p \approx N_A$ with $n\, p = n_i\, p_i$ and $p >> n$

A measure of impurity level is electrical conductivity or its inverse resistivity
e.g. Si impurity conc. of 10^{13} atoms/cm^3 $\Rightarrow$ resistivity of 500 Ω.cm

Heavily Doped Material *

unusually high concentration of impurity labelled n^+ or p^+
has very high conductivity - often used in making electrical contact

*
Since there is very low minority carrier density - allows 'blocking' contacts
Ohmic conyact - charges of either sign can flow freely
Steady state leakage currents using ohmic contacts are too high
Most approppriate type of blocking contacts are two sides of a p-n semiconductor junction

Properties of a p-n Junction

Bring into contact n- and p-type materials (done by doping a single crystal)

Begin with p-type crystal (original acceptor conc. N_A)

Assume surface left exposed to vapour of n-type impurity (left side becomes n-type material)

Density of electrons in n-type is much higher than in p-type

Net diffusion of conduction electrons into p-type material where they quickly recombine with holes

electrons moving out of n-type material leave immobile +ve charges and net -ve charge on p- side is established

Accumulated space charge creates electric field that diminishes tendency for further diffusion

Region over which charge imbalance exist is called the depletion region (conc. of e and h ≈ 100 /cm^3 !). In our case region will extend deeper into p- side than n- side

For electron-hole pairs created in depletion region, electrons swept toward n-type and holes toward p-type

Application of reverse bias (n- side made more +ve) extends the thin depletion region. The depletion depth is given by

$$d \cong \sqrt{\frac{2\varepsilon V}{eN}}$$

$$PDG: \quad d \approx 0.5\ (0.3)\ \mu m \times \sqrt{\rho V} \quad for\ \ n-type\ (p-type)$$

N - lower dopant conc. , ρ - resistivity (typically 1-10 kΩ.cm)
d ≈ 300 μm for ρ=5 kΩ.cm and Bias Voltage ≈ 70V

Concentration Profiles

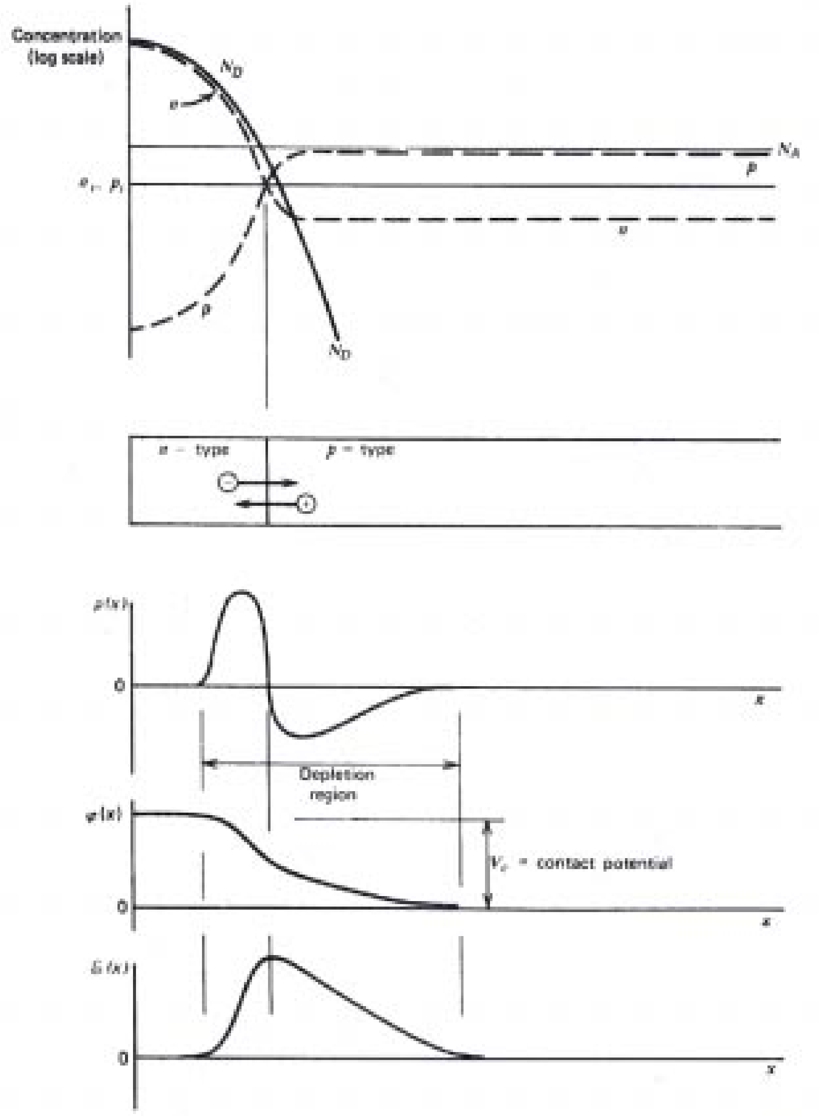

The assumed concentration profiles for the n-p junction shown at the top are explained in the text. The effects of carrier diffusion across the junction give rise to the illustrated profiles for space charge $\rho(x)$, electric potential $\varphi(x)$, and electric field $\mathscr{E}(x)$.

- In depletion region

conc. of e and h ≈ 100 /cm³ !.

- Reverse bias (n- side made more +ve) extends the thin depletion region.

$$d \cong \sqrt{\frac{2\varepsilon V}{eN}}$$

$$PDG: \quad d \;\approx\; 0.5\ (0.3)\ \mu m \times \sqrt{\rho V} \quad for\ \ n-type\ (p-type)$$

N - lower dopant conc. , ρ - resistivity (typically 1-10 kΩ.cm)

d ≈ 300 μm for ρ=5 kΩ.cm and

Bias Voltage ≈ 70V

Fabrication Of Si Detectors

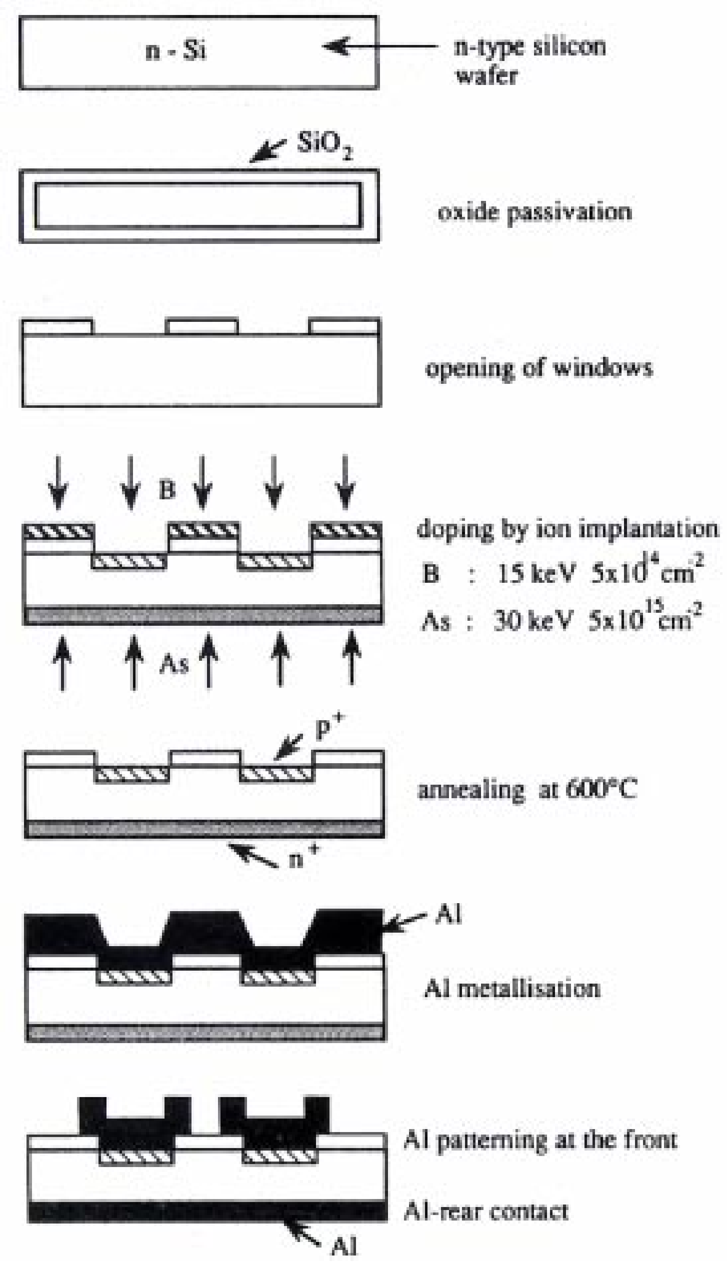

clean and polish wafer

oxidize at 1000^{o}C, passivate

apply photosensitive polymer and bake
expose to UV light thru mask, develop

form diode junctions by implantation/diffusion

anneal - implanted ions take-up lattice positions

aluminize surfaces

final photolithographic steps to pattern metal
for diode contacts

Si Microstrip Detectors

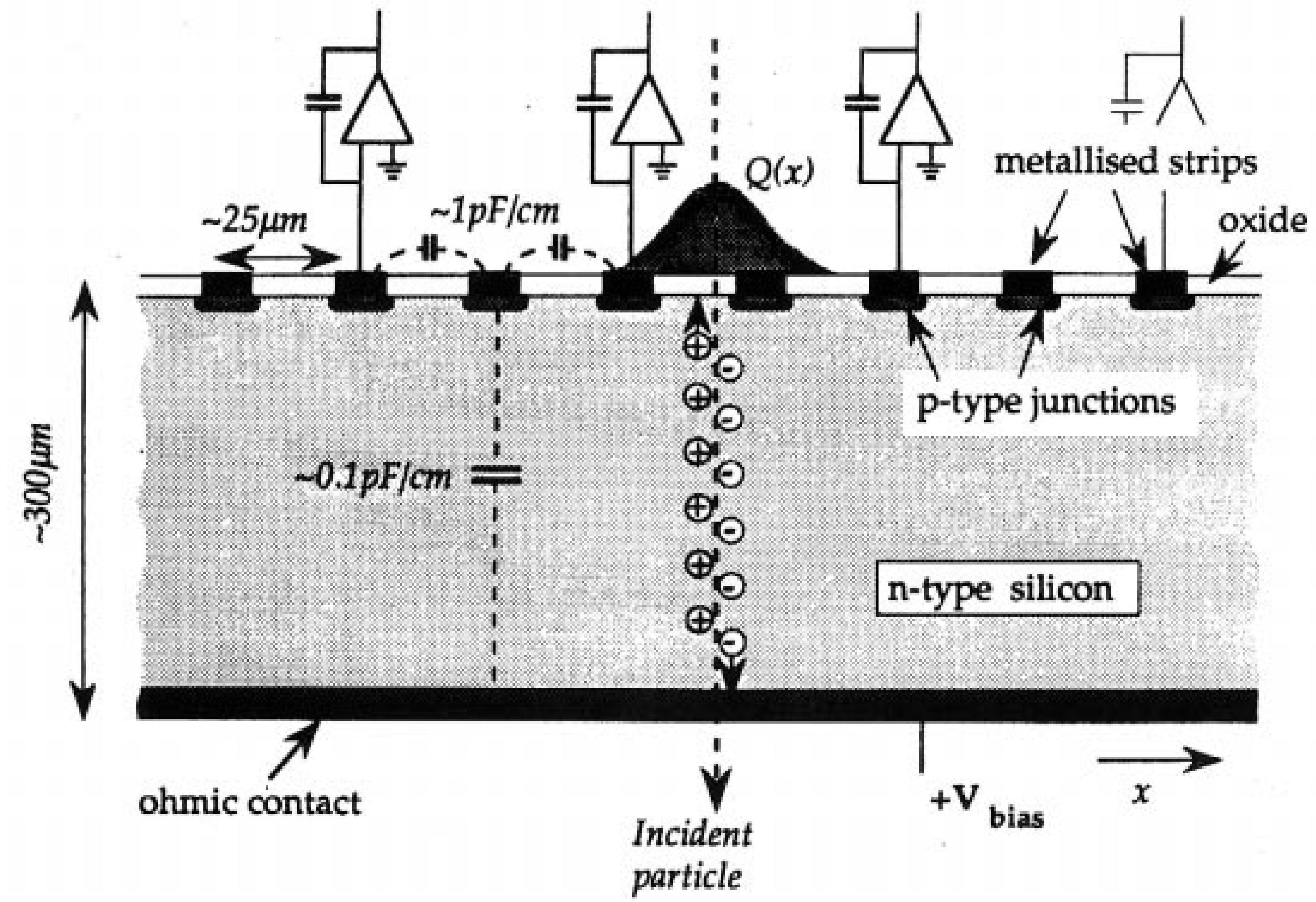

Schematic cross-section through a silicon microstrip detector. Diffusion distributes charge over multiple strips and capacitive charge division between readout amplifiers allows position interpolation.

Radiation Damage in Silicon

Bulk damage effects more important than surface damage

High energy hadronic particles displace Si atoms from their lattice positions (only ≈ 15 eV is required)

Simplest defects
- vacancies where Si atom is absent from its site
- Si atom occupies a position intermediate between atomic sites

Disruption of the symmetry causes formation of unwanted energy levels in the forbidden gap

increased leakage current $$\frac{\Delta I}{V} = \alpha \ \phi$$

where $\alpha \approx 2.10^{-17}$ A/cm for minimum ionizing protons and pions after long-term annealing and
V is the volume (in cm^3), ϕ is fluence in particles/cm^2

<u>dopant density changes during and after irradiation</u>

• effect is poorly understood
• n-type substrate eventually becomes p-type, whatever the initial type or resistivity
• dopant changes continue after irradiation has stopped BUT can be arrested if detectors <u>kept below 0 ºC</u>.
• with increasing particle fluence the depletion voltage increases

Manufacturing of Si detectors has improved substantially and high voltage operation (≥ 500 V) is nowadays possible.

Silicon Microstrip Detectors

Evolution of voltage for full depletion

V depletion

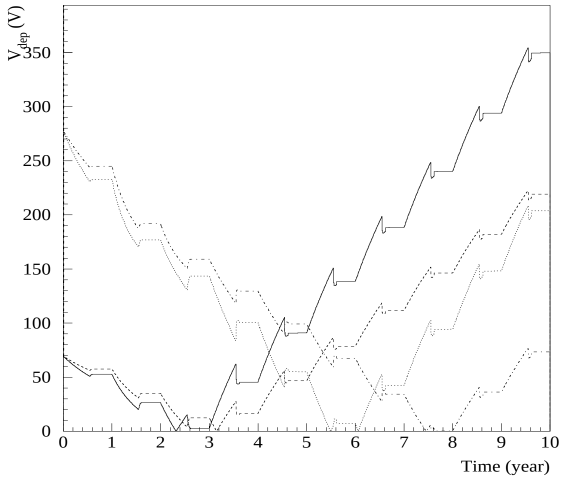

Time (years)

Results from neutron irradiation

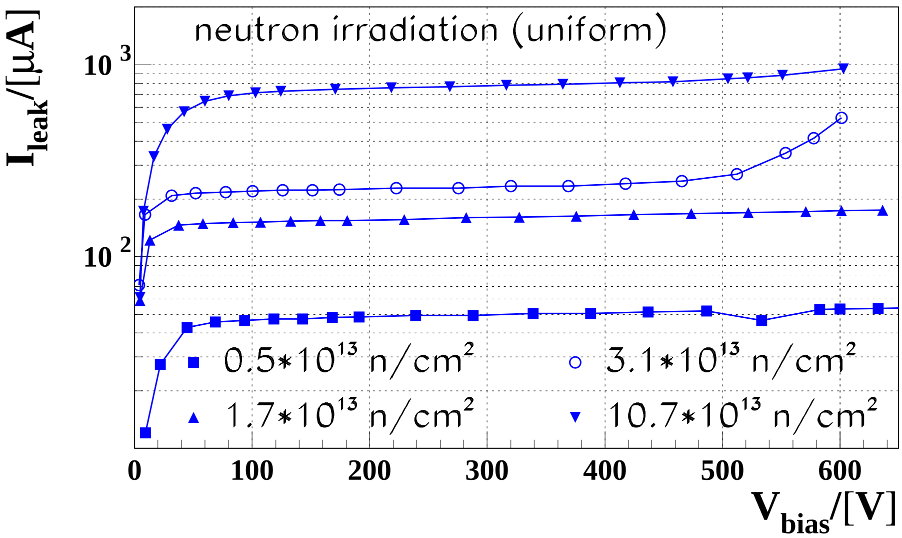

e.g. CMS Silicon Tracker

Area	70 m^2
# ch	5.2 M
r-ϕ pitch	62/83/125 µm
stereo	125/250 µm

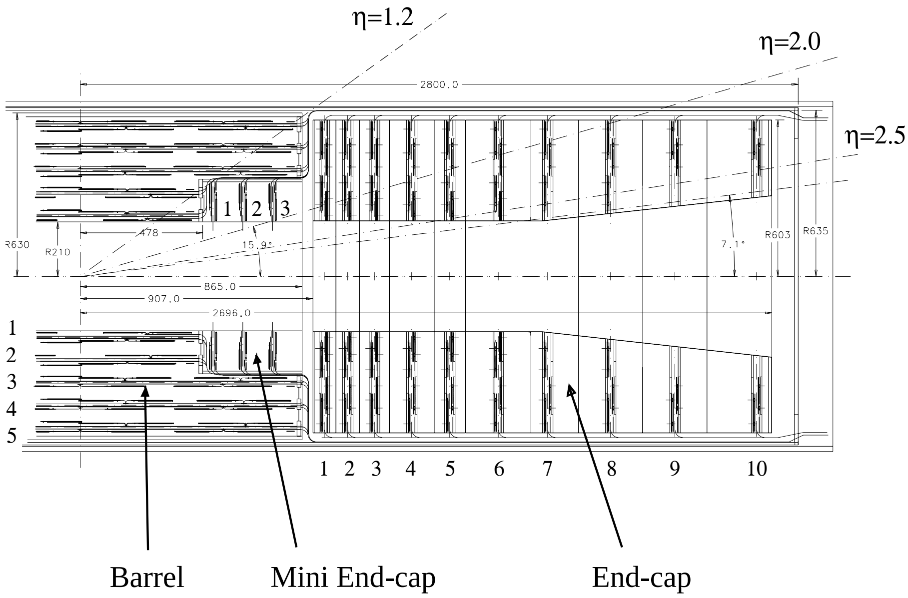

Pixel Detectors

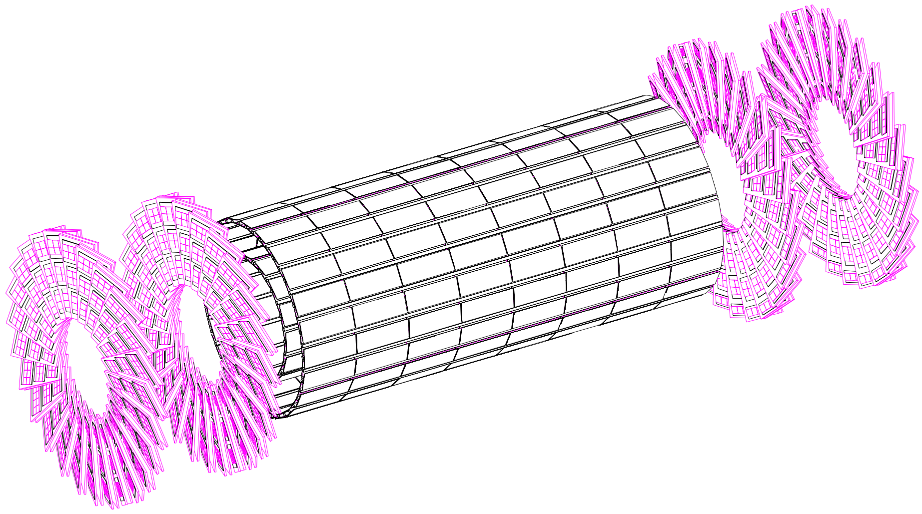

Characteristics of CMS pixel detectors

Size	150µm x 150 µm
n on n Si	large Lorentz angle (34°) allowing charge sharing
-5 °C	low leakge current, arrest reverse annealing

Irradiation of Si Pixel Detectors

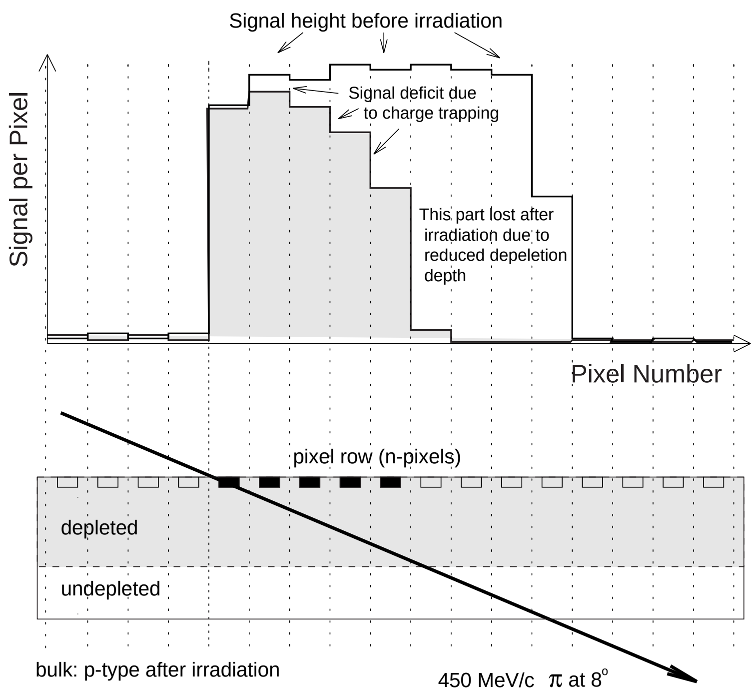

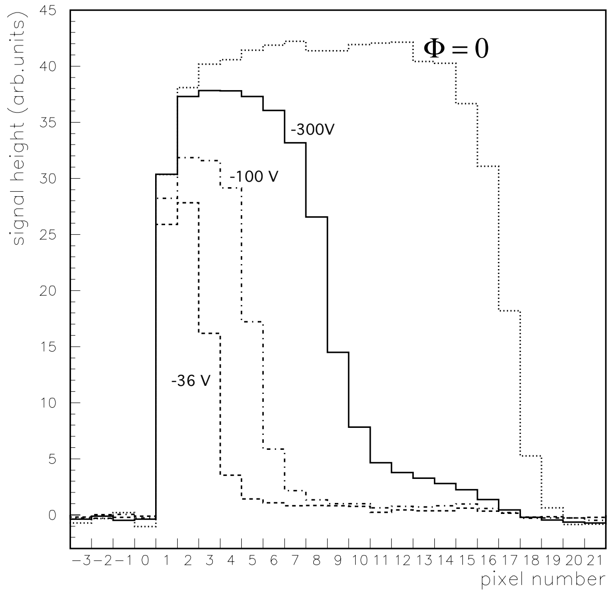

Depth profiles of charge collected from a pixel array irradiated with 6.10^{14} pion/cm^2

Electronics

- Electronics Noise
- Generic LHC Readout System
- Electronics for LHC Detectors
- Electronics of Sub-detectors
- CMS Tracker Electronics
- CMS Tracker Front-end
- Analog Optical Links

Electronics Noise

Amplifier Noise
Noise is any unwanted signal that obscures the signal.
Noise degrades accuracy of measurement

Intrinsic Noise : noise generated in the detector or electronics and cannot be eliminated, though possibly reduced
Extrinsic Noise : noise due to pickup from external sources or unwanted feedback (e.g. ground loops, power supply fluctuations, etc.)

Intrinsic Noise
• Thermal noise (Johnson, Nyquist) - series noise
any resistor, R, will develop a voltage across its ends whose average value is zero but r.m.s. is

$$\langle v^2 \rangle = 4kTR.\Delta f$$

• Shot noise - parallel noise
fluctuation in charge carriers

$$\langle i_n^2 \rangle = 2eI.\Delta f$$

The equivalent noise charge (ENC) is given by

$$ENC^2 = \frac{4kTR_s(C_d + C_{in})^2}{\tau} I_s + I_n\tau \; I_p$$

where C_d is detector capacitance
C_{in} is input capacitance of amplifier
I_n is leakage current
τ is shaping time
I_s, I_p are series and parallel noise integral (≈1 for $(RC)^2$ shaping)

e.g. for τ=50 ns, and a leakage current of 1 µA, ENC ≈ 800 e's

Electronics for LHC Detectors

Main components (systems) of Electronics

front-end, digital processing, ...
data transmission
power supplies, services, ...

What is different about electronics for LHC cf. e.g. LEP

high speed signal processing
signal pileup
high radiation levels
larger no. of channels (large data volumes)
new technologies

e.g. Challenge for Inner Tracker

- signals are small and fast response must be preserved
  preamplifiers must be mounted on detectors themselves
- must hold data in pipeline memories awaiting Level-1 decision
- it is not feasible to transfer data off the detector at a rate of 40 million events/s for millions of channels
  pipeline memories must be located on the detectors
  how are the signals taken out ?
  how are the electronics mounted on detectors ?
- several millions of channels will dissipate a considerable amount of heat (≈ several mW/ch)
  how is the cooling of electronics accomplished ?

⇒ v. difficult engineering and systems challenge
accomplish above whilst keeping the amount of material to a minimum

Electronics of Sub-detectors

Tracking

large channel count (10's M)	low power (few mW/ch)
limited energy precision	high radiation levels
limited dynamic range (<8-bit)	

Calorimetry

medium channel count (100's k)	power constraints
high energy precision(12-bit)	medium radiation levels
large dynamic range (17-bit)	
v. good linearity	
v. good stability in time	

Muon System

distributed over large area	low radiation levels

CMS Tracker Electronics

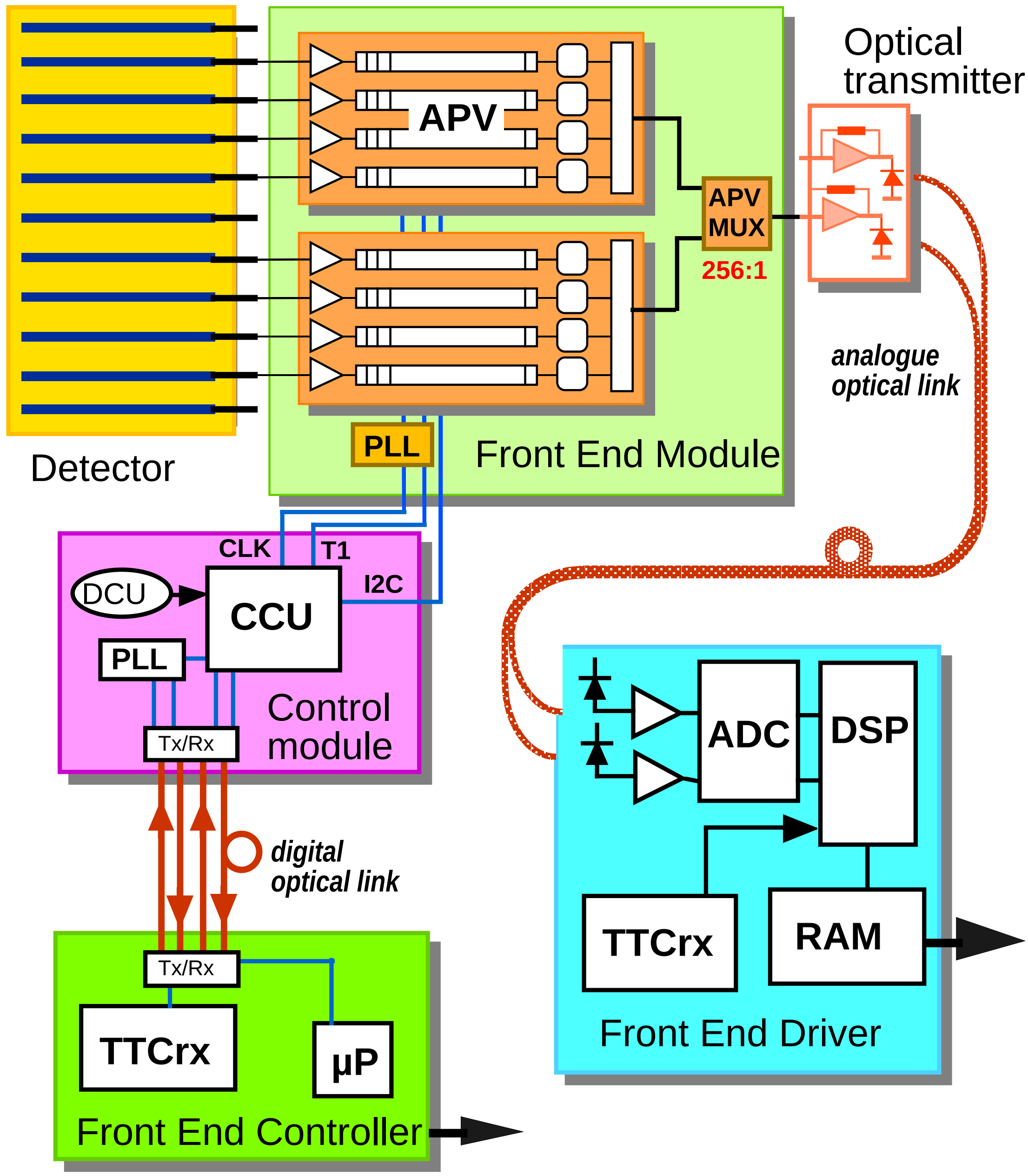

Each microstrip is read out by a charge sensitive amplifier with τ= 50 ns.
The o/p voltage is sampled at the beam crossing rate of 40 MHz.
Samples are stored in analog pipeline for up to Level-1 latency (3.2 µs)
Following a trigger form a weighted sum of 3 samples in analog circuit
This confines signal to single bx and gives pulse height
Buffered pulse height data multiplexed out on optical fibres
Output of laser modulated by the pulse height for each strip

CMS Tracker Front-end

Layout of APV6

Size 6.4 x 12 mm²

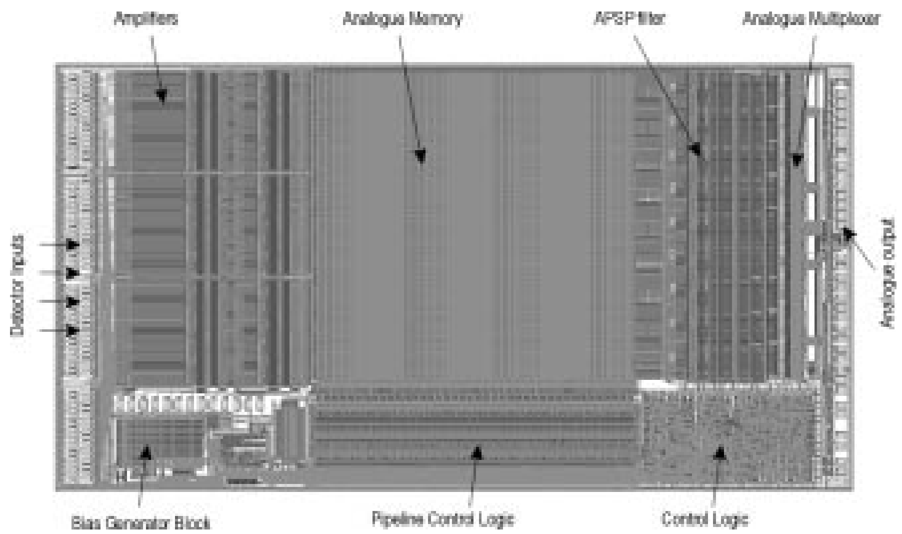

Pulse shape in peak and deconvolution mode of APV6

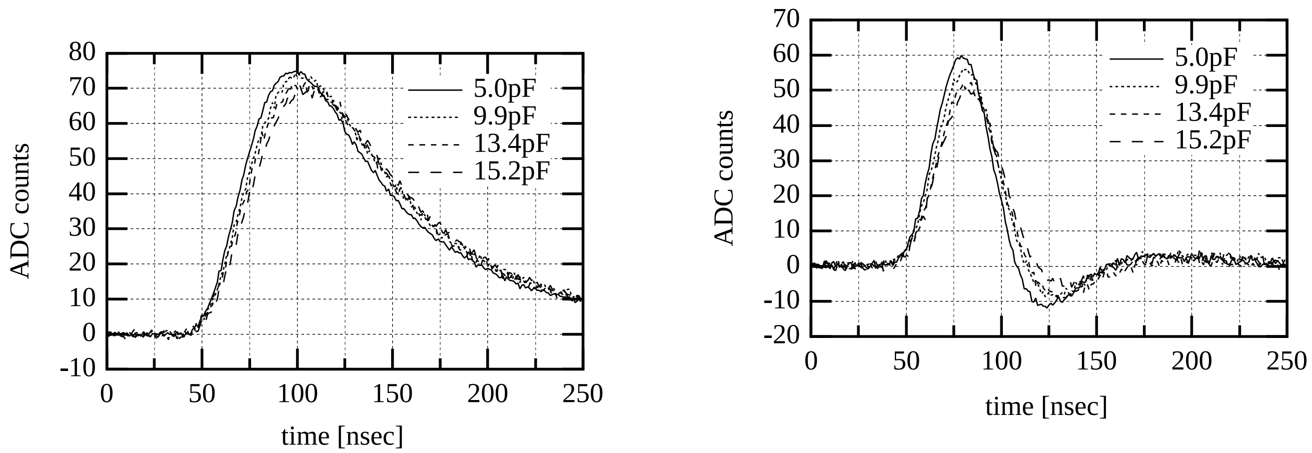

Si μ-strips

Overall Noise in e-

APV6	1500
i_l=2 μA	500
Opt. Lnk	750
Total	≈ 1750

cf mip signal 25 k e-

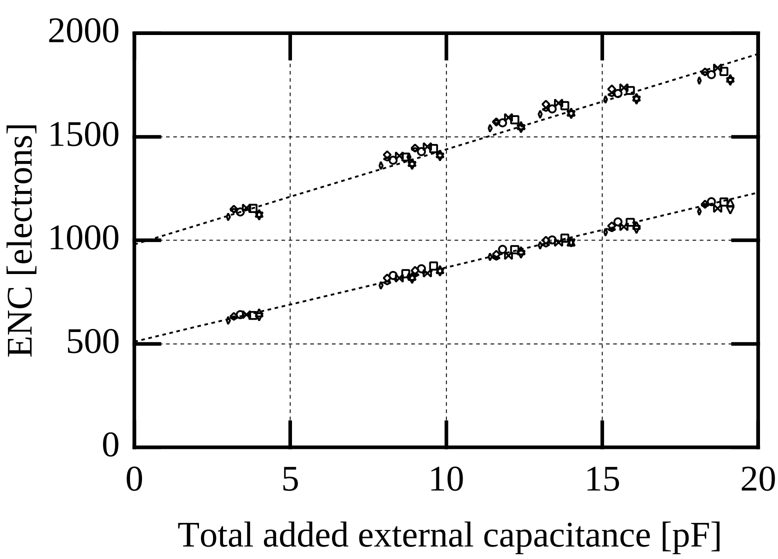

Analog Optical Links

Edge emitting 1.3 µm InGaAsP laser diodes

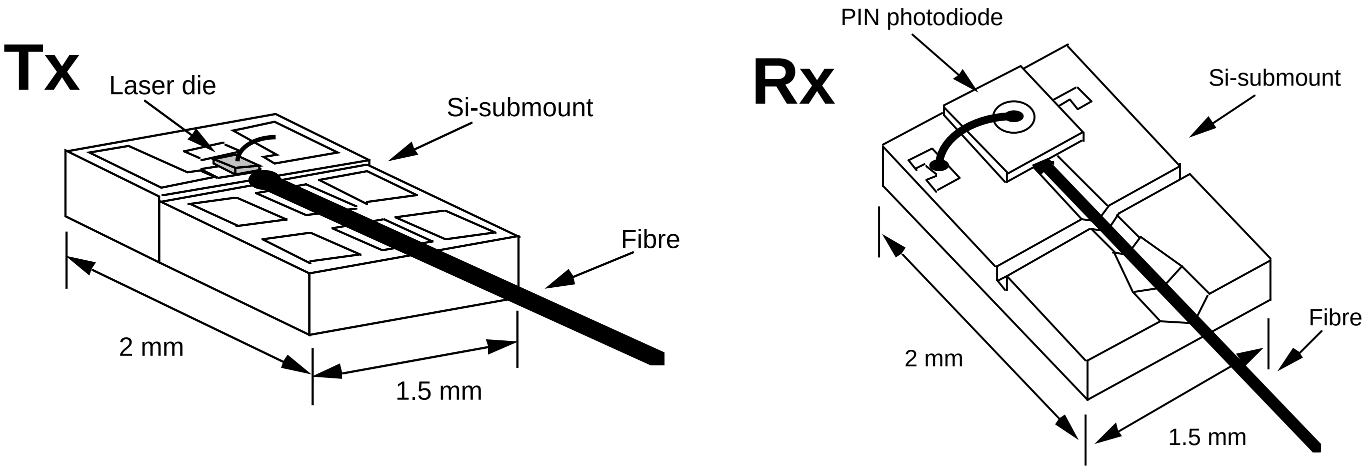

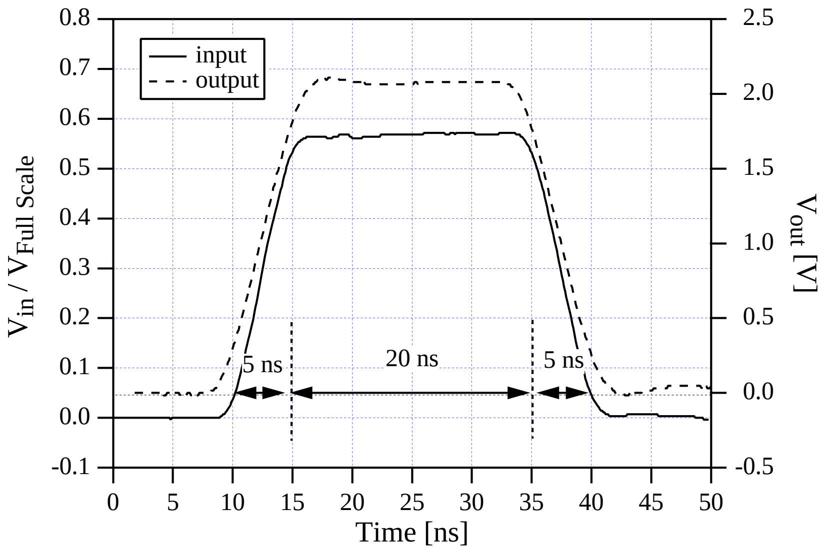

Pulse Response

Pre- and Post-Irradiation

OK to >> 10^{14} n/cm^2

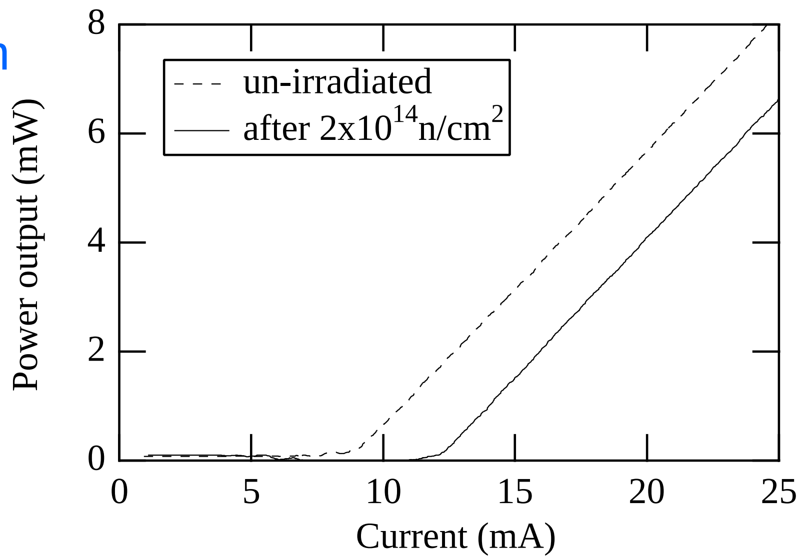

Features of Calorimetry

1. Calorimeters can measure energies of neutral and charged particles, jets and deduce the presence of neutrinos.

2. The relative energy resolution improves with energy as

$$\sigma/E \;\alpha\; 1/\sqrt{E}$$

This contrasts with momentum measurement of charged particles where the relative transverse momentum resolution $dp_t/p_t \;\alpha\; p_t$.

3. The longitudinal depth required to contain the cascades only increases logarithmically whereas for magnetic spectrometers the size increases as $\sqrt{p}$ for constant dp_t/p_t .

4. The cascade develops differently, longitudinally and laterally, for e/γ, hadrons and muons. This can be exploited for particle identification.

5. The pattern of energy deposit in a calorimeter with good lateral and longitudinal segmentation allows fast, efficient and very selective triggering on e/γ, jets and E_T^{miss}.

6. Good simulation codes exist to design of calorimeters (EGS4 for e.m. and FLUKA, GHEISHA, GCALOR for hadronic cascades).

7. Large precision electromagnetic calorimeter systems are operating well (CLEO, KTeV, NA48), will soon be commisioned (BaBar, Belle) or are under construction (CMS, ATLAS)

8. Calorimeter systems have played an important role in recent discoveries e.g. W, Z in UA1/UA2, top quark in CDF/D0 and will play a similarly crucial role in the next generation of experiments ATLAS/CMS.

Radiation Levels in LHC calorimeters

Dose and neutron fluence in and around the crystal calorimeter of CMS.

Bold Italics : dose in kGy (10^5 rads) at shower maximum and rear of calorimeter

Plain : neutron fluence in 10^{13} n/cm^2

Numbers corresponds to first ten years of LHC operation

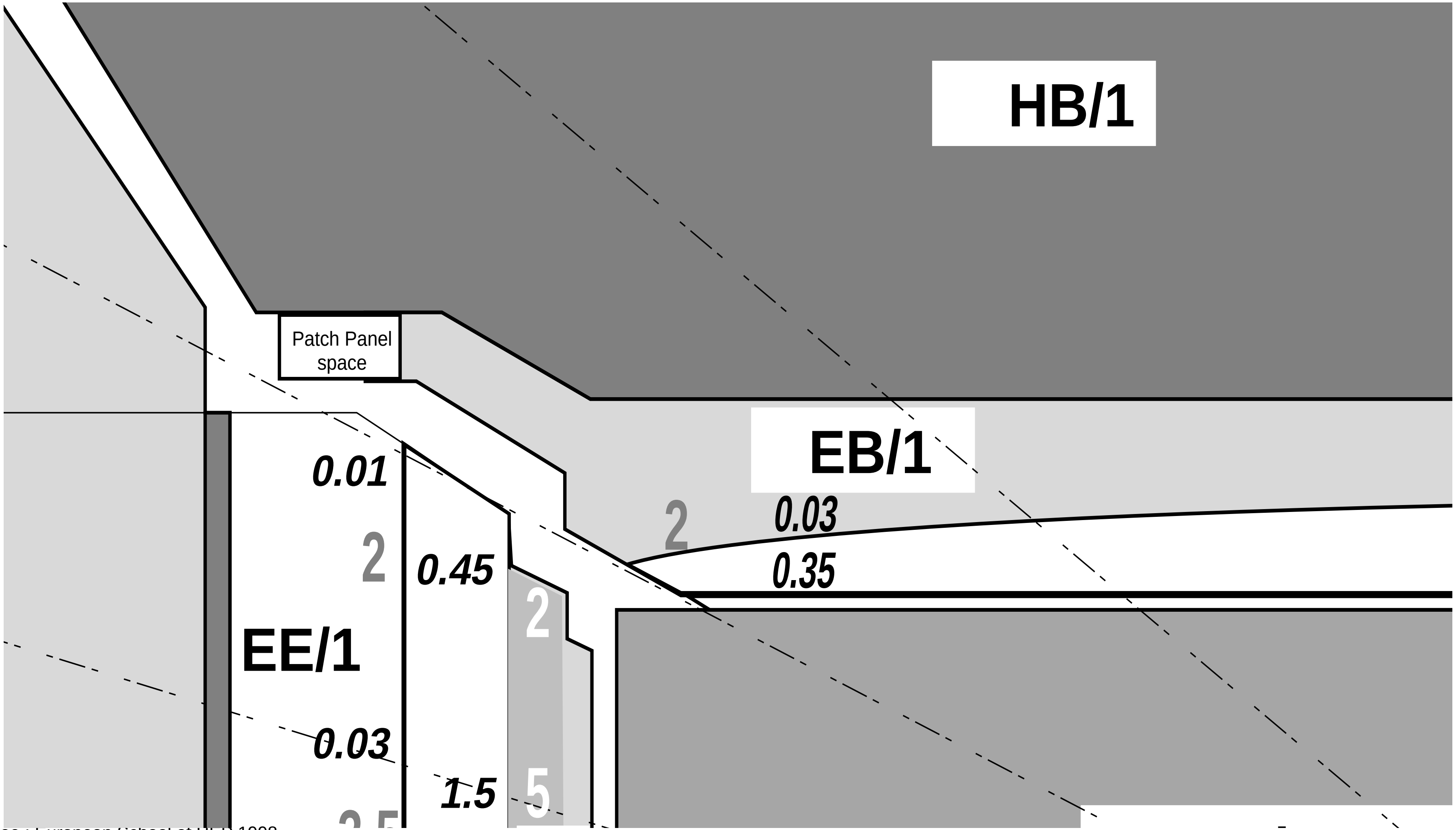

Crystal Calorimeters

- Inorganic Scintillators
- Radiation Damage in Crystals
- CMS ECAL
- PbWO4 Energy Resolution
- Response from 280 GeV electrons
- Si Avalanche Photodiodes
- Si Avalanche Photodiodes
- CMS $PbWO_4$ Crystals Assembly

Inorganic Scintillators

Desirable Properties

- high scintillation efficiency (energy $\rightarrow$ light)
- conversion (energy $\rightarrow$ light) linear
- medium transparent to its own emitted light
- short luminescence decay time
- n $\approx$ 1.5 for efficient coupling to photosensors
- radiation hard for LHC operation

No material simultaneously meets all these criteria

Inorganic: best light output and linearity (e.g. NaI)
Organic (eg. plastic scint.) faster (ns), smaller light yield ($\approx$ 1γ/100 eV), saturation

Fluorescence - prompt emission of visible radiation
Phospherescence - (slower) emission of longer wavelength

Inorganic Scintillators

Valence band - elctrons bound at lattice sites
conduction band - electrons free to move throughout the crystal

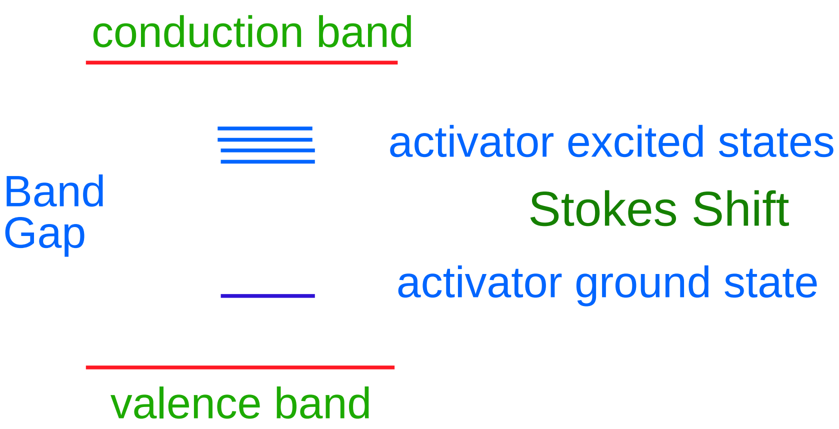

- Pure crystal - insufficient scintillation efficiency
- Add small amount of impurities (called activators) to increase prob. of visible γ emission
- Create energy states within forbidden gap through which an electron, excited to conduction band, can de-excite

Inorganic Scintillators

• a charged particle creates large no. of e-h pairs:
electrons elevated to conduction band
• +ve holes quickly drift to an activator and ionize it
• e migrates freely in crystal until it encounters an ionised activator,
• e drops into impurity site creating activator energy levels
• typically $T_{1/2}$ of activator sites ≈ 100 ns

Competing processes
• excited to state where transition to ground state is forbidden
• additional energy required to raise to a higher lying state from which de-excitation can take place
• one source of energy is thermal
⇒ slow component or afterglow
• radiationless transition (quenching processes)

• in wide category of materials, energy reqd. to create e-h pair
$W \approx 3\ E_g$

e.g in NaI, W ≈ 20 eV, NaI(Tl) : $N_\gamma \approx$ 40,000 γ/MeV of 3 eV

consequence of luminescence through activator sites
crystal is transparent to its own scintillation light

in pure crystal - emission and absorption spectra overlap -
substantial self absorption ⇒ need a Stokes shift

Radiation Damage in Crystals

All known crystals suffer from radiation damage
- absorption bands caused by colour centre formation or impurities
- light attenuation length is affected - loss of collected light (change of calibration)
- scintillation mechanism is not affected

Colour centre - crystal defect that absorbs visible (or near UV) light
most simple colour centre known as an F-centre (*farbe*-colour in German)

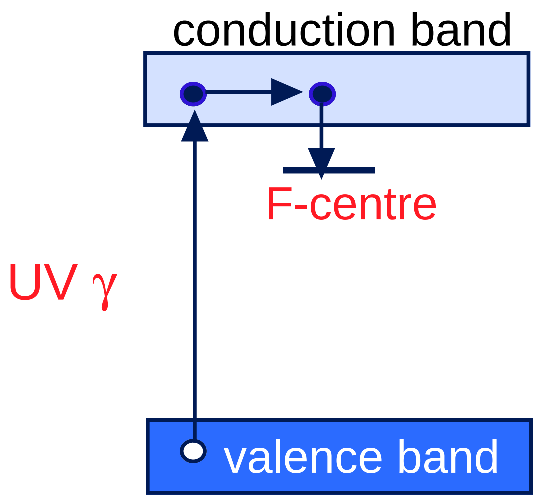

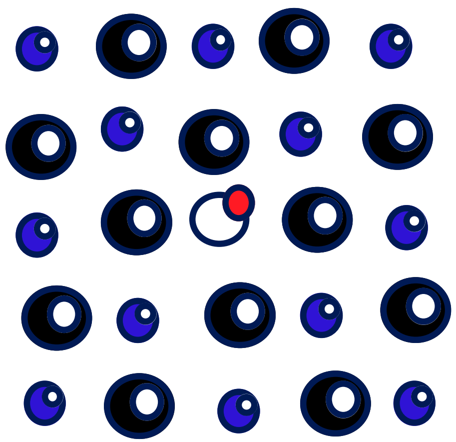

F-centre, electron captured in a cation vacancy

To improve radiation tolerance of $PbWO_4$ crystals
Decrease concentration of defects
stoechiometry, annealing
Compensation of remaining defects
control purity of raw material, specific doping-pentavalent of W site, trivalent on Pb site

Radiation Tolerance of $PbWO_4$ Crystals

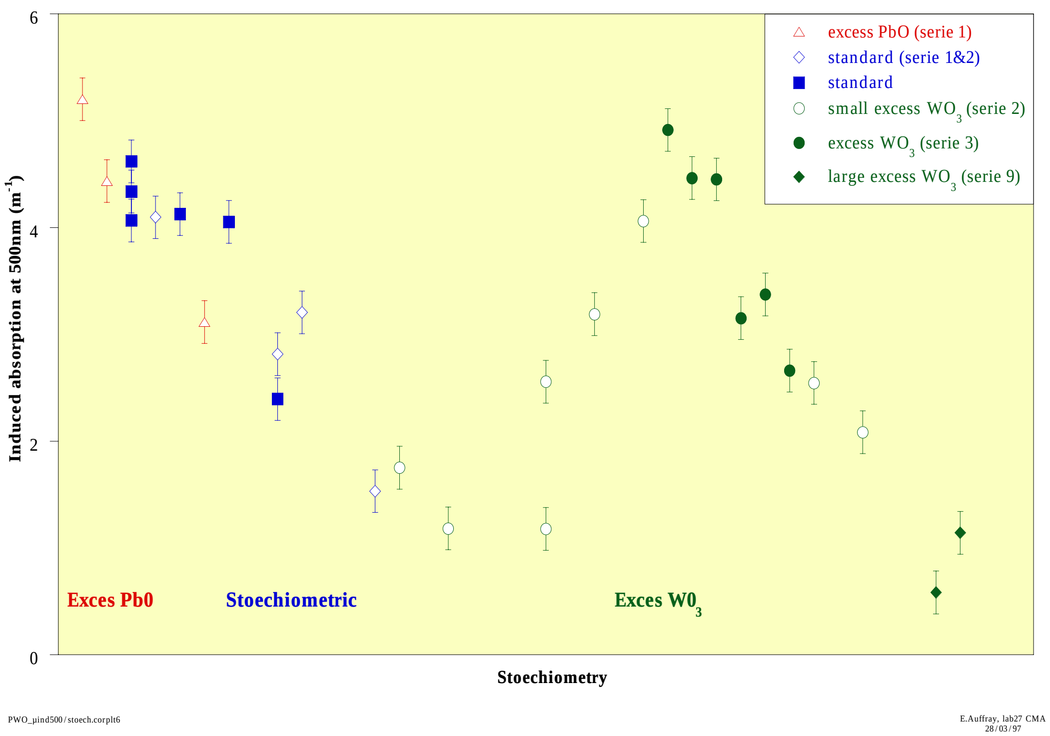

Specific Doping

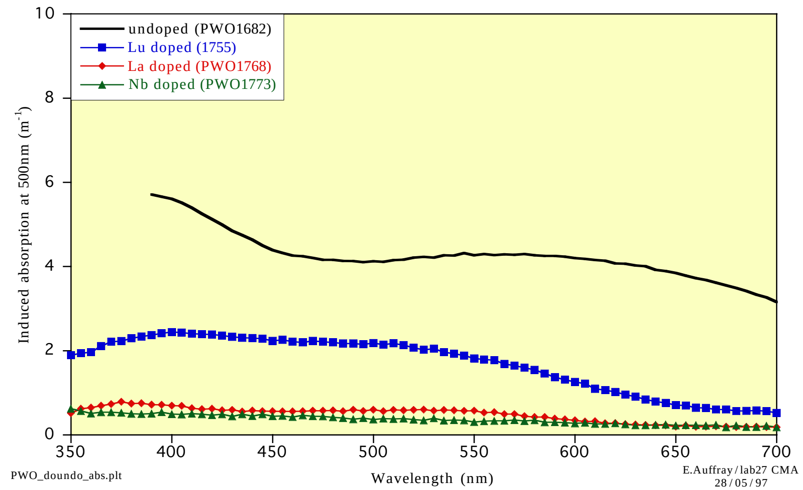

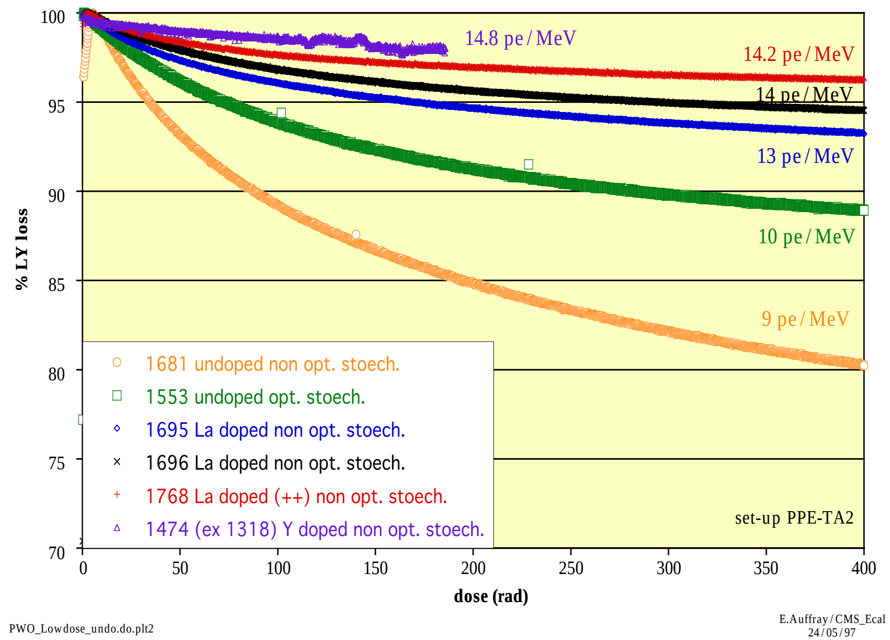

Low Dose Rate Front Irradiation v/s Specific Doping

Radiation Damage in Crystals

All known crystals suffer from radiation damage
- absorption bands caused by colour centre formation or impurities
- light attenuation length is affected - loss of collected light (change of calibration)
- scintillation mechanism is not affected
- dependence on dose rate

Colour centre - crystal defect that absorbs visible (or near UV) light
high concentration of blue colour centres makes crystals yellowish
crystal that is coloured after irradiation has poor radiation tolerance

most simple colour centre known as an F-centre (farbe-colour in German)
electron in an anion vacancy

E.g. R&D for improved radiation tolerance of $PbWO_4$ crystals

Decrease concentration of defects
- stoechiometry
- annealing

Compensation of remaining defects
- control purity of raw material
- specific doping, pentavalent of W site, trivalent on Pb site

Si Avalanche Photodiodes

Light output from $PbWO_4$ crystal is low, require a photodetector with amplification. Calorimeter will operate in 4T field !
Solution is to use Si avalanche photodiodes.

Working Principle

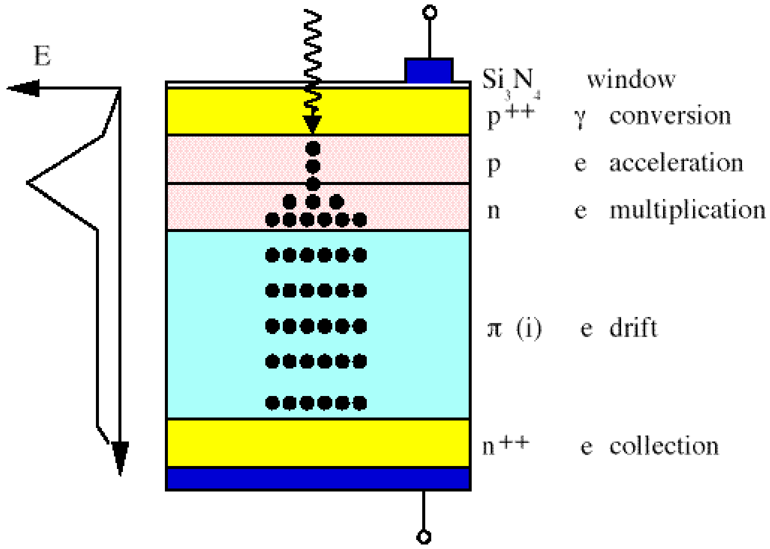

- Consider a crystal with a light yield of N_γ photons/MeV
- For deposited energy E, $N_\gamma.E$ photons hit APD
- For q.e. Q (can easily be 85%) $N_{pe} = N_\gamma EQ$
- photostatistics fluctuation $N_{pe} \pm \sqrt{N_{pe}}$
- If there is NO fluctuation in the gain, no. of electrons collected

$$M.N_{pe} \pm M\sqrt{N_{pe}}$$

but multiplication process in APD is noisy i.e. gain has a flctuation, σ_M

$$M \pm \sigma_M$$

because of this fluctuation no. of electrons collected is

$$M.N_{pe} \pm \sqrt{M^2+\sigma_M^2}\sqrt{N_{pe}}$$

so photostatistical contribution to energy resolution becomes

$$\frac{\sigma_{pe}(E)}{E} = \frac{1}{\sqrt{N_\gamma EQ}}\sqrt{\frac{M^2+\sigma_M^2}{M^2}} = \frac{1}{\sqrt{N_\gamma EQ}}\sqrt{F}$$

Si Avalanche Photodiodes

Parameter	Goal	Hamamatsu	EG&G
Active area	> 50 mm^2	25 mm^2	25 mm^2
Quantum efficiency @ 450 nm	> 80%	80%	75%
Capacity	<100 pF	100 pF	25 pF
Serial resistance	< 10 Ω	5 Ω	5 Ω
Excess noise factor	< 2	2.0	2.3
Operating bias voltage	< 500 V	400–420 V	350–450 V
Initial dark current	< 100 nA	2–3 nA	30–70 nA
dM/dV × 1/M @ M = 50	< 2%	5%	0.6%
|dM/dT| × 1/M @ M = 50	< –2%	–2.3%	–2.7%
Passivation layer	Si_3N_4	Si_3N_4	Si_3N_4
Packaging	non-magnetic	non-magnetic	non-magnetic

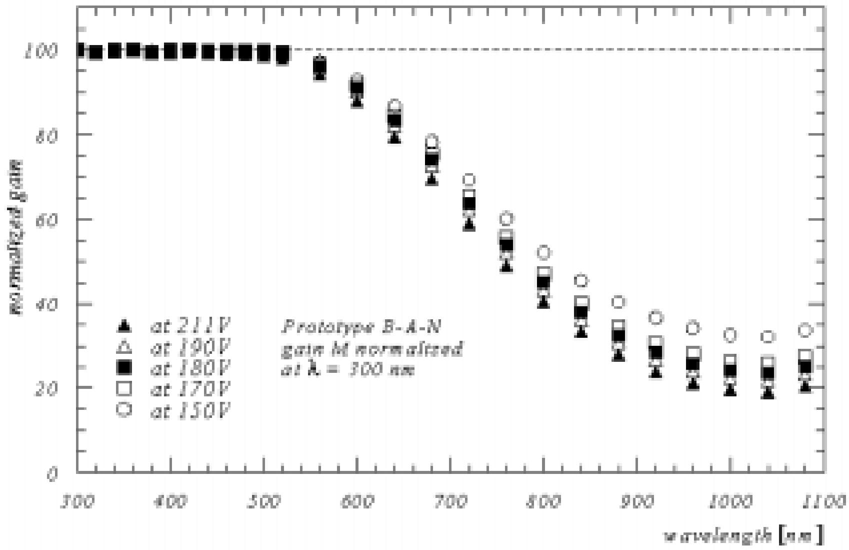

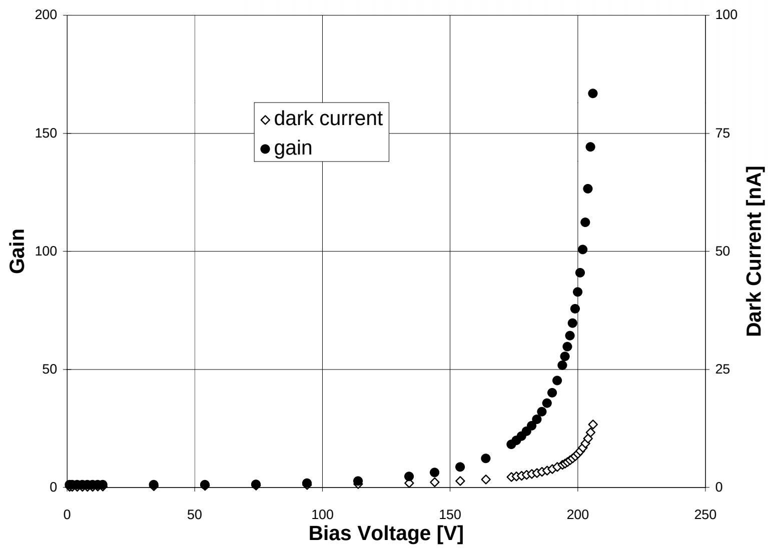

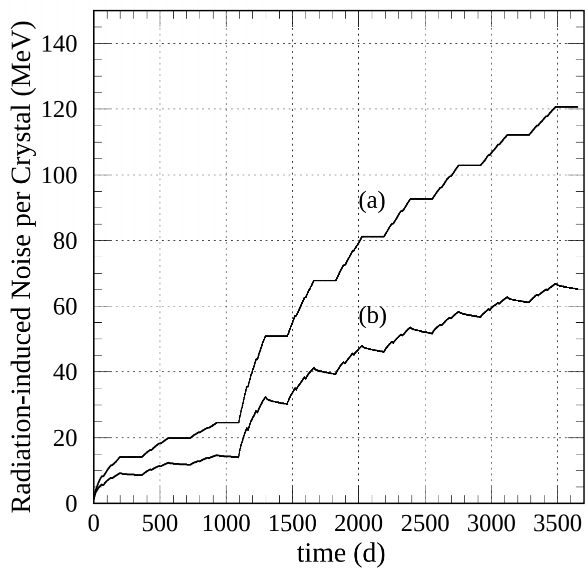

Noble Liquids Calorimetry

- Signal Generation in Noble Liquids
- Properties of Noble Liquids
- Charge Collection in Ionisation Chambers
- ATLAS LAr e.m. Calorimeter
- Performance of ATLAS ECAL

Signal Generation in Noble Liquids

- The number of ion pairs/100 eV ≈ that in gases.
- Not all electrons in liquids become "free". The motion of the electrons in liquids is governed by Coulomb attraction between the ions and by diffusion. A certain number of electrons will recombine with positive ions.

- Consider an e-ion pair. Assume r_c is the distance at which the Coulomb potential energy equals the mean thermal energy. Then

$$kT = \frac{e^2}{4\pi\varepsilon_0\varepsilon_r}\frac{1}{r_C}$$

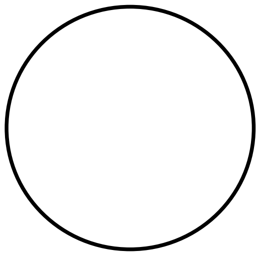

e.g. r_c ~ 1300Å in liquid argon (LAr).

- An electron will escape recombination if $\rho > r_c$ where ρ is the mean distance at which the electron thermalizes.

- In absence of an external electric field the escape probability is proportional to $\exp(-r_c/r)$.

- If G_{fi} is defined to be the number of "free" electrons per 100 eV of deposited energy, and W as the mean energy (in eV) required to create one electron-ion pair, then for low electric fields and low ionization density

$$G_{fi} = \frac{100}{W} e^{-r_C/r} (1+\alpha F) \qquad \text{Onsager}$$

where $\alpha = e^3 / 8\pi\varepsilon_0\varepsilon k^2T^2$, ε is the dielectric constant, F is the electric field strength and T is the absolute temperature.

Kramers - highly ionizing particles generate a dense column of electron-ion pairs and volume (or columnar) recombination has to be considered.

Properties of Noble Liquids

Desirable properties of liquids used in ionization chambers

- high free electron (G_{fi}) for large collected charge

.

- a high electron mobility (μ) leading to a high drift velocity and hence a rapid charge collection.

- a high degree of purity. The presence of electron scavenging impurities leads to the reduction of electron 'lifetime' and consequently a reduction in the collected charge.

Properties of Noble Liquids		LAr	LKr	LXe
Z/A		18/40	36/84	58/131
Density	g/cm^3	1.39	2.45	3.06
dE/dx <mip>	MeV/cm	2.11	3.45	3.89
Critical energy	MeV	41.7	21.5	14.5
Radiation Length	cm	14.3	4.76	2.77
Moliere Radius*	cm	7.3	4.7	4.1
W value	eV	23.3	20.5	15.
Drift vel (10kV/cm)	cm/μs	0.5	0.5	0.3
Dielectric Constant		1.51	1.66	1.95
Triple Point Temp	K	84	116	161

Charge Collection in Ionisation Chambers

• Ionisation chambers are essentially a pair of parallel conducting plates a few mm apart, at a PD in an insulating liquid (LAr, TMP etc.)

• Consider what happens to a single ion pair
(single carrier devices, +ve ions play no role in signal, ion mobility is much lower)

• Net charge induced on anode is $Q = -e\,\frac{(d-x)}{d}$

• Assume electron drifts with velocity v, and time of drift to cross the full gap is t_d

$$i(t) = \frac{dQ}{dt} = -e\,\frac{v}{d} = -\frac{e}{t_d}$$

• If ionisation is uniformly distributed, then fraction of electrons still moving after time t is $(t_d-t)/t_d$ for $t_d<t$.

$$\therefore \; i(t) = -Q_0\,\frac{v}{d}\left(1-\frac{t}{t_d}\right)$$

where Q_0 = Ne and current is max. at $t \approx 0$

$$q(t) = \int_0^t i(t)dt = -Q_0\left(\frac{t}{t_d}-\frac{t^2}{2t_d^2}\right) \quad t<t_d$$

• Total charge collected ($t \geq t_d$) is $Q_c = Q_0/2$ (2 because of uniform ionisation)
• If during drift, electrons are trapped by impurities, induced current will be reduced. If electron 'lifetime' is τ

$$i(t) = \frac{Q_0}{t_d}\left(1-\frac{t}{t_d}\right)e^{-t/\tau} \qquad t < t_d$$

Charge Collection in LAr Ionisation Chamber

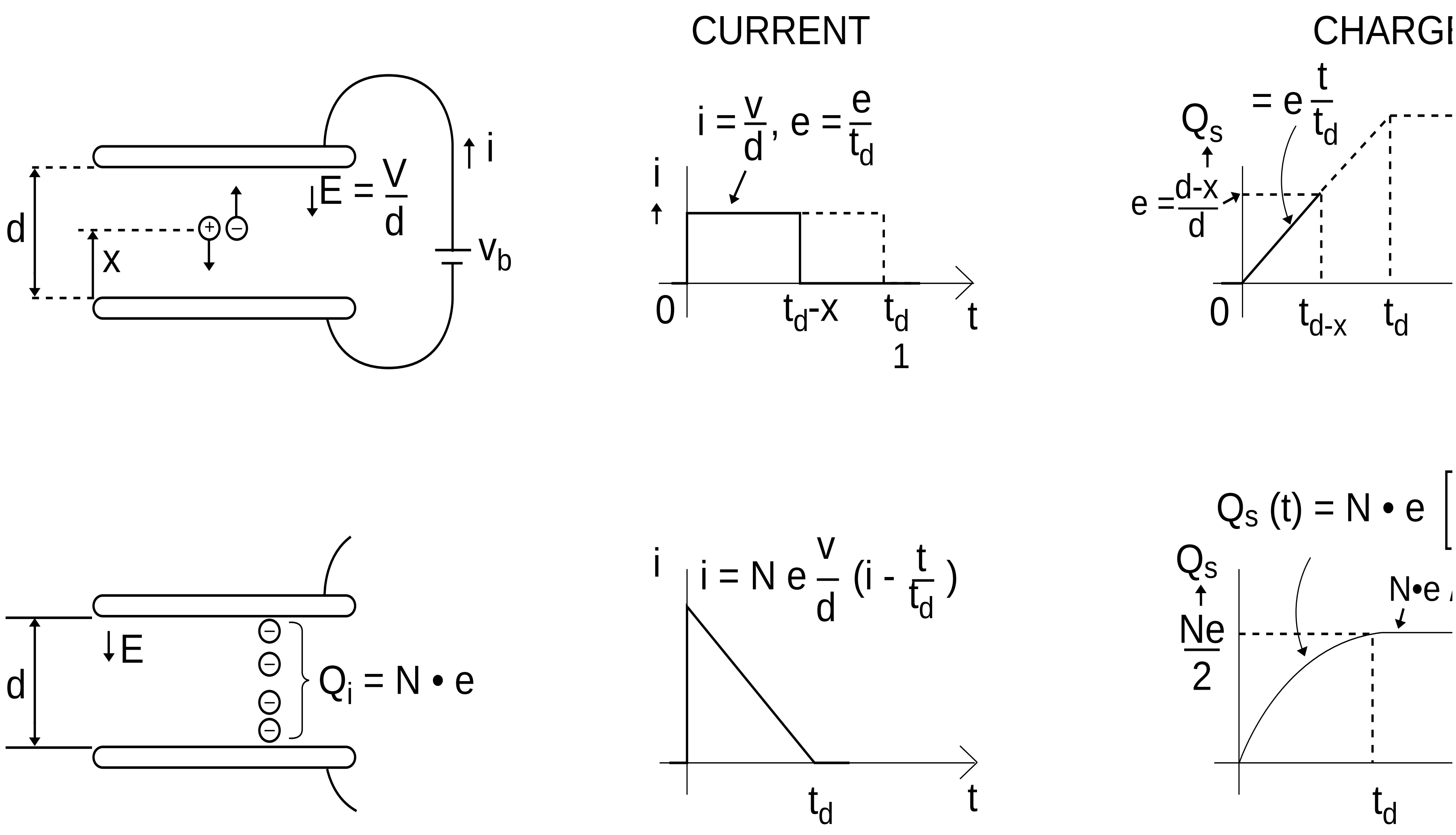

The current and charge for a) single electron-ion pair, b) uniformly distributed e-ion pairs

Signal Shapes

• Induced current duration = electron drift time t_d, with a triangular shape

• bipolar impulse response of chamber-preamp-shaper, most important condition for pulse shaping at high rates is

system impulse response should have zero area

pileup then does not produce a baseline shift

• for $t_p << t_d$, i.e. peaking time much faster than drift time, output response becomes 1st derivative of current pulse

energy info. fully contained in the initial current i_0

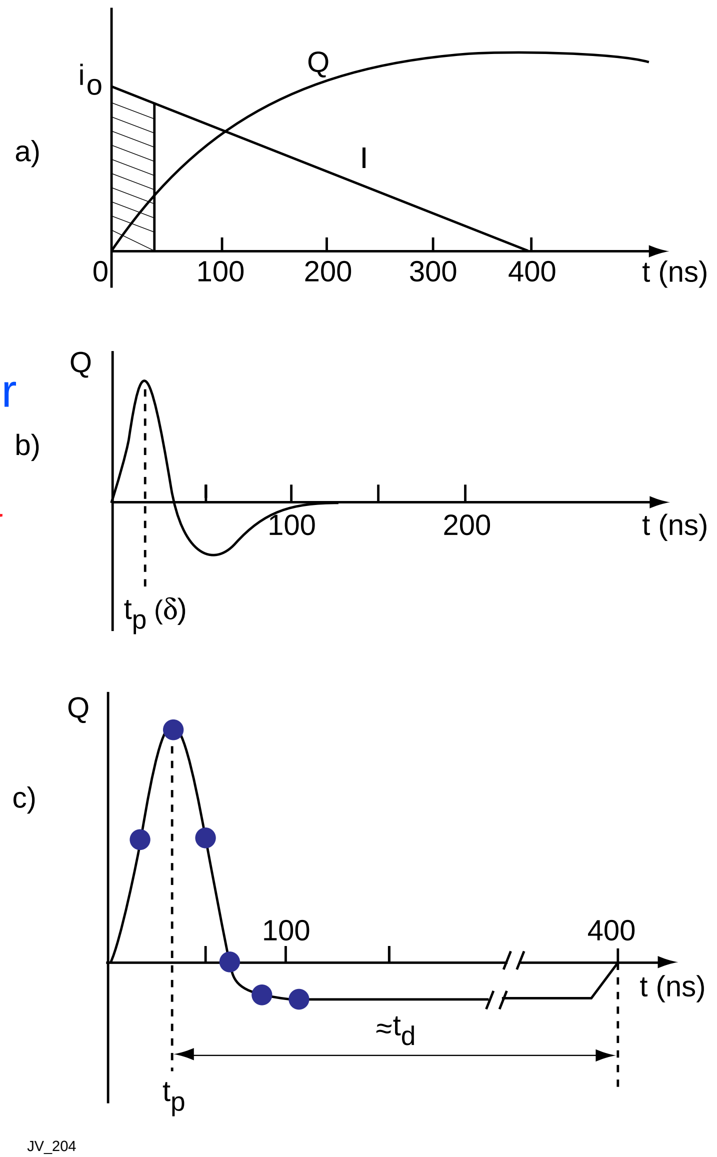

ATLAS LAr e.m. Calorimeter

The "accordion" concept, with electrodes essentially parallel to incoming particle's direction allows:

• high rate operation
avoid long connections between calorimeter cells to the electronics chain which lead to a slow response and high ENC

• high granularity readout in a barrel geometry with tower dimensions of ≈ Moliére radius

Features
• thin Pb-absorbers (1.2 mm for $|\eta| > 0.7$)
• towers project towards collision point, 3-fold longitudinal segmentation
• constant liquid argon gap is maintained
• fast response, by pulse shaping, exploits very fast rise of ionisation current, and reduces level of pileup

Quartz Fibre Calorimeters

- radiation hardness - quartz is one of most rad-hard solids
- fast - signal generated by C^v Iradiation
- narrow (and short showers) - only $e^{\pm}$ produced in shower development give an appreciable signal
- little sensitivity to induced radioactivity | Cv light emitted only by
- no sensitivity to evaporation neutrons | relativistic charged part.
- drawback - low light yield : 25% packing fraction $\Rightarrow$ 10 pe/GeV !

n=1.46 C^v thresholds : $e^{\pm}$ - 0.7 MeV, $\pi^{\pm}$ - 0.19 GeV, p - 1.3 GeV

Suitable for Very Forward Regions in LHC ($3<|\eta|<5$)

- em showers - 70% of energy deposited by $e^{\pm}$ with E>1 MeV
- hadronic showers - almost all non-em energy is invisible (e.g. $\approx$ 15% of non-em through $\pi^{\pm}$ in shower at 5 GeV in Fe)

expect e/h to be large (> 7) i.e. strongly non-compensating

Energy Resolution

- Hadronic signal determined by π^0s produced

- Expect hadronic energy resolution to be governed by event-to-event fluctuation in F_0 - will not obey Poissonnian statistics

$$F_0 \approx 0.435 - 0.052 \ln E$$

- For a calorimeter only sensitive to em shower component, energy resolution improves logarithmically with energy and not as $1/\sqrt{E}$

$\sigma(F_0)$ >> sampling or photostatistic (usually)

eg. 1 pe/GeV increase σ/E from 17 % to 19% at 150 GeV
at higher energies even better $\sigma(F_0) \approx 1/\ln E$ wheras $\sigma_{pe} \approx 1/\sqrt{E}$

Different ECAL/HCAL Calorimeter Structure

LHC pp experiments have put more emphasis on high precision e.m. calorimetry

High precision e.m. calorimetry is not compatible with perfect compensation

e.g. ZEUS :

$$\frac{\sigma_e}{E} = \frac{17\%}{\sqrt{E}} \quad and \quad \frac{\sigma_h}{E} = \frac{35\%}{\sqrt{E}}$$

BUT considerable importance has still to be placed on

- Gaussian hadronic energy response function (exact value of (σ/E) less important
- hemiticity
- linearity for jets

How do ATLAS and CMS calorimeter systems perform ?

Comparison with hadronic MC codes.

Trigger and Data Acquisition

The Challenge at the LHC
Purpose
Trends
Trigger Levels at LHC
Physical Trigger Levels - CMS
Level-1 Calorimeter Trigger - ATLAS
Calorimeter Trigger Rates - CMS
Muon Chamber Trigger Logic - CMS
Muon Rates
Summary - CMS
Selective Event Building and Higher Level Triggers
Trigger Rates and Physics
Super-Computing Trends
LHC Trigger/DAQ Perspectives

Trigger/DAQ : The Challenge at the LHC

Trigger is a key part of any HEP experiment

At LHC in pp general purpose experiments
select 100 events to record out of 10^9 interactions !

- very high efficiency of selection
  none of the few rare events should be missed

- select events without bias

- selection process should incur as little deadtime as possible

- reduce data flow as early and as quickly as possible
  <20> interactions every 25 ns $\Rightarrow$ 40,000 GB/s !!
  need information superhighway !

- must make sure selection process uses all subdetector data from the same crossing
  synchronise millions of channels to << 25 ns !

- can only store data at $\approx$ 100 Hz
  need to reject almost all events

- all done in real time
  cannot go back and recover events
  need to monitor selection process

Trigger Levels at LHC

Interaction rate 10^9 Hz

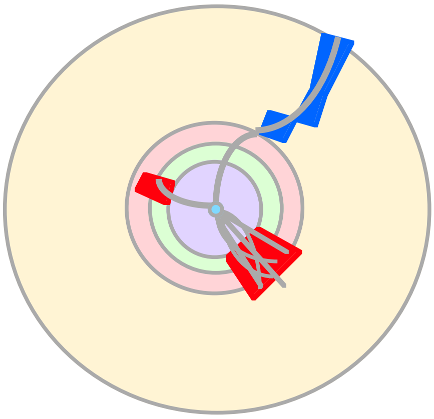

Trigger Objects

cut on p_T E_T of em clusters, muons, jets, missing E_T, isolation

- $\Delta t_{dec} \approx 3$ μs - no time to combine information from different sub-detectors
- Perform elementary operations with elementary conditions
- Local pattern recognition and energy evaluation using prompt reduced granularity information
- Parallel and pipelined processing

  custom made processors

Level-1 selected events 10^5 Hz

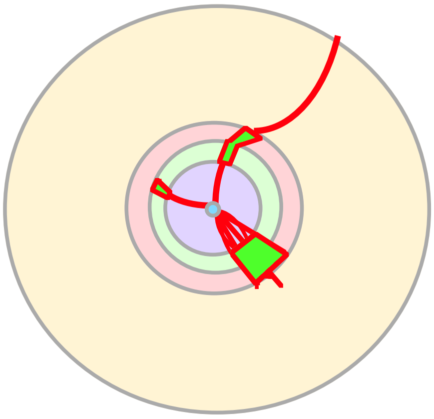

Clean particle signature (Z, W, ..)

- Full granularity used for precise meas.
- Kinematics. Effective mass cuts and event topology
- Track reconstruction and detector matching (shower shape, E/p etc)

Level-2 selected events 10^3 Hz

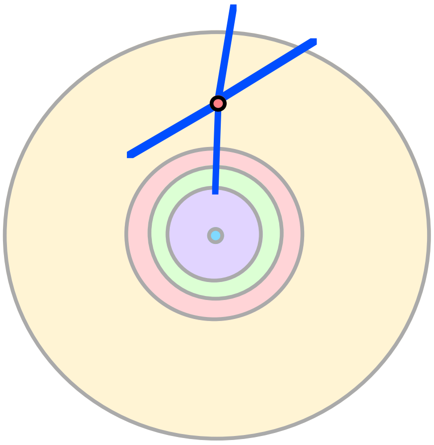

Physics process identification

- Event reconstruction and analysis

Level-3 events to tape 10..100 Hz

ATLAS Level-1Calorimeter Trigger

Isolated electron algorithm:

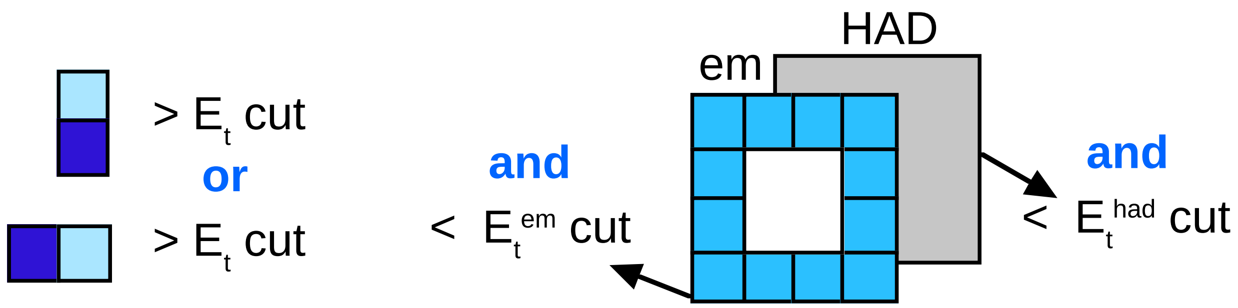

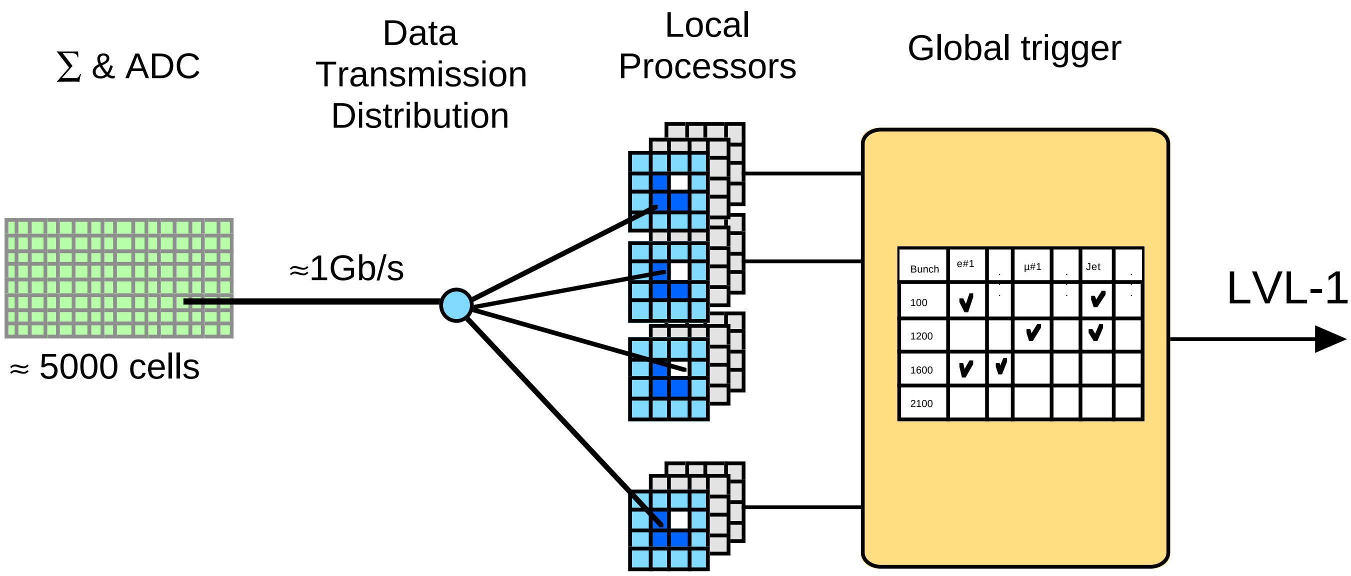

Sliding window for each tower

Extension to a τ-trigger

Vertical or horizontal sum of two trigger towers in both
ECAL + HCAL > E_t^{cut}
Isolation as before with different E_t^{cut}
Sliding window for each tower

Jet-trigger

Sum of energies in 4x4 trigger towers in ECAL and HCAL > E_t^{cut}
Sliding window for each block of 2x2 towers

Muon Trigger Segmentation and Efficiency

CMS RPCs

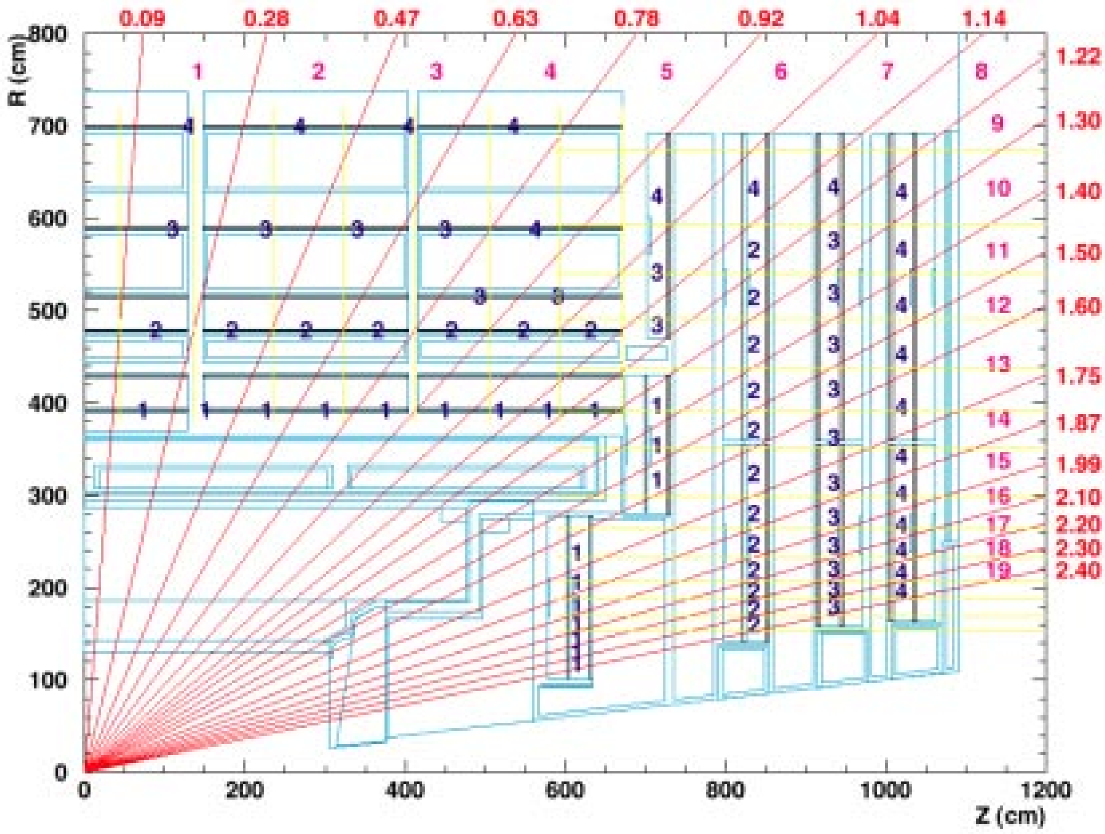

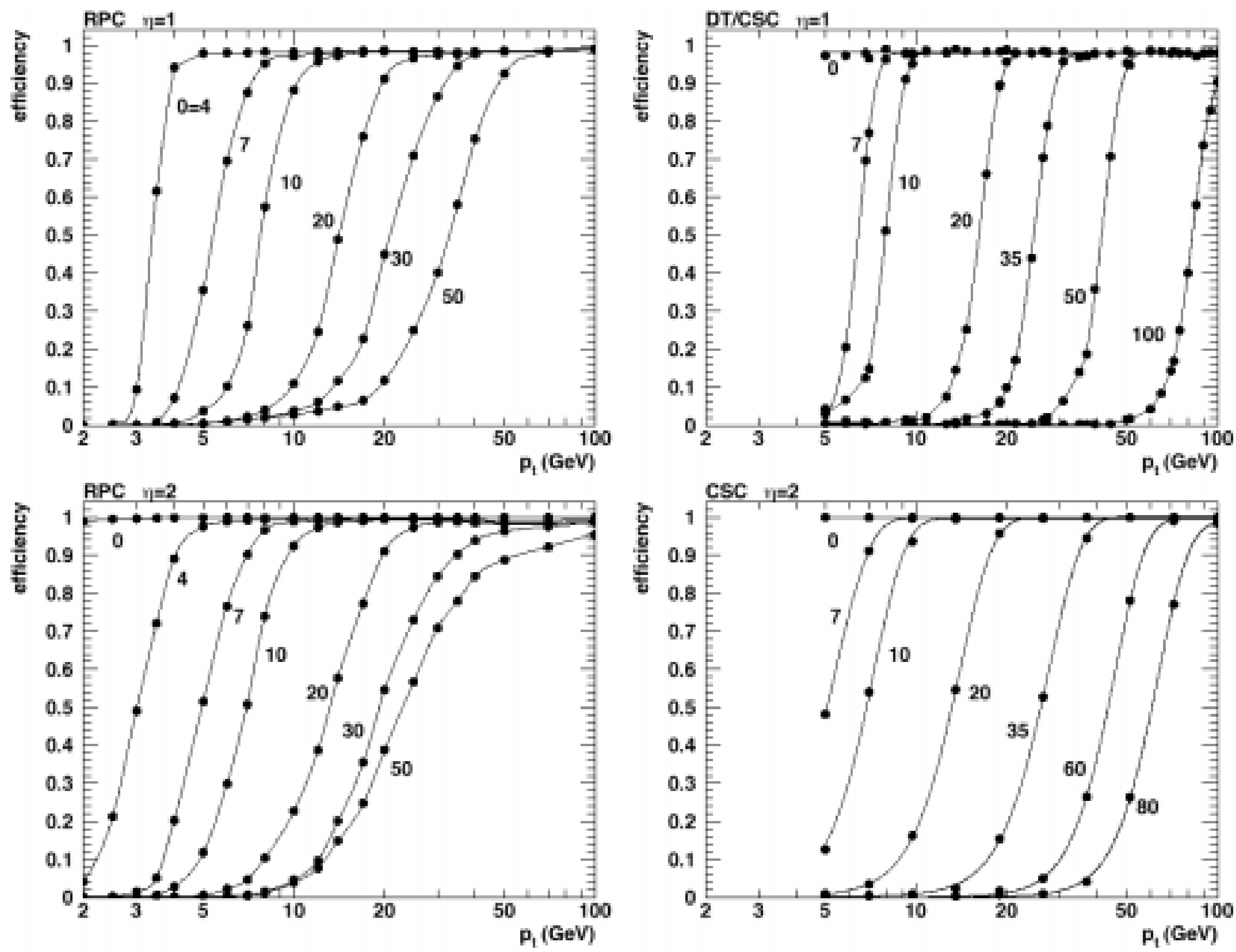

Trigger Rates and Physics

Calorimeter Trigger Rate at High Luminosity in CMS

Type	E_t^{cut} GeV	Individ. kHz	Increm. kHz
Sum E_t	400	0.3	0.3
E_t^{miss}	80	1.2	0.9
e	25	11.4	9.3
2-e	12	2.1	1.8
1- jet	100	1.5	1.0
2 - jet	60	1.2	0.7
jet + e	50/12	1.3	0.3
Cumulative		≈ 17	

Muon Trigger Rate at High Luminosity in CMS

Type	E_t^{cut} GeV	Individ. kHz	Increm. kHz
μ	20	7.8	7.8
2 -μ	4	1.6	9.2
μ e/γ	4/8	5.5	14.4
μ-jet	4/40	0.3	14.4
μ- E_t^{miss}	4/60	1.0	15.3
Cumulative		≈ 15	

Physics Efficiency

$H(80GeV) \rightarrow \gamma\gamma$	99%
$H(150\ Gev) \rightarrow 4l$	≈100 %
$pp \rightarrow tt \rightarrow eX$	88%
ΣSUSY	83%